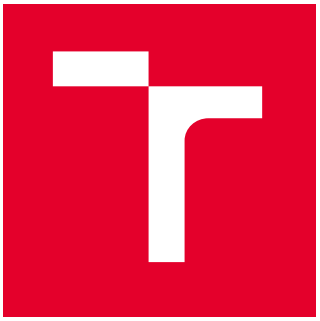

BRNO UNIVERSITY OF TECHNOLOGY

VYSOKÉ UČENÍ TECHNICKÉ V BRNĚ

FACULTY OF ELECTRICAL ENGINEERING AND COMMUNICATION

FAKULTA ELEKTROTECHNIKY
A KOMUNIKAČNÍCH TECHNOLOGIÍ

DEPARTMENT OF ELECTRICAL POWER ENGINEERING

ÚSTAV ELEKTROENERGETIKY

DEFINITION AND MEASUREMENT OF ELECTRICITY COMPONENTS IN ACTIVE DISTRIBUTION SYSTEMS

DEFINICE A MĚŘENÍ KOMPONENT ELEKTRICKÉ ENERGIE V AKTIVNÍCH DISTRIBUČNÍCH SÍTÍCH

DOCTORAL THESIS
DIZERTAČNÍ PRÁCE

AUTHOR — **Ing. Jan Klusáček**
AUTOR PRÁCE

SUPERVISOR — **prof. Ing. Jiří Drápela, Ph.D.**
ŠKOLITEL

BRNO 2025

Abstract

The measurement of electrical power and the registration of energy are fundamental for the management and control of active distribution systems. With the increasing number of active components in distribution networks—such as energy divertors, electrical drives, or inverters of battery storage systems and photovoltaic plants—energy flows fluctuate bidirectionally, fast and often in an unbalanced manner at low-voltage level, and are accompanied by various power quality disturbances. This thesis presents the results of several focused studies that (1) analyze the present condition of three-phase four-wire low-voltage distribution networks, with particular attention to the types of connected devices and their operational characteristics, (2) propose definitions of power components together with algorithms for their computation in measuring devices and (3) illustrate the interpretability of the individual components with respect to their subsequent applications (such as energy quantification and analysis), while also quantifying the deviations from the objective criteria, which are also unambiguously established in this thesis. Furthermore, the properties of power components are investigated, such as the implicit ability of symmetrical power components to quantify losses in the upstream distribution system resulting from unbalanced energy flows.

Overall, the thesis underlines the necessity of consistent methodologies to ensure fair energy sharing, reliable monitoring, and economically efficient operation of future decentralized energy systems. The thesis addresses both microgrids, representing the physical dimension of decentralization, and energy communities, reflecting rather its organizational dimension. The dissertation integrates methodological and technical aspects of power components measurement, offers a critical review of existing practices, examines them in the context of future decentralized network concepts, and outlines directions for further research.

Keywords

Energy registration, revenue meter, smart meter, power analyzer, power components, power theory, power quality, losses estimation, distribution system, microgrid, energy community.

Rozšířený abstrakt

Měření elektrického výkonu a registrování energie jsou základem pro řízení a správu aktivních distribučních soustav. S rostoucím počtem aktivních prvků v distribučních sítích, jako jsou regulátory pro řízení elektrického výkonu, elektrické pohony nebo střídače bateriových úložišť a fotovoltaických elektráren, dochází k obousměrným tokům energie, na úrovni nízkého napětí často nesymetrickým a doprovázeným rušením z oblasti kvality elektrické energie. Dizertační práce prezentuje a dává do kontextu výsledky několika konkrétních studií, které (1) analyzují současný stav třífázových čtyřvodičových nízkonapěťových distribučních sítí s důrazem na typy připojených zařízení a jejich provozní chování, (2) navrhují definice výkonových komponent spolu s algoritmy pro jejich výpočet v měřicích zařízeních a (3) demonstrují vypovídací schopnost jednotlivých komponent z hlediska jejich následného využití (například kvantifikace energie či analytické účely). V dizertační práci jsou jednoznačně stanovena objektivní kritéria, která umožňují jednoznačné kvantifikování odchylek měření u prosumerů, a která spojují odchylku výsledku měření s konkrétním dějem vedoucí k neefektivnímu využívání distribučních sítí. Za objektivní kritéria jsou považovány (1) skutečná energie/výkon přeměněná v jinou nebo z jiné formy energie každým jednotlivým zařízením prosumera, (2) ohmické ztráty (Joulovo teplo) ve vodičích nadřazené distribuční sítě, (3) skutečně importovaná a exportovaná energie v místě měření a (4) kompenzační proud virtuálního paralelního kompenzátoru v místě měření. Dizertační práce se vedle definic jednotlivých komponent také dále zabývá jejich vlastnostmi, například implicitní schopností souměrných složek výkonu kvantifikovat ty ztráty v nadřazené distribuční soustavě, které jsou vyvolané nesymetrickými energetickými toky v třífázových soustavách. Tento koncept je dále aplikován na numerický model mikrosítě připojené k nadřazené veřejné distribuční síti a s dvěma prosumery. Je ukázáno, že s využitím symetrických výkonů lze kvantifikovat příspěvek ke ztrátám v nadřazené distribuční síti od těch prosumerů, kteří využívají energetickou síť jako výkonový balancér. Dizertační práce se dále zabývá implementací definice činného výkonu a energie ve výpočetních modulech měřicích jednotek. Detailní numerické analýze je podrobeno pět algoritmů a jejich parametrické variant, které jsou v praxi využívány pro měření činného výkonu v různých aplikacích. Jsou porovnány výstupy jednotlivých algoritmů na rychlé změny směru toku energie.

Práce ukazuje odchylky různých implementací stejné definice výkonové komponenty (výpočetních algoritmů) v měřicích jednotkách a navrhuje systematická doporučení pro minimalizaci vlivu měřicích odchylek. Výsledky zdůrazňují význam harmonizace definic výkonových komponent a metrologických přístupů s cílem zajistit spravedlivé sdílení energie, spolehlivé monitorování a ekonomicky efektivní provoz budoucích decentralizovaných energetických systémů. Disertační práce propojuje metodologické a technické aspekty měření výkonových komponent, kriticky reviduje stávající přístupy, zkoumá je v kontextu budoucích konceptů decentralizovaných sítí a navrhuje směry dalšího výzkumu.

Bibliographic citation

KLUSÁČEK, Jan. *Definition and Measurement of Electricity Components in Active Distribution Systems.* Brno: Brno University of Technology, Faculty of Electrical Engineering and Communication, Department of Electrical Power Engineering, 2025. 125 p. Supervised by Jiří Drápela.

Author’s Declaration

I declare that I have written my treatise on doctoral thesis on the theme of “Definition and Measurement of Electricity Components in Active Distribution Systems”, under the guidance of the treatise on doctoral thesis supervisor and using exclusively the technical references and other sources of information cited in the treatise and listed in the comprehensive bibliography at the end of the treatise.

As the author, I furthermore declare that, with respect to the creation of this treatise on doctoral thesis, I have not infringed any copyright or violated anyone’s personal and/or ownership rights. In this context, I am fully aware of the consequences of breaking Regulation S 11 of the Copyright Act No. 121/2000 Coll. of the Czech Republic, as amended, and of any breach of rights related to intellectual property or introduced within amendments to relevant Acts such as the Intellectual Property Act or the Criminal Code, Act No. 40/2009 Coll., Section 2, Head VI, Part 4.

Brno …25.09.2025……. ----------

author’s signature

Acknowledgement

I am sincerely grateful to my supervisor, prof. Jiří Drápela, for his mentorship, valuable feedback, and guidance in my exploration of power systems and laboratory research. I would also like to extend my thanks to prof. Roberto Langella and prof. Jan Meyer for providing a kind and inspiring environment during my internships. Finally, my deepest gratitude goes to my family, especially beloved wife for her patience and endless support.

Brno ……25.09.2025…….

---

author's signature

Contents

FIGURES

1. INTRODUCTION

The transformation of modern energy systems is closely linked with several trends that increasingly shape the role and requirements of electricity metering. The liberalization of energy markets has placed growing emphasis on metering for accounting purposes, not only for traditional energy trading but also for energy sharing and the quantification of ancillary services [1]. In parallel, the decentralization of energy distribution has created the need for precise evaluation of power components in significantly smaller subsystems, including both physical subsystems such as microgrids and economic subsystems such as energy communities [2],[3]. Furthermore, the decentralization of generation capacities imposes new demands on the versatility of distribution networks, in which observability of network segments—dynamically and as close to real time as possible—represents a key requirement.

Real-time observability enables active and dynamic network control ([4], [A7]), thereby enhancing both the adaptability and robustness of distribution systems (DS). In the long-term perspective, observability is equally critical for system operators, who are responsible for maintaining supply quality and continuity. Reliable metering data form the basis for supply quality assessment ([5],[6]) as well as for the allocation of targeted investments to support grid development and modernization.

The concept of “smart metering devices” has thus become a fundamental element of modern DSs, often referred to as “smart distribution systems” [7]. Since the attribute “smart” is primarily associated with a metering device’s capability to participate in communication schemes, modern revenue meters (RMs) are required reflect the physical trends associated with the development of modern DSs, such us bidirectional energy flows (typically due to asymmetry, harmonic and interharmonic distortion, fast changing currents [8]). The metering devices should also be capable of identifying and detecting situations in which active participants possessing both generation and consumption units (active prosumers or, on a larger scale, aggregated flexibility providers) exploit gaps in the metering system in order to deliberately cause the registered energy flows to appear smaller than the actual physical exchange [9]. For example, this may occur when an active customer effectively utilizes the upstream DS as a temporal energy accumulator [10], or when energy is exported in one phase while simultaneously being imported in another phase at the customer’s point of connection (PoC) [A9].

The communication capabilities of smart meters represent a cornerstone for establishing smaller subnetworks, such as local distribution grids or community energy systems. In addition, smart meters can serve as integral components of home automation frameworks, as they are able to exchange data with other compatible household systems and devices [11].

The increasing complexity of modern electrical DSs—driven in particular by the decentralization of generation and distribution, market liberalization, and digitalization—

intensifies the demand for clear and consistent rules governing the measurement and registration of power and energy components in metering devices. The performance of metering equipment therefore plays a pivotal role not only from a technical perspective, by providing reliable data for system control and analysis, but also from an economic perspective, as it underpins energy trading and the allocation of distribution costs.

The initial motivation for this research is to investigate the limitations of accuracy in modern energy meters under conditions of bidirectional energy flows and to analyze how measurement errors introduced by implemented computational algorithms may affect subsequent processes. A further, associated, objective is to provide an unambiguous description of the actual energy flow in the system and to assess the extent to which individual power components and their algorithmic implementations adequately reflect, or fail to reflect, this physical energy transfer. Finally, the research aims to support the ongoing discussions, e.g. by means of formulation of recommendations for the enhancement of measurement methodologies and standards.

1.1 Historical Context

Historically, the earliest RMs were electromechanical induction-type devices, which converted the instantaneous energy flow into a rotary torque applied on an aluminum disc mechanically coupled to a registration mechanism [12], [13]. In three-phase systems, a single-disc arrangement was often employed, where the torques induced by the energy flows of all phases were summed. However, in installations with significant load unbalance, it was common practice to apply three independent single-phase meters, with their aggregated readings representing the registered value [14].

Since most end-users exhibited predominantly unidirectional energy transfer, inaccuracies occurring during transient phenomena—such as cycling industrial loads with switching periods much longer than the mechanical time constant of the meter—were tolerated under the assumption that deviations between instantaneous torque and actual power were compensated over a complete operating cycle due to the disc's inertia. Furthermore, under the premise of unidirectional power flow, temporary reverse power flows (e.g., regenerative braking in industrial drives [15]) were considered as a part of the metering process, as the short-term reverse torque was absorbed by the braking system of the disc.

Currently, almost all the electromechanical meters have been massively replaced by static meters, in which the results of measurement or registration is stored in the memory [16]. The electromechanical system for components calculation is replaced with metering integrated circuit processing the signals from signal acquisition chain. Although the static meters technically enable the measurement at higher resolution and enables faster dynamic response, the calculation algorithms derived from electromechanical meter are usually implemented in integrated circuits. However, due to the versatility of the microprocessors in static meters, there is a potential for implementation of additional (or

alternative) power components from power theories [17]. In combination with the alternative components, the energy flow might be described in more details than in case of power components being registered in RMs traditionally.

2. OBJECTIVES

The central objective of the thesis is to identify the current challenges in power metering in active distribution systems and contribute to definition and measurement of electricity components from the practical (bottom-up) point of view. The research and publication activities has been led by following research questions.

- What devices influence power metering in active distribution systems and how it corresponds with power quality?
- What are the main limitations of metering technologies in capturing rapidly changing or asymmetrical three-phase energy flows?
- How can active power algorithms be designed to clearly distinguish between energy import and export under dynamic conditions?
- Which power components describe the physical meaning of energy transfer in dynamic three-phase systems with bidirectional energy flow?
- How can inefficient energy transfer be quantified and evaluated?
- How severe are deviations arisen when control-based power metrics differ from those used in revenue metering in prosumer systems?
- How the ambiguities in metering of dynamic and unbalanced energy flows influence post-process computations in decentralized microgrids and energy communities?
- How the existing standards should be updated to reflect new trends and thus improve metering in active distribution systems and microgrids?

The research questions, which define the thesis objectives, are structured within the following areas of interest:

- Active customers and impact on grid quality, tariffs and billing paradigms
- Active customers - prosumers in microgrids
- „Energy self-sufficiency“ of active customers (devices & control)
- Definition of power components
- Computation algorithms for power components
- Commercial metering & monitoring devices in decentralized grids

2.1 Thesis Structure

In order to describe the answer to the research questions, the thesis is structurally divided into seven main sections. Each section provides a detailed and broader contextual discussion of the aspects considered during the research process and throughout the development of the author’s publications [A1]-[A12]. The work is thus designed to elaborate on and contextualize specific topics that originate from the individual research outputs.

- Section 3: presents a systematic review and categorization of typical applications of power component measurement in DSs, including a description of their significance and requirements, as well as a survey of the relevant standard framework of standards.
- Section 4: provides a systematic review of power component definitions.
- Section 5: focuses on the comparison of selected algorithms for calculating power and energy components in metering units.
- Section 0: introduces and explains objective criteria for evaluating the suitability of power components usage and implementation in metering devices. The inefficient energy transfer by means of oscillatory energy exchange at the PoC is illustrated.
- Section 6.4: evaluates the ability of selected power components to quantify DS losses that arise from inefficient utilization of the network.
- Section 8: addresses the context of small distribution networks (microgrids) with active participants (members). It analyzes the application of selected power components, the implementation of computational algorithms, and demonstrates their significance for energy sharing within communities. Moreover, it illustrates additional inaccuracies in energy allocation caused by subsequent computational steps in microgrids (e.g., allocation keys for energy sharing).
- Section 9: analyzes different control algorithms for active prosumers that divert active energy to target value of different power components in RMs, presents the requirements on diverter's hardware.
- Section 10: summarizes the contributions of the individual publications and the dissertation as a whole.

3. POWER METERING APPLICATIONS

Measurement of electrical power and energy parameters in metering devices serves three primary purposes:

1. Energy registration for billing and market transactions, typically performed by RMs.
2. Real-time power measurement for control of energy flows, implemented via smart meters or dedicated measurement units.
3. Measurement and temporal aggregation of power values for power system diagnostics and analysis, carried out by power analyzers and advanced metering devices.

The typical roles, locations, and data flows of these devices within the power system are illustrated in Fig. 3.1.

At the local level, measured quantities—primarily active and reactive power—are used in behind-the-meter energy management systems. These applications concern:

- Individual end-users connected at low-voltage (LV) and medium-voltage (MV) levels, and
- Local distribution subsystems (such as microgrids) interconnected with regional distribution networks. Relevant hardware includes specialized metering units or RMs communicating with local control systems such as programmable logic controllers (PLCs), embedded control boards in active converters, or compensation equipment.

At the intermediate level, time-aggregated and registered data (i.e., time-integrated values) are utilized for billing of energy consumption and distribution services, based on revenue metering. These data are often reused for grid-related tasks such as power flow analysis, planning, voltage regulation, or energy flow control. In these contexts, the focus lies on aggregated values of active/reactive power and energy. Additionally, RMs may store further parameters, such as aggregated current and voltage values, enhancing their role in grid analytics. For more detailed analyses, power analyzers may supplement the measurement infrastructure. These devices are installed temporarily or permanently at key locations in the grid, such as transformer terminals (substations, customer-owned distribution transformers) or points of common coupling (PCC) between multiple consumers.

At the system level, measured data support enhanced visibility of distribution system operator (DSO) assets and optimization of grid control strategies. Applications include long-term infrastructure planning, adjustment of voltage/frequency control parameters, evaluation of power quality indices, equipment diagnostics, and maintenance scheduling.

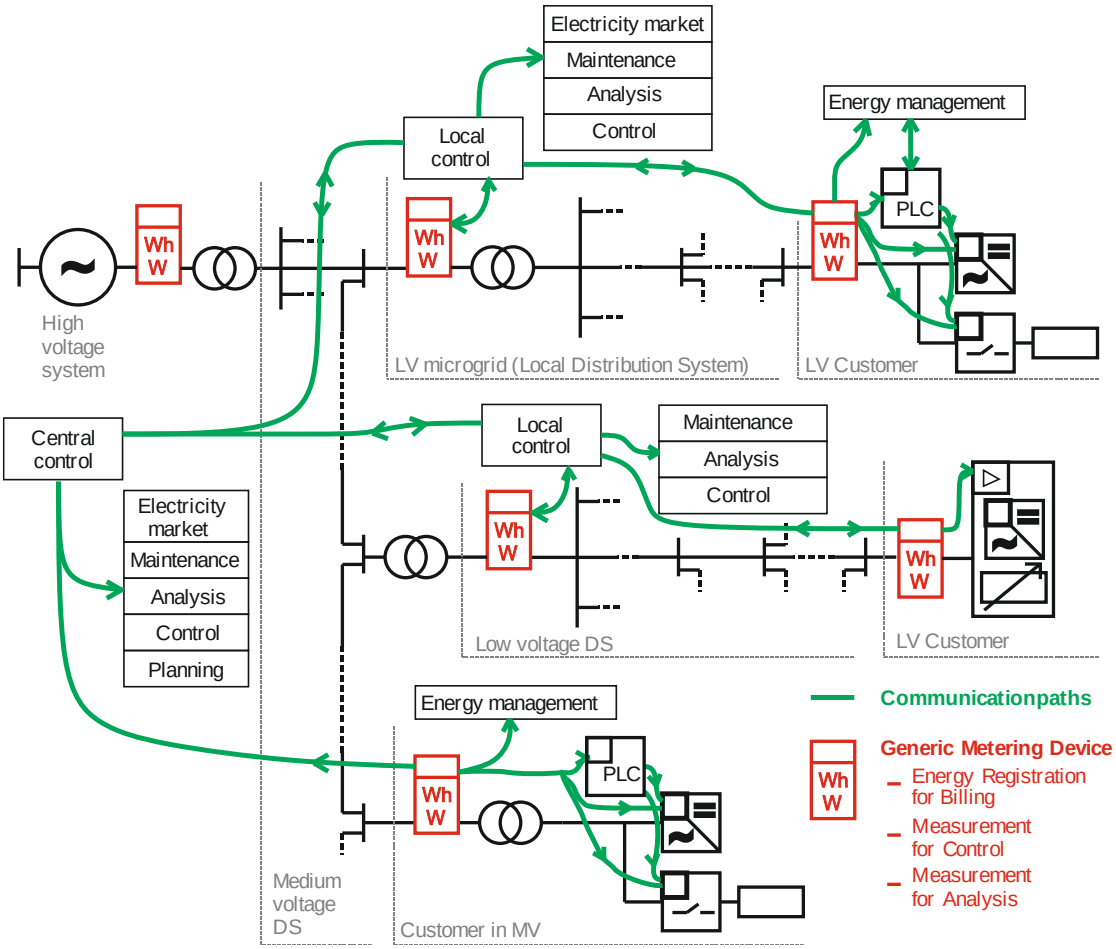

Fig. 3.1. Location of metering devices in DS, application and data flow in power systems.

Power and energy components measured by individual devices are acquired either on demand (both locally and remotely), or regularly by automated communication networks. Subsequently, the components processed either locally or at central levels. Based on their purpose, the utilization of these data can be categorized into the following groups:

1. Electricity distribution billing – supporting cost allocation for the delivery of electrical energy through the distribution network.
2. Electricity trading – providing the basis for commercial transactions related to active energy production and consumption.
3. Operational control – enabling real-time or near-real-time regulation of energy flows, voltage levels, and device coordination.
4. Grid visibility and diagnostics – facilitating power system monitoring, condition assessment, and analytical tasks supporting planning and maintenance.

The diagram in Fig. 3.2 illustrates the scope of the thesis. The work focuses on power metering units from the perspective of the physical flow of electrical energy, considering both its quantitative and qualitative aspects, while also addressing their relevance to

practical applications. Although the analyses presented throughout the thesis are primarily demonstrated using RMs, the findings and methodologies are applicable to a broad range of metering devices used in power systems, including:

- Generic energy monitors, which provide basic energy measurements to support energy management and visibility in end-user systems.
- Generic power meters, which deliver real-time power measurements suitable for operational control.
- RMs, primarily used for electricity billing, but also capable of supporting diagnostics and grid analysis when equipped with advanced functionalities.
- Power analyzers, offering high-resolution measurements of both power quality and quantity, enabling detailed diagnostics and visibility at critical locations within the power system.

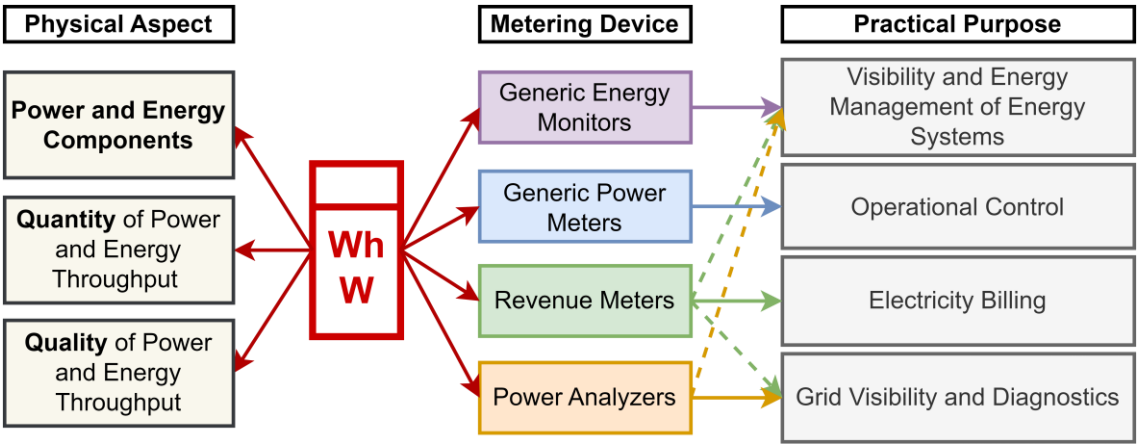

Fig. 3.2. Practical and physical aspects of power metering.

3.1 Regulatory Requirements and Standards on Power and Energy Measurement

The definitions of power theory and power and energy components relevant to power metering are established in IEEE 1459-2010 [18]. This standard provides a formal framework for decomposing electrical power under non-sinusoidal and unbalanced conditions. The IEC 61557-12 Ed.2 [19], particularly in Annex B, extends this framework by introducing power quality indicators and offering practical insights into the interpretation of measured quantities. Additionally, Annex C of the same standard introduces power components classified according to the quadrants of the active–reactive power plane, effectively expanding the set of defined components when active and reactive power are categorized by their directional characteristics.

Furthermore, IEC 62052-41 [20] complements these definitions by specifying classification and sorting methods for power components in multiphase systems. It also defines the measured quantities and their aggregation to be stored in the registers of RMs

for billing purposes, including both active and reactive energy components and their time-dependent profiles.

The above-mentioned standards define the power and energy components, but do not provide specific implementation guidelines for their realization in power metering devices. In contrast, power analyzers designed for voltage quality assessment are supported by detailed standards that precisely define the measurement methods and algorithms for individual parameters:

- IEC 61000-4-7 [21]: defines algorithms and methods for the measurement of harmonics and interharmonics.
- IEC 61000-4-15 [22]: specifies the algorithm and method for flicker measurement.
- IEC 61000-4-30 [23]: defines the measurement parameters for frequency, RMS voltage, voltage dips, interruptions, overvoltages, harmonics and interharmonics, flicker, voltage unbalance, and rapid voltage changes, along with the associated accuracy classes (Class A and Class S).

In contrast, the methods and algorithms for the measurement of power and energy components are not standardized in such detail. Their specification is addressed only indirectly, typically via accuracy class requirements, leaving the exact implementation to the manufacturer's discretion (see Tab. 3.1). Relevant standards include:

- IEC 61557-12 [19]: sets accuracy requirements for indicative power and energy meters, including classification into categories PMD-I, PMD-II, and PMD-III, depending on the application.
- IEC 62053-21/-22/-23/-24/-41 [24]-[28] and IEC 62052-11 [29]: specify accuracy limits and testing procedures for revenue-grade meters used for billing, defining accuracy classes such as 2, 1, 0.5, 0.2, 0.1, and their "special" variants (e.g., 0.5S, 0.2S, 0.1S) which maintain specific accuracy at lower minimal currents.
- MID Directive 2014/32/EU [30], implemented via EN 50470-1 [31] and EN 50470-3 [32], establishes requirements for billing meters in Europe, using accuracy classes A, B, and C, harmonized with the IEC test procedures.
- OIML R 46-1/-2 [33], [34]: provides an alternative accuracy framework adopted in non-European regions such as Latin America and parts of Asia, also using accuracy classes A, B, and C.

As a result, the correctness of the measurement is dependent on definition of the tests, which include a limited number of test procedures preventing selected external conditions (e.g. electromagnetic environment, dynamic power flow) using a testbench defined in IEC 62057 series [35].

Furthermore, the power/energy meters are tested including complete measuring chain (signal measurement in sensors/probes, signal acquisition and processing in digitization unit, signal processing unit and calculation unit of the power/energy components). Thus,

the contribution by the individual stages to the total uncertainty, especially calculation unit being the main scope of the thesis, is difficult to separate and identify.

Consequently, the accuracy of power and energy measurements depends primarily on the test definitions, which typically encompass only a limited set of procedures and do not fully reflect certain external conditions—such as electromagnetic interference or dynamic variations in power flow. Moreover, power and energy meters are evaluated as a complete measurement chain, which includes:

1. Signal acquisition via sensors or probes,
2. Analog-to-digital conversion and preprocessing, and
3. Numerical processing and computation of power and energy components.

As a result, it is challenging to isolate and quantify the contribution of individual stages to the overall measurement uncertainty. In particular, the calculation stage, which is the main focus of this thesis, cannot be easily assessed independently of the entire system.

Tab. 3.1 Sorting of standards related to power meters and power quality analyzers.

Standard	**Generic Power Monitors**	**Static Revenue Meters**	**Power Analyzers**	**External Power Meters**
Definition of power and energy components				
IEEE Std. 1159-2010	✔	✔	✔	✔
IEC 61557-12	✔	✔	✔	✔
IEC 62052-41	X (optional)	✔	X (optional)	X
Standard testing, sorting to accuracy classes				
IEC 62052-11	X (optional)	✔	X (optional)	X (optional)
IEC 62053 (-21/-22/-23/-24/-41)	X (optional)	✔	✔	X (optional)
IEC 61557-12	✔	✔	✔	✔
EN 50470 (-1 / -3)	X	✔	X (optional)	X
MID (2014/32/EU)	X	✔	X	X
OIML R 46 (-1/-2)	X	✔	X	X
IEC 62058 (-11/-31)	X	✔	X	X
IEC 62586-2	X	X (optional)	✔	X
Voltage and current sensors				
IEC 61869 (-1/-2/-3/-4/-5/-6/-9/-10/-11/-12/-14/-15)	✔ (indirect measurement)	✔ (indirect measurement)	✔ (indirect measurement)	✔ (indirect measurement)

3.2 Metering Units for Distribution Network Charges

This section focuses on the measurement processes within RMs, which serve as the basis for calculating electricity distribution charges imposed on grid users. In the context of the European Union, customer charges are typically structured into several categories [36]:

- Fixed charge for active power – based on reserved capacity, typically expressed in €/kW/month.
- Variable charge for active energy – calculated according to the registered energy consumption, in €/kWh.
- Fixed periodic charge – independent of energy consumption, usually specified per billing period (e.g. €/month).
- Charge for reactive energy – applied when reactive power exceeds allowable limits, e.g. when the power factor falls below 0.95.
- Specific regulatory charges – including fees for renewable energy support schemes, market operator services, or other policy-driven levies.

The reserved capacity is stipulated in the connection agreement and is typically monitored using the maximum 15-minute average active power, as recorded by RMs, to verify compliance with the contracted demand—this applies primarily to larger customers connected at the MV level or above.

For smaller customers (typically with a maximum current of up to ~80 A per phase at the LV level), the reserved capacity might be also implicitly determined by the rated current of the main circuit breaker at the PoC (e.g. 20 A, 25 A, 32 A). In such cases, capacity monitoring is not based on RM measurements, but rather enforced through the physical limitations of the connection.

The variable component of distribution charges is typically derived from the active energy values registered in the RM's registers [37]. Each register may be associated with a different tariff rate, depending on the energy flow direction (import or export) [38], or on time-based pricing schemes such as time-of-use tariffs [39], [40].

Both fixed and variable charges are thus generally based on power or energy components measured and recorded by RMs. As a result, any systematic measurement errors [A9], or even inconsistencies in the definition of measured components [A12], can impact the fairness and accuracy of cost allocation within the electricity DS.

To ensure that distribution charges are technically justified and economically fair, the measurement processes should:

- Reflect the actual energy flow in the network, to enable proper loss allocation and grid operation assessment.
- Capture the quality of energy consumption or generation, in order to identify and discourage behaviors that degrade system efficiency or violate voltage quality requirements [41].

3.2.1 Distribution Network Costs Allocating

The expenditures of European DSOs are generally categorized into the following cost components [36]:

- Capital expenditures (CAPEX) – including return on capital employed and asset depreciation.
- Operational expenditures (OPEX) – covering maintenance, administrative, and personnel costs.
- Network losses – comprising both technical and non-technical losses.
- Metering-related costs – involving procurement, installation, and maintenance of metering infrastructure.
- System services – such as voltage regulation, reactive power compensation, and ancillary services.
- Policy-driven costs – including support schemes for renewable energy sources (RES), combined heat and power (CHP) units, or social tariffs.

The core principles guiding the design of distribution tariffs include cost reflectivity—ensuring that users contribute in proportion to the costs they impose on the system—along with transparency, non-discrimination, and consumer protection [38], [42].

In [38], the authors examine five methods for cost allocation among grid users. These methods differ based on whether the direction of energy flow (import vs. export) is taken into account and whether they consider the intensity of power consumption. Some approaches also incorporate the topological structure of the grid, aiming to reflect the so-called proximity effect—i.e., assigning a greater share of the cost to users who are physically closer to the infrastructure in use (e.g., specific feeders or lines) [A12]. While this can naturally align cost allocation with each user's contribution to system losses, caution must be exercised to avoid discriminatory treatment of users connected via circuits with higher impedance, which may not directly correspond to their actual cost impact.

Although system losses represent only a fraction of the total expenditures of a DSO and therefore should not serve as the sole basis for cost allocation, they provide an objective and technically grounded indicator of a user's impact on the network. As highlighted in the preceding paragraph, system losses are frequently considered in both academic literature and in the context of this thesis as a relevant criterion for allocating distribution costs.

In [43], the authors conduct an extensive review of methodologies for allocating system losses among consumers. They identify two primary technical challenges in implementing such allocation schemes:

1. The availability and accuracy of metering data, and
2. The integration of distributed generation into the DS.

Loss allocation can be implemented at different levels of granularity. The methods discussed in [43] focus on allocating the total network losses, typically based on the registered active energy in standard RMs.

By contrast, the approaches proposed in author's publications [A5] and [A12] introduce additional power components that aim to charge users whose behavior contributes disproportionately to system losses. These methods assess the non-ideal power exchange at the user's PoC, particularly focusing on unbalanced phase loading. The user's impact is quantified through their contribution to losses arising from phase asymmetry, and penalization is implemented by adjusting billing registers—either by:

1. Adding a portion of energy to the import register, or
2. Subtracting it from the export register.

The methodology leverages the concept of positive sequence power, which serves as an implicit indicator of unbalanced behavior and its associated additional losses in the DS. Notably, the authors demonstrate the effectiveness of this approach in highly unbalanced scenarios, such as when a user imports power in one phase while exporting in another within a three-phase connection.

An alternative approach to quantifying a user's impact on DS costs in AC networks is based on the concept of apparent power, which emphasizes the ideally balanced and efficient power transfer within the system. Although apparent power does not directly correspond to the user's contribution to network losses, it serves as a signal for power quality compliance at the PoC. By encouraging users to minimize non-active (nonactive) power components, it helps to reduce the propagation of undesired power through the grid.

Apparent power can also be decomposed into distinct components, some of which are directly associated with specific categories of non-active power, such as reactive power arising from capacitive or inductive elements. These components—while not causing direct energy consumption—may contribute to the inefficiency and over-dimensioning of network assets and are thus considered in advanced cost allocation schemes.

3.3 Metering Units for Commodity Billing

The liberalization of electricity markets, combined with the increasing availability of affordable distributed generation, energy storage systems, and responsive (active) loads, has enabled even small-scale end-users to act as active participants in energy markets. Accurate and reliable power metering is therefore a fundamental prerequisite for enabling energy trading at all levels of the system.

Electricity consumers typically purchase active energy from suppliers via fixed-price contracts or through access to spot electricity markets. These transactions are settled based on metered energy consumption, often aggregated over 15-minute intervals [44], with a trend toward even shorter settlement periods [45]. In this context, two distinct sources of error can affect the validity of settlement data:

- Improper calibration of the metering device itself, which introduces a systematic measurement bias specific to the given unit, and
- Inaccurate time synchronization, which does not affect the internal measurement accuracy but may lead to misalignment of data with contractual time intervals during subsequent processing and evaluation.

Both types of errors can result in deviations between contracted and delivered volumes that exceed the allowed tolerance defined by the meter's accuracy class.

Electricity producers, on the other hand, inject energy into the grid and are remunerated based on the quantity of energy delivered, either via feed-in tariff schemes or market-based pricing mechanisms. In such cases, precise metering of generated energy is essential to ensure correct compensation for producers.

Aggregators combine multiple distributed energy resources and utilize them for energy balancing, either on spot electricity markets or within balancing markets coordinated by the transmission system operator. Their operation depends on sub-metering infrastructures and the ability to issue control signals to active customers in accordance with their business models. Inaccurate metering or data acquisition may lead to overcommitment or under-delivery, resulting in financial penalties or loss of market position [46].

Finally, grid users may participate in energy communities or collective schemes, where peer-to-peer energy exchange occurs either within private sub-grids (e.g., apartment complexes or microgrids) or via the infrastructure of the regional DSO. In such configurations, precise and synchronized power metering is essential for balancing imports and exports among participants and for ensuring transparent and fair settlement.

The measurement system must therefore deliver time-aligned readings of acceptable precision, enabling the reconciliation of consumption and generation—thus forming the foundation for a shared operational and economic concept.

3.4 Metering Units for Control

Local energy-management systems (EMS, Fig. 3.3)—ranging from individual households and industrial campuses to private neighborhood networks—are designed to control generation, storage and demand without compromising following DS-side constraints (Fig. 3.4) [A4].

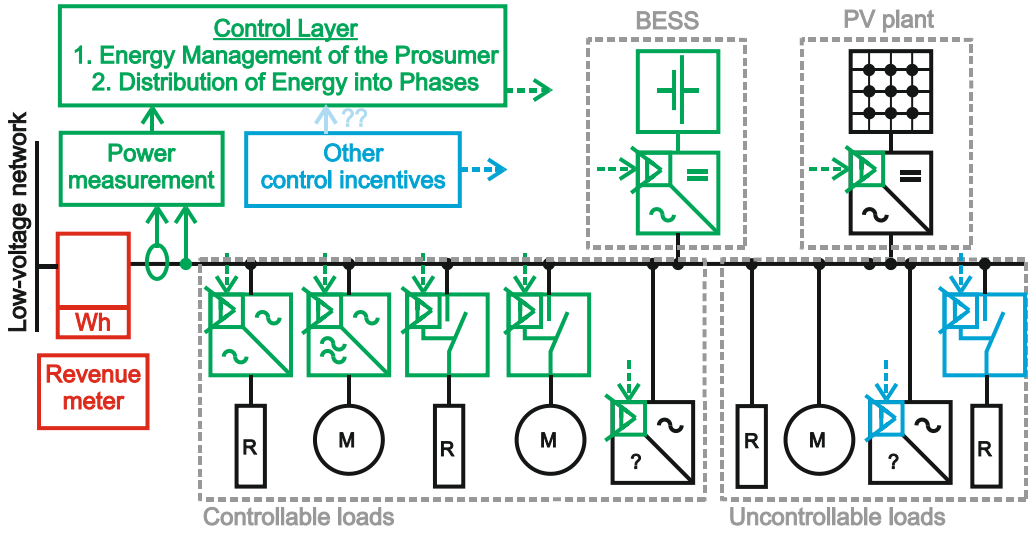

Fig. 3.3. Model of generic EMS and energy metering oriented on comparison of control strategies [A5].

Every EMS action may degrade voltage quality at the PoC according to relevant standatd. This requirement places an upper limit on how aggressively power flow may be modulated—avoiding voltage swings and flicker [A4]—and, in turn, on the necessary measurement refresh rate. Yet the achievable control speed is also set by the switching behavior of the power-electronic hardware (active hardware), whose commutation negatively affects PoC voltage quality alongside measurement granularity [A1], [A4]. It is concluded that raising the switching frequency diminishes energy fluctuations at the PoC, thus improves power quality, and reduces the cost of mitigation measures. The impact of the commercial energy diverters on flicker and emission of current DC component is described in [A6].

Modern smart meters still inherit simplifications rooted in an era of uni-directional flows; for instance, they may assume unidirectional energy flow in phases of multiphase systems or assume unidirectional dynamic changes of energy flow in time. Control algorithms must not rely on such weaknesses—regulation that intentionally masks a real export by toggling polarity within the meter's dead-band (both in time and across the phases) is detrimental to system visibility and to power quality [A3].

The Fig. 3.4 also shows a technology for mitigation of detrimental current draw according to switching strategy of the deployed hardware, which is derived from commercial devices [10] and relevant designs [47].

Based on outcomes of [A1] and [A5], additional requirements on active energy diverting device might be specified:

- Metric alignment with the billing meter. When the control objective is to hold the net energy exchange at the PoC within a target envelope, the controlled variable must be defined exactly as the billing meter defines it, e.g. same component separation (component definition), same sign convention, same

sorting method in three-phase systems [A3], [A5], an integration window that is no longer than, and preferably shorter than, that used for settlement in billing meter [A1].

- Measurement and control speed. A stable controller cannot react faster than it observes; therefore the measurement refresh-rate must outpace the control bandwidth—typically by at least one decade to guarantee adequate phase margin. If, for example, the EMS is required to limit export within 200 ms, active-power samples should be available every 20 ms or faster [A1]. The disproportions between measurement and control bandwidth may lead to control stability issues, affecting the voltage quality in PoC [A2].

At the system level, the same distributed energy resource (DER) assets, that a household EMS controls locally, form a pool of flexibility that can be marshalled by aggregators to deliver ancillary services—frequency containment, congestion relief or balancing reserves [48]. The importance of specified constraints is applicable to metering devices for evaluation of the aggregated ancillary services. Beside the settlement, ancillary-service verification demands time-synchronized measurements so that delivered up- and down-regulation can be unambiguously attributed to each resource [1].

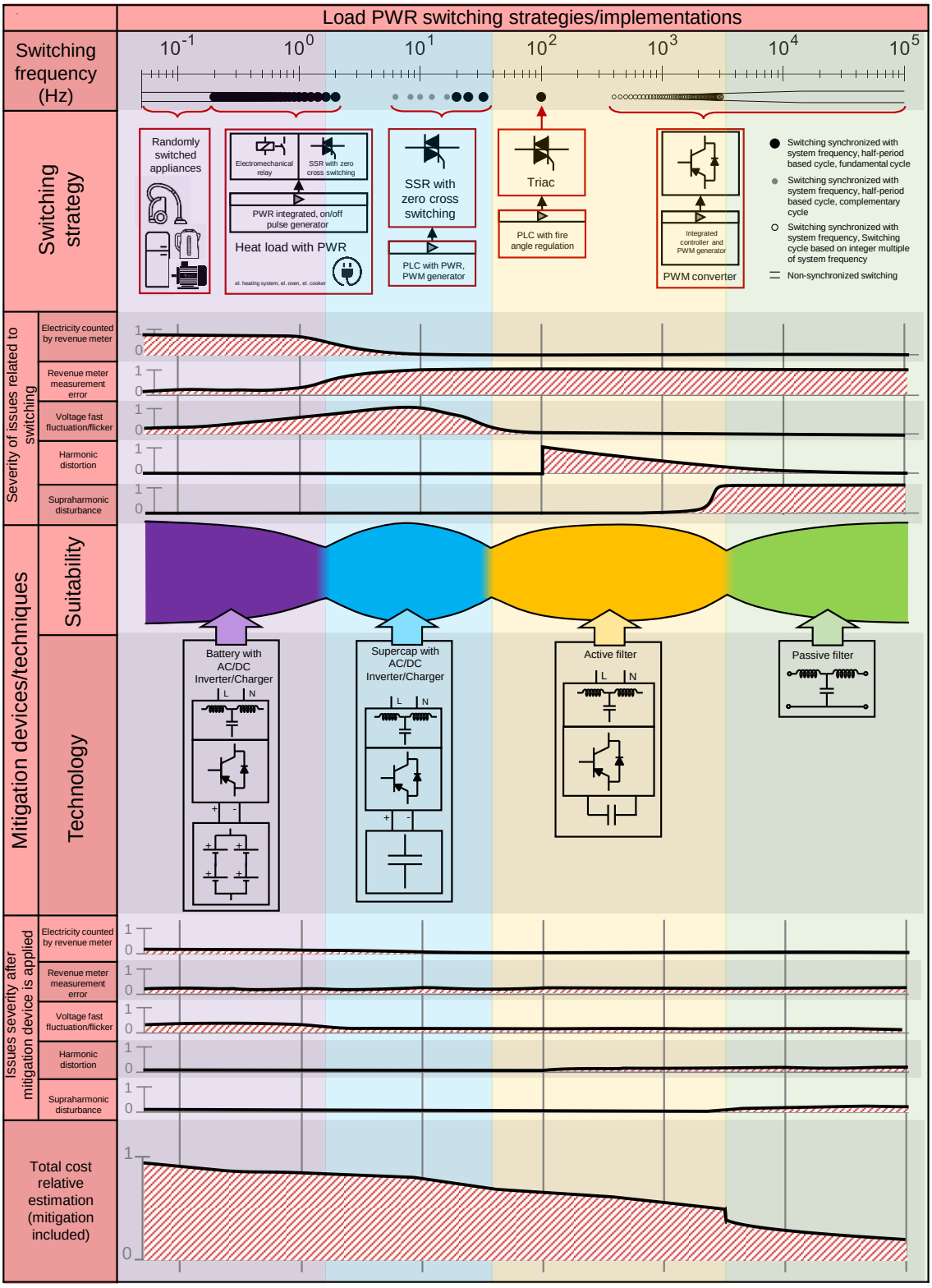

Fig. 3.4. EMC and energy metering oriented comparison of switching strategies [A4].

Whether in a household micro-grid or across an entire DS—depends on timely and physically consistent information about the energy flow being quantified using components of electrical power. Achieving the control goals, aligned definitions of power

components, algorithms and trusted synchronization is required. From perspective of power components definition, the authors in [17] show that aggregate kWh and period-averaged kvarh are too coarse for sub-second EMS decisions. They call for meters to provide real-time, sign-aware instantaneous active power and rolling energy integrals, plus directional components of reactive power. Distinguishing clearly between settlement quantities (kWh/kvarh) and control-oriented quantities (instantaneous, per phase, import/export) furnishes the EMS with actionable data.

3.4.1 Voltage Control in DS

DSOs face challenge with to voltage and reactive power-flow across feeders and distribution transformer substations (DTS). Within a single DTS, on-load tap changers, capacitor banks and inverter-based DERs are coordinated to maintain voltage and reactive power [A7], [A8]. Controllers require granularity and uncertainty at least equal to, and ideally better than, those used in the governing algorithms. Moreover, in the context of local voltage regulation, the definition of reactive power should be derived from the effect which reactive current component produces as it flows through a power line (Fig. 3.5).

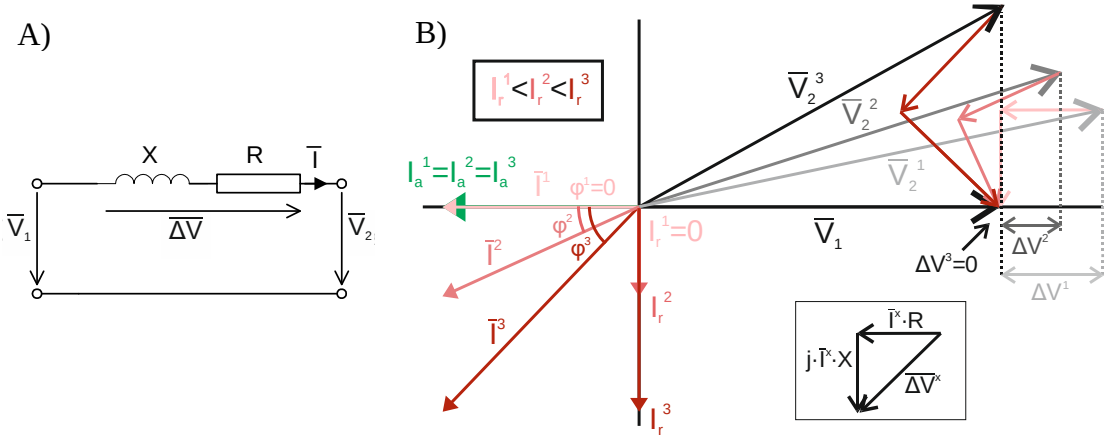

Fig. 3.5. Single phase power line model (A) and principle of voltage control using reactive power (B) [A7].

Voltage-control measurements at medium-voltage and higher levels are generally obtained from dedicated instrumentation—power-quality analyzers and other specialized metering units. Smart RMs, by contrast, furnish a densely distributed sensing network but with limited temporal resolution. Consequently, they are better suited to broad-scale monitoring and post-analysis that enhance grid visibility rather than to real-time voltage control.

3.5 Grid Analysis and Visibility

Reliable operation of a distribution grid depends on visibility and analyzes based on measurements of voltage and current quality and also measurements of power quality components. Such measurements make it possible not only to reconstruct events after

they occur, but also to predict impending deviations and intervene before faults or regulatory limits are breached. Moreover, network visibility enables the preparation of regular final reports and the monitoring of network conditions over time [5].

Typical metering devices used for measurement and registration of power components are:

- Power analyzers: relatively costly devices; deployed selectively where the potential damage from poor power and voltage quality outweighs measurement cost (PoC with industrial customers, complaint hot-spots, distribution transformers)
- Smart meters: deployed as part of mandated roll-outs; furnish a densely distributed sensing network but with limited temporal resolution, which enhance grid visibility diagnostics and analyses.

The devices monitoring power quality must comply with standards defining calculation algorithms and testing procedures specified in related standards (Tab. 3.2).

Tab. 3.2 Standards related to power quality monitoring.

Standard	Generic Power Monitors	Static Revenue Meters	Power Analyzers	External Power Meters
Voltage/Power quality measurement methods				
IEC 61000-4-7	X (optional)	X (optional)	✔	X (optional)
IEC 61000-4-30	X (optional)	X (optional)	✔	X
IEC 61000-4-15	X (optional)	X (optional)	✔	X
Methodology for application of measured quantities				
IEC 62586-1	X	X (optional)	✔	X

A denser network of measurement points—mostly smart meters and in combination with specialized measurements from power analyzers (or phasor measurement units – PMUs [49]) at strategic nodes—allows DSOs to apply the state estimation techniques to calculate voltage profiles and power flows with acceptable accuracy [50]. In turn, on-load tap changers, capacitor banks or battery storage can be suitably designed, placed, and even proactively controlled to keep voltage in statutory limits, e.g. due to dynamic high photovoltaic (PV) production. Although smart meters offer limited temporal granularity, they form a dense sensor network whose aggregated data reliably expose long-term trends and anomalies (persistent undervoltage, phase imbalance, steadily rising peak demand). Furthermore, the enhanced observability provided by state estimation allows operators to track, how power flow is loading individual network components. In addition, smart meters might continuously monitor that the droop characteristics—mandatory grid-

support functions required of distributed generators by the grid code (in EU defined by RfG [51] and national implementation, e.g. in the Czech Republic [52])—are functioning properly, although such metering data are not legally definitive.

4. POWER AND ENERGY COMPONENTS REVIEW

In static measuring units, the components of electrical energy are typically calculated from sampled phase current and voltage waveforms, obtained by digitizing continuous-time analog signals through the analog-to-digital (A/D) converters of the measurement front-end. The fundamental measured quantities are therefore sampled signals (n^{th} sample) of phase currents and voltages with a sampling period T_s:

$$v^{Lx}(t) \rightarrow v^{Lx}(nT_s) \text{ and}$$
$$i^{Lx}(t) \rightarrow i^{Lx}(nT_s).$$

By applying an appropriate filter to the input signals—either in the analog or digital stage of the measurement front-end—it is possible to obtain signals within the frequency band limited to the fundamental power system frequency f_1 (corresponding to the angular frequency ω_1). These signals represent the fundamental harmonic components of the measured phase voltage and current waveforms:

$$v_1^{Lx}(t) \rightarrow v_1^{Lx}(nT_s) \text{ and}$$
$$i_1^{Lx}(t) \rightarrow i_1^{Lx}(nT_s).$$

It should be noted that, in three-phase systems, the same fundamental frequency is assumed for all phases, implying an inherent coupling between them (e.g., the common shaft of three-phase rotating machines, or coupled bridge control in active front-ends).

The sampled digital signals can then be processed using algorithms for calculating the total RMS values of voltage and current ((4.1) and (4.6), respectively), as well as the RMS values of only the fundamental harmonics ((4.2) and (4.7), respectively) [19]. It is important to point out that, to suppress ripple caused by intermodulation, the number of samples within the RMS computation interval kT must be an integer multiple of the sampling period $kT/T_s \in N$), which in practice necessitates fundamental frequency ω_1 detection and resampling of the input signals. Another source of oscillations and measurement inaccuracy is the presence of interharmonic components in the signals. As demonstrated in [18] and [53], with a focus on subharmonics, the longer the measurement window (i.e., larger *k* in kT), the smaller the resulting error.

Although in practice the algorithms in static electricity meters are implemented in discrete form, all component definitions in this section are expressed in the continuous domain to maintain consistency with the definitions in relevant standards and literature.

From the calculated RMS values, it is further possible to derive the RMS values of the remaining harmonic and interharmonic components ((4.3) a (4.8), respectively), as well as the Total Harmonic Distortion (THD) index, which expresses the ratio of the energy contained in frequency components different to the fundamental harmonic frequency. This coefficient is widely used in power quality assessment. In practice, RMS values of the fundamental and other harmonics—particularly for power quality evaluation

[21]—are obtained using the Fourier transform (FT) algorithm. From the perspective of signal pre-processing, this is essentially the same procedure, since the FT is also evaluated over integer multiples of the fundamental period. When the FT is applied, the individual harmonic components of the signal are computed as phasors, meaning they possess both magnitude and phase angle. This allows for determining the phasors of the first harmonic voltages and currents, including their phase angles—so-called complex RMS quantities ((4.4) and (4.9), respectively).

Tab. 4.1 Voltage and current RMS fundamental components.

Component	**Symbol**	**Definition**	
RMS voltage	V^{Lx}	$V^{Lx} = \sqrt{\frac{1}{kT}\int_{\tau}^{\tau+kT} v^{Lx}(t)^2 \cdot dt}$	(4.1)
Fundamental RMS voltage	V_1^{Lx}	$V_1^{Lx} = \sqrt{\frac{1}{kT}\int_{\tau}^{\tau+T} v_1^{Lx}(t)^2 \cdot dt}$	(4.2)
Non-fundamental RMS voltage	V_H^{Lx}	$V_H^{Lx} = \sqrt{V^{Lx^2} - V_1^{Lx^2}}$	(4.3)
Fundamental RMS voltage phasor	$\underline{V_1^{Lx}}$	$\underline{V_1^{Lx}} = V_1^{Lx} \cdot e^{-j\delta_1^{Lx}}$	(4.4)
Total harmonic distortion of voltage	THD_V^{Lx}	$THD_V^{Lx} = \sqrt{\left(\frac{V^{Lx}}{V_1^{Lx}}\right)^2 - 1}$	(4.5)
RMS Current	I^{Lx}	$I^{Lx} = \sqrt{\frac{1}{kT}\int_{\tau}^{\tau+kT} i^{Lx}(t)^2 \cdot dt}$	(4.6)
Fundamental RMS Current	I_1^{Lx}	$I_1^{Lx} = \sqrt{\frac{1}{kT}\int_{\tau}^{\tau+kT} i_1^{Lx}(t)^2 \cdot dt}$	(4.7)
Non-fundamental RMS current	I_H^{Lx}	$I_H^{Lx} = \sqrt{I^{Lx^2} - I_1^{Lx^2}}$	(4.8)
Fundamental RMS current phasor	$\underline{I_1}^{Lx}$	$\underline{I_1}^{Lx} = I_1^{Lx} \cdot e^{-j\psi_1}$	(4.9)
Total harmonic distortion of current	THD_I^{Lx}	$THD_I^{Lx} = \sqrt{\left(\frac{I^{Lx}}{I_1^{Lx}}\right)^2 - 1}$	(4.10)

Furthermore, various transformations can be applied to the fundamental quantities, such as the Clarke transformation into stationary α-β coordinates or the Park transformation into the rotating *d*-*q* reference frame [54]. Tab. 4.2 presents the Fortescue transformation, i.e., the computation of voltage and current symmetrical components using the rotation operator $\underline{a} = 1e^{j\frac{2}{3}\pi}$ and the complex RMS values of the fundamental harmonics ((4.11) - (4.16)). The Fortescue transformation is applied specifically to the fundamental harmonic values due to its validity being restricted to sinusoidal waveforms, where only the fundamental positive-sequence component is meaningful to extract [55].

The symmetrical components of voltage and current are particularly useful for assessing voltage and current unbalance [23], as well as for calculating component-based powers [A9][A12].

Tab. 4.2 Symmetrical components of voltage and current.

Component	Symbol	Definition	
Positive sequence fundamental RMS voltage phasor	$\underline{V_1}^+$	$\underline{V_1}^+ = \frac{1}{3}\left(\underline{V_1}^{L1} + \underline{a} \cdot \underline{V_1}^{L2} + \underline{a}^2 \cdot \underline{V_1}^{L3}\right)$	(4.11)
Negative sequence fundamental RMS voltage phasor	$\underline{V_1}^-$	$\underline{V_1}^- = \frac{1}{3}\left(\underline{V_1}^{L1} + \underline{a}^2 \cdot \underline{V_1}^{L2} + \underline{a} \cdot \underline{V_1}^{L3}\right)$	(4.12)
Zero sequence fundamental RMS voltage phasor	$\underline{V_1}^0$	$\underline{V_1}^0 = \frac{1}{3}\left(\underline{V_1}^{L1} + \underline{V_1}^{L2} + \underline{V_1}^{L3}\right)$	(4.13)
Positive sequence fundamental RMS current phasor	$\underline{I_1}^+$	$\underline{I_1}^+ = \frac{1}{3}\left(\underline{I_1}^{L1} + \underline{a} \cdot \underline{I_1}^{L2} + \underline{a}^2 \cdot \underline{I_1}^{L3}\right)$	(4.14)
Negative sequence fundamental RMS current phasor	$\underline{I_1}^-$	$\underline{I_1}^- = \frac{1}{3}\left(\underline{I_1}^{L1} + \underline{a}^2 \cdot \underline{I_1}^{L2} + \underline{a} \cdot \underline{I_1}^{L3}\right)$	(4.15)
Zero sequence fundamental RMS current phasor	$\underline{I_1}^0$	$\underline{I_1}^0 = \frac{1}{3}\left(\underline{I_1}^{L1} + \underline{I_1}^{L2} + \underline{I_1}^{L3}\right)$	(4.16)

For completeness, [18] defines the equivalent RMS values of voltage and current in three-phase systems, i.e., the values that would produce the same power losses under ideal transmission conditions—namely, balanced power transfer with voltage and current waveforms containing only the fundamental harmonic. The definitions of voltage and current are provided both for the total RMS values ((4.18) and (4.21), respectively) and for the RMS values of the fundamental harmonic only ((4.17) and (4.20), respectively).

The relationships are first defined in general form for three-phase (four-wire) networks, including the coefficients ζ (expressing the ratio between the resistance of the phase conductors and that of the neutral conductor), κ_h (accounting for the skin effect and proximity effect of the conductors for harmonic h), and ρ_h (expressing the ratio of conductor resistances for harmonic h). A detailed description of these coefficients can be found in [18]. In practice, these coefficients are specific parameters of the actual conductors in the real system; however, their determination is often challenging.

Therefore, the definitions of equivalent RMS values are often approximated for the case where the coefficients are unknown, by assuming $\zeta = 1$, $\kappa_h = 1$ a $\rho_h = 1$.

Tab. 4.3 Equivalent RMS components of voltage and current in three-phase systems.

Equivalent fundamental RMS L-N voltage	V_1^e	$V_1^e = \sqrt{\frac{3\left(V_1^{L1^2} + V_1^{L2^2} + V_1^{L3^2}\right) + \zeta\left(V_1^{L12^2} + V_1^{L23^2} + V_1^{L31^2}\right)}{9(1+\zeta)}}$ $V_1^e \approx \sqrt{\frac{3\left(V_1^{L1^2} + V_1^{L2^2} + V_1^{L3^2}\right) + \left(V_1^{L12^2} + V_1^{L23^2} + V_1^{L31^2}\right)}{18}}$	(4.17)
Equivalent RMS L-N voltage	V^e	$V^e = \sqrt{\frac{3\left(V^{L1^2} + V^{L2^2} + V^{L3^2}\right) + \zeta\left(V^{L12^2} + V^{L23^2} + V^{L31^2}\right)}{9(1+\zeta)}}$ $V^e \approx \sqrt{\frac{3\left(V^{L1^2} + V^{L2^2} + V^{L3^2}\right) + \left(V^{L12^2} + V^{L23^2} + V^{L31^2}\right)}{18}}$	(4.18)

Equivalent harmonic RMS L-N voltage	V_H^e	$V_H^e = \sqrt{(V^e)^2 - (V_1^e)^2}$	(4.19)
Equivalent fundamental RMS current	I_1^e	$I_1^e = \sqrt{\frac{{I_1^{L1}}^2 + {I_1^{L2}}^2 + {I_1^{L3}}^2 + \rho_1 {I_1^N}^2}{3}}$ $I_1^e \approx \sqrt{\frac{{I_1^{L1}}^2 + {I_1^{L2}}^2 + {I_1^{L3}}^2 + {I_1^N}^2}{3}}$	(4.20)
Equivalent RMS current	I^e	$I^e = \sqrt{\frac{\sum_{h=1}^{H}\left[\kappa_h\left({I_h^{L1}}^2 + {I_h^{L2}}^2 + {I_h^{L3}}^2\right) + \rho_h {I_h^N}^2\right]}{3}}$ $I^e \approx \sqrt{\frac{{I^{L1}}^2 + {I^{L2}}^2 + {I^{L3}}^2 + {I^N}^2}{3}}$	(4.21)
Equivalent harmonic RMS current	I_H^e	$I_H^e = \sqrt{(I^e)^2 - (I_1^e)^2}$	(4.22)

4.1 Single Phase Definitions

In [18], the power components that can theoretically be computed from voltage and current waveforms are defined. For the purposes of this work, these components are grouped according to a physical–practical criterion, specifically based on the type of energy exchange they describe within the system. The classification adopted in this thesis is as follows.

- Active powers – quantities expressing the rate of transfer of active (watthour) energy, which is demonstrably converted into another form of energy (e.g., mechanical energy, heat, etc.).
- Apparent powers – quantities representing the theoretical maximum active power that could be transferred by voltage and current of given RMS values under ideal conditions (i.e., in-phase sinusoidal voltage and current waveforms).
- Reactive powers – quantities characterizing the exchange of non-active energy (with zero average value in the computation interval) between the reactive elements of the DS (e.g., inductors, capacitors).
- Distortion powers – quantities describing the exchange of non-active energy arising from voltage and current waveform distortion due to harmonic components.
- Non-active power –quantity describing general non-active energy exchange.

Fig. 4.1 illustrates the relationship between selected single-phase components based on [18], with the components grouped according to the above classification.

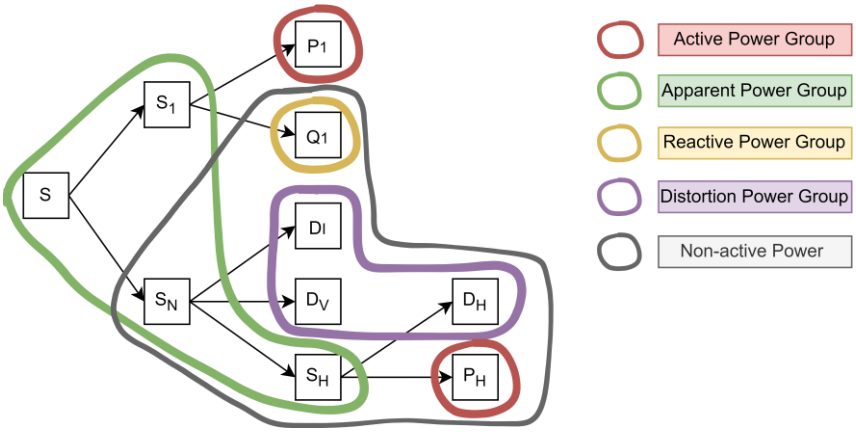

Fig. 4.1. Relation of power components in single-phase system [18].

4.1.1 Active Power Group

Active (watt) power generally expresses the rate of transfer of active energy and represents the portion of energy that is demonstrably converted into another form of energy (4.23). By definition, it is the portion of the instantaneous power that does not average to zero. The theory presented in [18] further distinguishes between the active power transferred by the fundamental harmonic components of voltage and current (4.24) and the active power transferred by higher-order harmonic components of voltage and current, i.e., by voltage–current pairs of the same harmonic order (4.25).

Specifically in the context of revenue metering, the selection of a particular power definition is critically examined in [56], where the author highlights an implicit consequence of (4.25). This definition, which relies on measuring power associated only with fundamental frequency components (4.24), inherently penalizes sites emitting harmonic distortion due to nonlinear loads—by yielding a higher measured value—when compared to definition (4.23). Conversely, it favors (or "rewards") sites with linear loads operating under distorted supply voltages, as it results in a lower measured value. Consequently, (4.24) is considered more equitable and potentially incentivizing for operating linear loads, as it aligns the measurement outcome with the nature of the consumed load rather than the voltage quality.

However, the practical difference between the power values computed using (4.23) and (4.24) at a site generating harmonics is significantly influenced by the local connection impedance. As a result, the perceived fairness—based on the discrepancy between these two power definitions—becomes a function of the customer's distance from the source (e.g., MV/LV transformer) in low-voltage networks. Since end-users have no control over their PoC to the grid, this introduces a structural inequality: customers located closer to the supply point, with lower connection impedances, are systematically favored in the measurement process. Thus, the concept of fairness in power metering should also account for this infrastructural dependency.

Tab. 4.4. Active power components – single-phase definitions.

Component	Symbol	Definition	
Active power	P^{Lx}	$P^{Lx} = \frac{1}{kT}\int_{\tau}^{\tau+kT} v^{Lx}(t) i^{Lx}(t) \cdot dt$	(4.23)
Fundamental active power	P_1^{Lx}	$P_1^{Lx} = \frac{1}{kT}\int_{\tau}^{\tau+kT} v_1^{Lx}(t) i_1^{Lx}(t) \cdot dt$ $P_1^{Lx} = V_1^{Lx} \cdot I_1^{Lx} \cdot \cos(\psi_1 - \delta_1)^{Lx}$ $P_1^{Lx} = V_1^{Lx} \cdot I_1^{Lx} \cdot \cos(\varphi_1)^{Lx}$	(4.24)
Harmonic Active Power	P_H^{Lx}	$P_H^{Lx} = P^{Lx} - P_1^{Lx}$	(4.25)

4.1.2 Apparent Power Group

The concept of apparent power represents the theoretical maximum active power that could be transferred by voltage and current of given RMS values under ideal conditions (i.e., in-phase sinusoidal voltage and current waveforms)—while causing the same power losses in the upstream DS (neglecting skin-effect). It therefore describes the power transfer potential of the supply system and serves as a measure of effectiveness in active energy transfer.

According to [18] (Fig. 4.1), under harmonically distorted voltage and current waveforms (4.26), apparent power can be further decomposed into fundamental apparent power (4.27), representing the ineffectiveness due to the phase displacement between the fundamental voltage and current waveforms, and harmonic apparent power (4.28), which represents the ineffectiveness in transferring active power to nonlinear loads.

For completeness, the complex power (4.29) is also provided, defined as the product of the fundamental voltage and current phasors, with the current phasor taken as the complex conjugate. From a practical perspective, complex power is primarily a mathematical construct used in subsequent calculations assuming quasi-steady-state conditions.

Finally, harmonic apparent power (4.30) describes the energy exchange exclusively associated with non-fundamental harmonic components of voltage and current. This component can also be expressed as the sum of product of non-fundamental harmonic voltage and current components of both equal and different order (Annex B [18]) and can be further decomposed into active and non-active parts.

Tab. 4.5 Apparent power components – single-phase definitions.

Component	Symbol	Definition	
Apparent power	S^{Lx}	$S^{Lx} = V^{Lx} \cdot I^{Lx}$	(4.26)
Fundamental apparent power	S_1^{Lx}	$S_1^{Lx} = V_1^{Lx} \cdot I_1^{Lx}$	(4.27)
Nonfundamental apparent power	S_N^{Lx}	$S_N^{Lx} = \sqrt{(S^{Lx})^2 - (S_1^{Lx})^2}$	(4.28)
Complex power	$\underline{S_1}^{Lx}$	$\underline{S_1}^{Lx} = \underline{V_1}^{Lx} \cdot \left(\underline{I_1}^{Lx}\right)^* = P_1^{Lx} + jQ_1^{Lx}$	(4.29)
Harmonic apparent power	S_H^{Lx}	$S_H^{Lx} = \sqrt{(P_H^{Lx})^2 + (D_H^{Lx})^2}$	(4.30)

4.1.3 Reactive Power Group

Reactive power can be a useful quantity for following purposes.

1. Quantifying system losses arising from the operation of reactive loads, i.e., the injection of current that is not in-phase with voltage waveform.
2. Determining the required capacity of passive compensation equipment designed to offset the reactive current of loads and system reactive elements.
3. Quantifying the power that effectively contributes to voltage control in devices actively involved in voltage regulation within distribution networks [A7], [A8].

Annex D of IEC 61557-12 [19] specifies two approaches for calculating reactive power: the quadrature-phase-shift method applied to one of the signals (4.31) and the direct summation of the reactive powers of all harmonic components according to Budeanu (4.32). However, Annex A [18] states that both definitions may be misleading in the case of waveforms with significant harmonic distortion, since applying these definitions to distorted signals systematically (and mathematically provably) may lead to mutual cancellation of the contributions from individual harmonic components.

Therefore, [18] recommends defining reactive power solely for the fundamental harmonic (4.33) – (4.35), which is also consistent with the use of the reactive power component as described in points 2) and 3) of the preceding paragraph. While this definition does not represent a measure of the overall inefficiency of energy transfer (i.e., it is not the geometric complement of active power to apparent power—other components serve this purpose), it enables the practical isolation of the portion of non-active power that is relevant for voltage control in power networks and for quantifying the required capacity of passive compensators for the reactive current of reactive loads.

Although definition derived from varmeters (4.33) (and, similarly, (4.34)) is shown in Annex A [18] to be potentially misleading when applied to distorted signals, it remains valid when only the fundamental harmonic components v_1^{Lx} a i_1^{Lx} are considered for calculating Q_1^{Lx}. In the frequency domain, the relationship given in (4.35) can be also employed for this purpose, if the voltage and current RMS components are calculated among the same interval kT.

Tab. 4.6 Reactive power components – single-phase definitions.

Component	**Symbol**	**Definition**	
Quadrature-shift definition of reactive power	Q^{Lx}	$Q^{Lx} = \frac{1}{kT}\int_{\tau}^{\tau+kT} v^{Lx}(t) \cdot i^{Lx}\left(t - \frac{T}{4}\right) \cdot dt$	(4.31)
Budenau's reactive power	Q^{Lx}	$Q^{Lx} = \sum_{h=1}^{H} V_h^{Lx} \cdot I_h^{Lx} \cdot \sin\varphi_h^{Lx}$	(4.32)
Fundamental reactive power	Q_1^{Lx}	$Q_1^{Lx} = \frac{-1}{kT\omega_1}\int_{\tau}^{\tau+kT} i_1^{Lx}(t)[\int v_1^{Lx}(t) \cdot dt] \cdot dt$	(4.33)
		$Q_1^{Lx} = \frac{\omega_1}{kT}\int_{\tau}^{\tau+kT} i_1^{Lx}(t) \cdot \frac{dv_1^{Lx}(t)}{dt} \cdot dt$	(4.34)
		$Q_1^{Lx} = V_1^{Lx} \cdot I_1^{Lx} \cdot \sin\varphi_1^{Lx}$	(4.35)

4.1.4 Distortion Power Group

The distortion power describes an exchange of energy that is oscillatory in nature, non-active (its average value over the measurement period is zero), and arises due to the presence of voltage and current harmonics of mutually exclusive orders. As discussed in [18], distortion power can be further classified according to its origin 1) fundamental voltage and non-fundamental current harmonics (4.36), 2) fundamental current and non-fundamental voltage harmonics (4.37), and 3) non-fundamental harmonic components only (4.38).

Tab. 4.7 Distortion power components – single-phase definitions.

Component	**Symbol**	**Definition**	
Current distortion power	D_I^{Lx}	$D_I^{Lx} = V_1^{Lx} \cdot I_H^{Lx}$	(4.36)
Voltage distortion power	D_V^{Lx}	$D_V^{Lx} = V_H^{Lx} \cdot I_1^{Lx}$	(4.37)
Harmonic distortion power	D_H^{Lx}	$D_H^{Lx} = V_H^{Lx} \cdot I_H^{Lx}$	(4.38)

4.1.5 Other Non-active Power Components

In this work, the term “other non-active power components” refers to components that either combine multiple previously defined power terms—thus not distinguishing between their individual origins—or partially or fully overlap with existing definitions in terms of their physical meaning. For example, Annex D of [19] presents an expression for reactive power based on the power triangle approach, also referred to as the geometrical (complementary) method (4.39). However, as discussed in section 4.1.3, the definition of reactive power in [18] is restricted to the fundamental frequency component only. Consequently, the given formulation for reactive power is valid solely under ideal sinusoidal conditions of voltage and current waveforms. Under non-sinusoidal conditions, it should instead be interpreted more generally as a non-active power component.

Furthermore, under harmonic distortion, there arises an issue concerning the sign of the reactive power, since the sign convention is typically used to distinguish the nature of the reactive power—i.e., whether the corresponding current is inductive or capacitive (based on the theoretical behavior of an inductor or capacitor in the presence of harmonic voltage). In the presence of multiple harmonic components, this interpretation becomes ambiguous, as (4.39) does not clearly specify which harmonic orders should be considered when evaluating the initial phase angles. In practice, it is reasonable to consider the initial phase angles of the fundamental components of current and voltage (denoted as δ_1^{Lx} and ψ_1^{Lx}, respectively). However, if only these angles are used, the meaning of the magnitude of the resulting component does not correspond directly to the physical meaning of its polarity.

Although the definition provided in (4.39) is not practically suitable for quantifying the need for reactive load compensation or voltage control, it does, in general, quantify a portion of power associated with the inefficient transfer of active energy. In this context, the definition may still be useful for assessing non-effective active energy transfer. In [18], this component is referred to as non-active power, defined without regard to its sign, and is formulated in (4.40) accordingly.

Tab. 4.8 Other non-active power components – single-phase definitions.

Component	Symbol	Definition	
Signed non-active power	N^{Lx}	$N^{Lx} = T \cdot \sqrt{(S^{Lx})^2 - (P^{Lx})^2}$ $T = +1$ if $\left(\delta^{Lx} - \psi^{Lx}\right) \in (0° - 180°)$ $T = -1$ if $\left(\delta^{Lx} - \psi^{Lx}\right) \in (180° - 360°)$	(4.39)
Unsigned non-active power	N^{Lx}	$N^{Lx} = \sqrt{(S^{Lx})^2 + (P^{Lx})^2}$	(4.40)

4.1.6 Quality Indicators of Active Energy Transfer

For completeness, [18] also introduces indicators of active power transfer quality, commonly referred to as power factors. A generalized definition is provided in (4.41), which expresses the ratio of active power to apparent power. This ratio reflects the portion of total power that is effectively converted into useful work, or alternatively, it quantifies the proportion of total loading (and associated losses) in the DS that is inherently required for the transmission of active energy in the ideal case and actual loading (and associated losses). Equation (4.42) presents a similar concept, but considers only the ineffectiveness caused by reactive power due to inductive or capacitive loads. Finally, Eq. (4.43) quantifies the ratio between the apparent power associated with harmonic components and that of the fundamental frequency. This indicator serves as a measure of the degree to which harmonic distortion affects the energy transfer across the point of measurement.

Tab. 4.9 Quality indicators of energy transfer – single-phase definitions.

Indicator	Symbol	Definition	
Power Factor	PF^{Lx}	$PF^{Lx} = \frac{P^{Lx}}{S^{Lx}}$	(4.41)
Fundamental power factor	PF_1^{Lx}	$PF_1^{Lx} = \frac{P_1^{Lx}}{S_1^{Lx}}$	(4.42)
Harmonic pollution factor	PF_H^{Lx}	$PF_H^{Lx} = \frac{S_N^{Lx}}{S_1^{Lx}}$	(4.43)

4.2 Three Phase Definitions

The preceding section introduced the definitions of electrical power components in single-phase systems. In this section, these definitions are extended—primarily following the framework proposed in [18]—to include components applicable to measurements in three-phase systems. The components are categorized into the same groups of power

quantities as in section 4.1, maintaining consistency in classification.

4.2.1 Active Power Group

In a three-phase four-wire system, the active power can be determined as the sum of the phase powers—either based on the total instantaneous powers (4.44) or restricted to the fundamental frequency components only (4.45). In both cases, the resulting active power corresponds to the average energy transferred through the point of measurement over the observation period kT, averaged across all three phases (L1–L3).

Furthermore, [18] defines the active power associated with the symmetrical components of voltage and current—specifically, the powers of the positive-sequence, negative-sequence, and zero-sequence components, given in (4.46), (4.47) and (4.48), respectively. The author in [56] argues that, particularly for billing applications, the measurement of active power associated with the positive-sequence components (4.46) is more equitable and potentially incentivizes end-users in DSs to operate their loads more symmetrically across phases.

Although this fairness argument is subject to the same limitations discussed in Section 4.1.1—namely, that it does not account for the impact of the customer's connection impedance—the concept of measuring symmetrical component powers is further developed in [A9]. There, the use of symmetrical components is explored in the context of bidirectional energy flows, with a focus on their ability to indicate power losses caused by unbalanced power exchange in the upstream DS (see also section 6.4). In [A12], the relevance of symmetrical component is further demonstrated as an indicator of bidirectional energy flow in the context of realistic prosumer behavior, particularly with respect to achieving energy self-sufficiency in microgrids (see also section 8).

Tab. 4.10 Active power components – three-phase definitions.

Component	**Symbol**	**Definition**	
Three phase active power	P	$P = \frac{1}{kT}\int_{\tau}^{\tau+kT}[v^{L1}(t)i^{L1}(t) + v^{L2}(t)i^{L2}(t) + v^{L3}(t)i^{L3}(t)] \cdot dt$ $P = P^{L1} + P^{L2} + P^{L3}$	(4.44)
Three phase fundamental active power	P_1	$P_1 = \frac{1}{kT}\int_{\tau}^{\tau+kT}[v_1^{L1}(t)i_1^{L1}(t) + v_1^{L2}(t)i_1^{L2}(t) + v_1^{L3}(t)i_1^{L3}(t)] \cdot dt$ $P_1 = P_1^{L1} + P_1^{L2} + P_1^{L3}$	(4.45)
Three phase positive sequence fundamental active power	P_1^+	$P_1^+ = 3 \cdot \lvert\underline{V}_1^+\rvert \cdot \lvert\underline{I}_1^+\rvert \cdot \cos\varphi_1^+$	(4.46)
Three phase negative sequence fundamental active power	P_1^-	$P_1^- = 3 \cdot \lvert\underline{V}_1^-\rvert \cdot \lvert\underline{I}_1^-\rvert \cdot \cos\varphi_1^-$	(4.47)
Three phase negative sequence fundamental active power	P_1^0	$P_1^0 = 3 \cdot \lvert\underline{V}_1^0\rvert \cdot \lvert\underline{I}_1^0\rvert \cdot \cos\varphi_1^0$	(4.48)

4.2.2 Apparent Power Group

As in the single-phase case, the apparent power in a three-phase four-wire system reflects the efficiency of active power transfer. However, in three-phase systems, inefficiencies in active power transmission arise not only from reactive currents and harmonic components, but also from asymmetrical loading. In other words, when the transfer of active energy is unbalanced across the phases, the phase conductors and the neutral conductor are more heavily loaded compared to a scenario in which the same amount of active energy is transmitted symmetrically.

Not all definitions in [18] account for this type of inefficiency. For instance, the definition based on the arithmetic sum of the phase-wise apparent powers—as given in (4.49), and in (4.51) for the fundamental components—does not reflect whether the energy is being transferred symmetrically or not. Similarly, the definition based on the vector sum of the phase powers—as in (4.50) and (4.52) for the fundamental components—also ignores the symmetry of energy transfer. Moreover, this vector-sum formulation allows for the mutual compensation of reactive power between phases: for example, if one phase exhibits capacitive behavior and another inductive, the resulting reactive powers may partially or even fully cancel out. This is problematic from a physical standpoint, as real currents still flow through the conductors and contribute to energy losses. Both the arithmetic and vectorial definitions of apparent power are considered conceptually outdated in [18].

In contrast, the effective apparent power defined in (4.53) (and (4.54) for the fundamental frequency) does account for the inefficiencies caused by unbalanced energy transfer. According to the derivation in [18], this formulation quantifies the losses in a four-wire system attributable to asymmetrical energy flow. Analogously to the single-phase case, a harmonic effective apparent power is also defined in (4.55).

Furthermore, [18] introduces apparent power definitions based on the symmetrical components of current and voltage ((4.57)-(4.59)), though these apply only to the fundamental frequency. In addition, a so-called unbalanced apparent power is defined (4.60).

In addition to the definitions presented above, the literature provides further formulations of apparent power, which are associated with specific, purpose-driven interpretations and conceptually overlap with the aforementioned definitions. For instance, [58] introduces the definition of asymmetrical power to determine an asymmetry coefficient as part of power quality assessment.

Tab. 4.11 Apparent power components – three-phase definitions.

Component	Symbol	Definition	
Fundamental arithmetic apparent power	S^A	$S^A = S^{L1} + S^{L2} + S^{L3}$	(4.49)
Fundamental vector apparent power	S^V	$S^V = \left\lvert P^{L1} + P^{L2} + P^{L3} + j(Q^{L1} + Q^{L2} + Q^{L3}) \right\rvert$	(4.50)
Fundamental arithmetic apparent power	S_1^A	$S_1^A = S_1^{L1} + S_1^{L2} + S_1^{L3}$	(4.51)
Fundamental vector apparent power	S_1^V	$S_1^V = \lvert P_1^{L1} + P_1^{L2} + P_1^{L3} + j(Q_1^{L1} + Q_1^{L2} + Q_1^{L3}) \rvert$	(4.52)
Effective fundamental apparent power	S_1^e	$S_1^e = 3 \cdot V_1^e \cdot I_1^e$	(4.53)
Effective apparent power	S^e	$S^e = 3 \cdot V^e \cdot I^e$	(4.54)
Harmonic apparent power	S_H^e	$S_H^e = 3 \cdot V_H^e \cdot I_H^e$	(4.55)
Nonfundamental effective apparent power	S_N^e	$S_N^e = \sqrt{(S^e)^2 - (S_1^e)^2}$	(4.56)
Three phase positive sequence fundamental apparent power	S_1^+	$S_1^+ = 3 \cdot \left\lvert \underline{V}_1^+ \right\rvert \cdot \left\lvert \underline{I}_1^+ \right\rvert$	(4.57)
Three phase negative sequence fundamental apparent power	S_1^-	$S_1^- = 3 \cdot \left\lvert \underline{V}_1^- \right\rvert \cdot \left\lvert \underline{I}_1^- \right\rvert$	(4.58)
Three phase negative sequence fundamental apparent power	S_1^0	$S_1^0 = 3 \cdot \left\lvert \underline{V}_1^0 \right\rvert \cdot \left\lvert \underline{I}_1^0 \right\rvert$	(4.59)
Unbalanced power	S_1^U	$S_1^U = \sqrt{(S_1^e)^2 - (S_1^+)^2}$	(4.60)

4.2.3 Reactive Power

According to [18], the reactive power in a three-phase system can be calculated as the sum of the phase-wise reactive powers—generally as defined in (4.61), or restricted to the fundamental frequency in (4.62). However, a notable limitation of (4.62) is that it does not distinguish the actual need for reactive power compensation in each individual phase when the character of the reactive power differs between phases. When using Q_1 for compensation in such scenarios, it is highly likely that, although the total reactive power Q_1 may be reduced to zero, reactive power will still be present in the individual phases. As a result, despite the reactive power compensation, reactive currents will continue to flow in the upstream DS, contributing to conductor loading and additional losses. As such, the total three-phase value Q_1 may be inadequate for voltage control in networks where phase-wise differences in reactive behavior are common, such as in LV DS.

For completeness, [18] also defines the reactive powers of the symmetrical components of the fundamental currents and voltages, as presented in (4.63)-(4.65).

Together with the corresponding symmetrical components of active and apparent power, these quantities form a power triangle.

Tab. 4.12 Reactive power components – three-phase definitions.

Component	Symbol	Definition	
Three phase reactive power	Q	$Q \quad = Q^{L1} + Q^{L2} + Q^{L3}$	(4.61)
Three phase fundamental reactive power	Q_1	$Q_1 = Q_1^{L1} + Q_1^{L2} + Q_1^{L3}$	(4.62)
Three phase positive sequence fundamental active power	Q_1^+	$Q_1^+ = 3 \cdot \left\|\underline{V_1}^+\right\| \cdot \left\|\underline{I_1}^+\right\| \cdot sin\varphi_1^+$	(4.63)
Three phase negative sequence fundamental active power	Q_1^-	$Q_1^- = 3 \cdot \left\|\underline{V_1}^-\right\| \cdot \left\|\underline{I_1}^-\right\| \cdot sin\varphi_1^-$	(4.64)
Three phase negative sequence fundamental active power	Q_1^0	$Q_1^0 = 3 \cdot \left\|\underline{V_1}^0\right\| \cdot \left\|\underline{I_1}^0\right\| \cdot sin\varphi_1^0$	(4.65)

4.2.4 Distortion Power Group

Distortion powers in three-phase systems are defined in [18] in a manner analogous to the single-phase case presented in section 4.1.4 ((4.66)-(4.67)). These powers are formulated based on equivalent RMS values, which inherently account for the inefficiencies associated with asymmetrical energy flows caused by harmonic components.

Tab. 4.13 Distortion power components – three-phase definitions.

Component	Symbol	Definition	
Current distortion power	D_I^e	$D_I^e = 3V_1^e I_H^e$	(4.66)
Voltage distortion power	D_V^e	$D_V^e = 3V_H^e I_1^e$	(4.67)
Harmonic distortion power	D_H^e	$D_H^e = \sqrt{(S_H^e)^2 - (P_H^e)^2}$	(4.68)

4.2.5 Other Non-active Power Components Group

The non-active power is defined in [18] by (4.69). This definition does not account for inefficiencies arising from asymmetrical utilization of the three-phase network.

Tab. 4.14 Other non-active power components – three-phase definitions.

Component	Symbol	Definition	
Three phase non-active power	N	$N = N^{L1} + N^{L2} + N^{L3}$	(4.69)

4.2.6 Quality Indicators of Active Energy Transfer

In [18], a total power factor for three-phase systems is defined as (4.70), which accounts

for all sources of inefficiency that may arise during power transmission due to the operation of unbalanced, reactive, and nonlinear loads. This definition reflects the combined effects of asymmetry, reactive power, and voltage and current waveforms distortion. The fundamental positive-sequence power factor, defined in Eq. (4.71), carries the same interpretation as the fundamental power factor in the context of single-phase systems. The unbalance power factor might be defined as (4.72) in order to quantify the asymmetry in the point of measurement.

Tab. 4.15 Quality indicators of energy transfer – three-phase definitions.

Indicator	**Symbol**	**Definition**	
Power factor	PF	$PF = \frac{P}{S_e}$	(4.70)
Fundamental positive-sequence power factor	PF_1^+	$PF_1^+ = \frac{P_1^+}{S_1^+}$	(4.71)
Unbalance power factor	PF^U	$PF^U = \frac{S_1^U}{S_1^+}$	(4.72)

4.3 Sorting of Power Components

In addition to the power components jointly defined as part of a specific power theory (previous sections), the direction of active power and the nature of reactive power—based on the behavior of passive reactive elements under sinusoidal voltage—are typically distinguished for two main purposes: 1) energy billing and settlement, and 2) power quality monitoring (e.g., power factor assessment). This distinction introduces a binary classification criterion applied to the basic definitions of these power components. As a result, the components are mapped into a complex plane, where the active and reactive powers are is represented along the axes [26]. The resulting point's position in this plane (Fig. 4.2), defined by its coordinates (i.e., the active and reactive power components), determines its radial distance from the origin, which corresponds to the apparent power. The interpretation of this magnitude depends on the specific definitions of active and reactive power employed, as discussed in sections 4.1.2 and 4.2.2.

Fig. 4.2 illustrates that, for the purpose of network analysis based on measured quantities, it is beneficial to select definitions of active and reactive power in such a way that the geometrically derived apparent power aligns with one of the formally defined concepts in sections 4.1.2 and 4.2.2. For instance, in analytical tools that apply state estimation algorithms based on complex phasors at the fundamental frequency, it is natural to consistently adopt power components defined exclusively at the fundamental harmonic.

The complex power plane is further divided into four quadrants, Q1 through Q4. The components assigned to these quadrants represent an additional layer of classification built upon the foundational definitions of power components introduced in sections 4.1 and 4.2. This quadrant-based interpretation provides the conceptual basis for the Object

Identification System (OBIS), which defines a standardized set of codes used to uniquely identify data items within the DLMS/COSEM communication protocol [37].

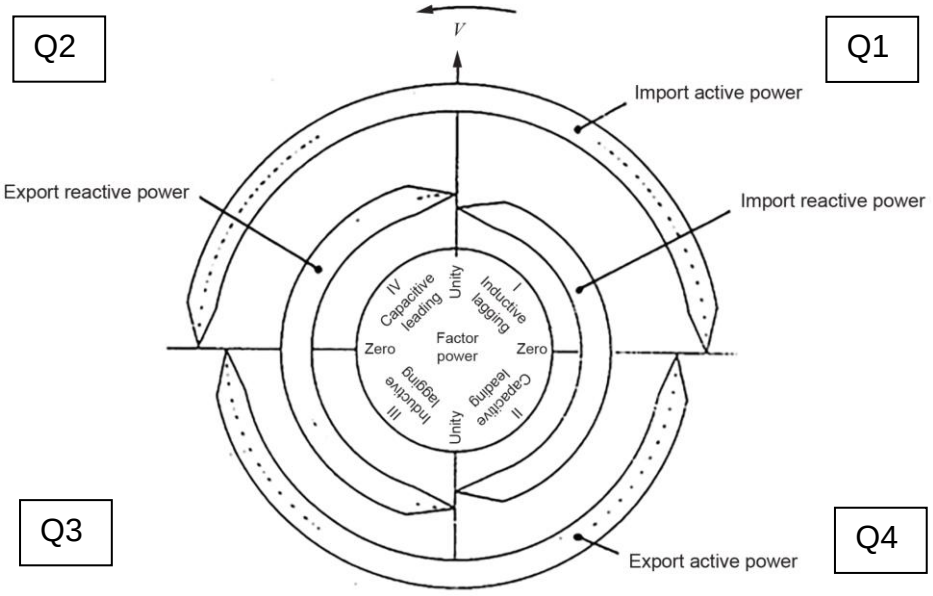

Fig. 4.2: Four-quadrant representation of energy flow directions [26].

The components represented in the complex power plane ((4.73) - (4.77)) are denoted in a generalized form in the summary Tab. 4.16, since—in principle—all definitions of active and reactive power that assign both direction and character to the quantities can be mapped to the corresponding quadrants. Active power is classified according to its direction, distinguishing between import and export (denoted $P^{y_P}_{z_P,imp}$ and $P^{y_P}_{z_P,imp}$, respectively), while reactive power components are explicitly assigned to specific quadrants: $Q^{y_Q}_{z_Q,1Q}$, $Q^{y_Q}_{z_Q,2Q}$, $Q^{y_Q}_{z_Q,3Q}$, $Q^{y_Q}_{z_Q,4Q}$, corresponding to Q1 through Q4.

Tab. 4.16. Sorting of power components based on position in complex plane [37].

Component	**Symbol**	**Definition**	
Imported active power	$P^{y_P}_{z_P,imp}$	$P^{y_P}_{z_P,imp} = \begin{cases} \lvert P^{y_P}_{z_P}\rvert & if \quad P^{y_P}_{z_P} \geq 0 \\ 0 & if \quad P^{y_P}_{z_P} < 0 \end{cases}$	(4.73)
Exported active power	$P^{y_P}_{z_P,exp}$	$P^{y_P}_{z_P,exp} = \begin{cases} \lvert P^{y_P}_{z_P}\rvert & if \quad P^{y_P}_{z_P} \leq 0 \\ 0 & if \quad P^{y_P}_{z_P} > 0 \end{cases}$	(4.74)
1st quadrant reactive power	$Q^{y_Q}_{z_Q,1Q}$	$Q^{y_Q}_{z_Q,1Q} = \begin{cases} \lvert Q^{y_Q}_{z_Q}\rvert & if \quad Q^{y_Q}_{z_Q} \geq 0 \wedge P^{y_P}_{z_P} \geq 0 \\ 0 & if \quad otherwise \end{cases}$	(4.75)
2nd quadrant reactive power	$Q^{y_Q}_{z_Q,2Q}$	$Q^{y_Q}_{z_Q,2Q} = \begin{cases} \lvert Q^{Lx}_1\rvert & if \quad Q^{y_Q}_{z_Q} \geq 0 \wedge P^{y_P}_{z_P} < 0 \\ 0 & if \quad otherwise \end{cases}$	(4.76)
3rd quadrant reactive power	$Q^{y_Q}_{z_Q,3Q}$	$Q^{y_Q}_{z_Q,3Q} = \begin{cases} \lvert Q^{Lx}_1\rvert & if \quad Q^{y_Q}_{z_Q} < 0 \wedge P^{y_P}_{z_P} < 0 \\ 0 & if \quad otherwise \end{cases}$	(4.77)
4th quadrant reactive power	$Q^{y_Q}_{z_Q,4Q}$	$Q^{y_Q}_{z_Q,4Q} = \begin{cases} \lvert Q^{Lx}_1\rvert & if \quad Q^{y_Q}_{z_Q} < 0 \wedge P^{y_P}_{z_P} \geq 0 \\ 0 & if \quad otherwise \end{cases}$	(4.78)

In this notation, the index *y* indicates either phase association or the type of three-phase definition. The index *z* identifies the category of the power definition in terms of the harmonic components included. In general, the definitions of active and reactive power may vary depending on the selected definition, and are therefore marked accordingly with the subscript identifiers *P* and *Q* to reflect their respective associations.

4.4 Aggregation and Integration of the Components

The definitions of power components (Sections 4.1 and 4.2), including their classification (section 4.3), generally describe steady-state conditions. However, in practice, all components are computed over specific time intervals (greater than or equal to the sampling period T_s), with the actual measurement interval determined by the selected measurement algorithm and its parameterization (see section 5). Within these intervals, the system is assumed to be in a quasi-steady state. To reduce the volume of measurement data over time, it is often necessary to aggregate or integrate component values in time and/or aggregate across phases depending on the intended application. Fig. 4.3 illustrates the use of aggregated and integrated power components in selected metering applications.

For the purpose of billing for active energy (Commodity bill in Fig. 4.3), integrated values over longer time periods (typically monthly or yearly) are predominantly used. In the context of electricity trading and sharing within energy communities, the integration period is aligned with the shortest evaluation interval defined by the respective market or sharing platform (~15 minutes). Billing for distribution (Distribution fees in Fig. 4.3) commonly employs both integrated (monthly or yearly) and aggregated values (~15-minutes) of active and reactive power components.

For feedback control purposes (Control in Fig. 4.3), raw component values evaluated at or near the sampling interval T_s are typically required. However, aggregated components may be used for slow control loops or for adaptive tuning of control parameters. Analytical applications (Analysis in Fig. 4.3) utilize all types of components; nonetheless, in long-term monitoring scenarios, aggregated values (~1–15 minutes) are often preferred to reduce data volume.

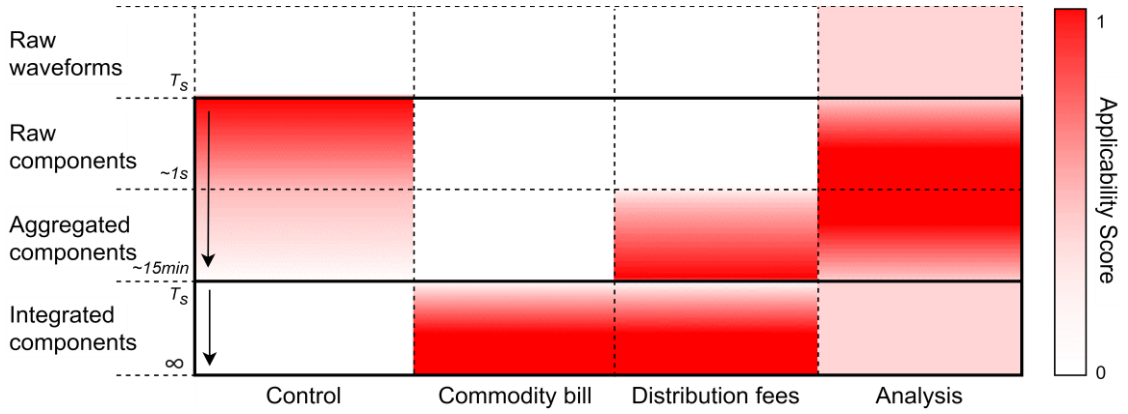

Fig. 4.3: Typical data granularity for selected metering applications.

4.4.1 Aggregation in Time

The fundamental time series of power components, evaluated over defined measuring intervals, can be aggregated into a single representative value over a longer period. Although temporal information is reduced, the essential energetic impact of the component over the aggregation interval is preserved. The aggregated value thus carries the same physical meaning as if the component were computed from instantaneous voltage and current directly over the entire aggregation interval. Furthermore, additional statistical descriptors—such as minimum, maximum, or percentile values—may complement the aggregated data to capture significant variations within the interval.

However, when applying temporal aggregation, careful consideration must be given to the specific definitions of the power components to ensure that the aggregated value retains the physical meaning of the underlying quantity. The aggregation formulas provided in this section are applicable to selected groups of components, regardless of the particular definitions or the types of inefficiencies being addressed. General aggregation relations (with the aggregated quantity denoted as X) for these groups are summarized in Tab. 4.17. The aggregated quantity consists of *M* components X_p, fundamentally defined on intervals k_pT_p. If all the X_p are defined in the same intervals (kT), the definitions may be reduced as indicated in Tab. 4.17.

When aggregating RMS values, it must be acknowledged that the RMS definition (see Tab. 4.1) inherently represents a quadratic mean over the interval kT. Therefore, when aggregating already computed RMS values, an appropriate aggregation expression must be used—namely, the quadratic mean of RMS components over time, as defined in Equation (4.79), which also corresponds to the discrete-time RMS definition [19].

Tab. 4.17. Generic time-aggregation formulae.

Component group	**Symbol**	**General aggregation formula**	
RMS of voltage and current	$V^{y}_{z,aggT}$ $I^{y}_{z,aggT}$	$X = \sqrt{\frac{\sum_{p=1}^{M} X_p^2 \cdot k_p T_p}{\sum_{p=1}^{M} k_p T_p}} \approx \sqrt{\frac{\sum_{k=1}^{M} X_k^2}{M}}$	(4.79)
Active power	$P^{y}_{z,aggT}$	$X = \frac{\sum_{k=1}^{M} X_k \cdot k_p T_p}{\sum_{p=1}^{M} k_p T_p} \approx \frac{\sum_{k=1}^{M} X_k}{M}$	(4.80)
Reactive power	$Q^{y}_{z,aggT}$	$X = \frac{\sum_{k=1}^{M} X_k \cdot k_p T_p}{\sum_{p=1}^{M} k_p T_p} \approx \frac{\sum_{k=1}^{M} X_k}{M}$	(4.81)
Apparent power	$S^{y}_{z,aggT}$	$X = \sqrt{\frac{\sum_{p=1}^{M} X_p^2 \cdot k_p T_p}{\sum_{p=1}^{M} k_p T_p}} \approx \sqrt{\frac{\sum_{k=1}^{M} X_k^2}{M}}$	(4.82)
		$S^{y}_{z,aggT} = V^{y}_{z,aggT} \cdot I^{y}_{z,aggT}$	(4.83)
Power factor	$PF^{y}_{z,aggT}$	$PF^{y}_{z,aggT} = \frac{P^{y}_{z,aggT}}{S^{y}_{z,aggT}}$	(4.84)

The active power, as defined in Tab. 4.4, represents the average rate of useful energy transfer over the interval kT. Thus, temporal aggregation of active power is performed using a simple arithmetic mean (4.80).

Reactive power—particularly when defined as the response of passive reactive components to the fundamental voltage waveform, as discussed in section 4.1.3—is calculated as the mean value of the instantaneous product of input sinusoidal waveforms, phase-shifted via integration or differentiation by $\pi/2$ ((4.33) and (4.34)). In this case, reactive power values in the base intervals can also be aggregated using the arithmetic mean (4.81).

The aggregation of apparent power over time is more complex. The definition of apparent power (section 4.1.2) describes it as the theoretical upper limit of active power transfer under ideal conditions—i.e., sinusoidal and phase-aligned voltage and current waveforms at the fundamental frequency, and, in three-phase systems, under perfectly balanced operation [18]. However, in real-world systems, an additional form of ineffectiveness—temporal unevenness—emerges during the aggregation interval. This term refers to the fact that power components, and the associated currents that cause losses, fluctuate within the interval. Since resistive losses are proportional to the square of the current, these variations lead to higher total losses than if the system operated steadily at the aggregated levels of power components. Thus, Tab. 4.17 provides two distinct expressions for calculating the aggregated apparent power: one that neglects the effect of temporal unevenness (4.82), and another that accounts for it (4.83), providing a more accurate representation of transmission inefficiencies over time [59]. For completeness, the aggregated power factor should be calculated from already aggregated components according to its definition, as it is defined as a ratio of power components.

However, a number of measuring devices, in which the voltage measurement is only a secondary function (typically smart RMs), and which are deployed both in MV and LV DS, aggregates both power and rms components using arithmetic mean (4.80). The deviation in the representativeness of the aggregated components may thus become non-negligible, particularly when large differences exist among the individual aggregants.

4.4.2 Aggregation over Phases

The IEC 62052-41 [20] defines procedures for aggregating active power components across multiple phases of a polyphase system. Specifically, it introduces three distinct methods: 1) the vectorial computation method ($3ph$), 2) the algebraic computation method ($\Sigma 1ph$), and 3) the absolute computation method (abs). Each method yields different results depending on how it accounts for phase relationships and the sign of the contributing quantities.

Tab. 4.18 illustrates the application of these computational methods to the sorted active power components from section 4.3, where $y = Lx$. The definition of the vectorial method essentially overlaps with the standard three-phase definitions ((4.44), (4.45)),

while the algebraic and absolute methods complement the set of three-phase active power components in section 4.2.1. The output of the vectorial method is the component P_z^{3ph} (4.85), which can be further sorted according to section 4.3. The algebraic method is applied separately to import and export components, resulting in $P_{z,imp}^{\Sigma 1ph}$ and $P_{z,exp}^{\Sigma 1ph}$ ((4.86) and (4.87), respectively). The absolute method, on the other hand, yields inherently a non-negative value P_z^{abs} (4.88).

The vectorial and algebraic summation methods for active power are discussed in greater detail in section 5.2, particularly in the context of opposite directional energy flows in the individual phases.

Tab. 4.18. Phase-aggregation formulae for active power group of components.

Component group	**Symbol**	**Aggregation formula**	
Active power – vectorial method	P_z^{3ph}	$P_z^{3ph} = \sum_{x=1}^{X}(P_{z,imp}^{Lx} - P_{z,exp}^{Lx})$	(4.85)
Importing/exporting active power – algebraic method	$P_{z,imp}^{\Sigma 1ph}$	$P_{z,imp}^{\Sigma 1ph} = \sum_{x=1}^{X}(P_{z,imp}^{Lx})$	(4.86)
	$P_{z,exp}^{\Sigma 1ph}$	$P_{z,exp}^{\Sigma 1ph} = \sum_{x=1}^{X}(P_{z,exp}^{Lx})$	(4.87)
Active power – absolute method	P_z^{abs}	$P_z^{abs} = \sum_{x=1}^{X}\lvert P_{z,imp}^{Lx} - P_{z,exp}^{Lx}\rvert$	(4.88)

The aggregation methods presented above may, in principle, also be applied to the reactive power group of components in individual phases, as reactive power is likewise subject to sorting (based on its sign) as discussed in section 4.3. Tab. 4.19 presents the resulting components. For a three-phase system, conclusions analogous to those for active power hold: the vectorial method (4.89) replicates the three-phase definitions provided in section 4.2.3 ((4.61), (4.62)), whereas the algebraic and absolute methods ((4.90)-(4.94)) complement them.

Tab. 4.19. Phase-aggregation formulae for reactive power group of components.

Component group	**Symbol**	**Aggregation formula**	
Reactive power – vectorial method	Q_z^{3ph}	$Q_z^{3ph} = \sum_{x=1}^{X}(Q_{1Q}^{Lx} + Q_{2Q}^{Lx} + Q_{3Q}^{Lx} + Q_{4Q}^{Lx})$	(4.89)
Reactive power in Q1-Q4 – algebraic method	$Q_{z,Q1}^{\Sigma 1ph}$	$Q_{z,Q1}^{\Sigma 1ph} = \sum_{x=1}^{X}(Q_{z,Q1}^{Lx})$	(4.90)
	$Q_{z,Q2}^{\Sigma 1ph}$	$Q_{z,Q2}^{\Sigma 1ph} = \sum_{x=1}^{X}(Q_{z,Q2}^{Lx})$	(4.91)
	$Q_{z,Q3}^{\Sigma 1ph}$	$Q_{z,Q3}^{\Sigma 1ph} = \sum_{x=1}^{X}(Q_{z,Q3}^{Lx})$	(4.92)
	$Q_{z,Q4}^{\Sigma 1ph}$	$Q_{z,Q4}^{\Sigma 1ph} = \sum_{x=1}^{X}(Q_{z,Q4}^{Lx})$	(4.93)
Reactive power – absolute method	Q_z^{abs}	$Q_z^{abs} = \sum_{x=1}^{X}\lvert Q_{1Q}^{Lx} + Q_{2Q}^{Lx} + Q_{3Q}^{Lx} + Q_{4Q}^{Lx}\rvert$	(4.94)

Phase-wise aggregation methods are not specifically applied to the remaining components, as the other groups—namely, apparent and distortion power group of

components—are inherently non-negative (i.e., they do not carry an implicitly assigned direction or character through their sign). In three-phase systems, all aggregation methods merely replicate the definitions of the respective component groups presented in section 4.2—specifically, those formulations that involve summation of the corresponding component across all phases.

4.4.3 Integration

By integrating power components over time—whether derived from the fundamental measurement interval kT or from aggregated values (as discussed in sections 4.4.1 and 4.4.2)—a single scalar value is obtained that quantifies the cumulative temporal effect of the respective power component. From a mathematical standpoint, this operation corresponds to the area under the power components waveform in time, therefore energy. However, from a physical and practical perspective, the term energy is appropriately reserved exclusively for integrals of active power components (4.95), which represent energy that has been demonstrably converted into another, useful form (e.g., mechanical or thermal energy).

Although it is mathematically possible to integrate all defined power components over time, in practice, mostly the integrals of active and reactive power components are commonly utilized. The integration of reactive power components yields what is also referred to as reactive energy (4.96). A general expression for the time integration of any power component is provided by (4.97).

A special case of time-integrated quantities is the integrated square of RMS current, denoted as $A2h$ (4.98). This component can be employed as an alternative indicator of energy loss due to current flow in power lines. Specifically, by multiplying $A2h$ by the resistance of a conductor, one directly obtains the losses incurred within that conductor. The quantity $A2h$ inherently captures the effect of a specific current component (denoted by z), including any temporal variability in the load profile, therefore including temporal unevenness [59].

The formulas for temporal integration provided in Tab. 4.20 are expressed in discrete form, using summation. Each integrated energy value is computed as the product of a power component and the corresponding time interval during which it is active—typically the basic evaluation interval defined by the parametrization of the employed measurement algorithm ($k_g T_g$).

Tab. 4.20 Integrated values of power components groups.

Integrated Component	**Symbol**	**Integration formula**	
Integrated active power components (active energy in kWh)	$A_{z,int}^{y}$	$A_{z,int}^{y} = \sum_{g=1}^{G} P_{z,int,g}^{y} \cdot k_g \cdot T_g$	(4.95)
Integrated reactive power components (reactive energy in kvarh)	$R_{z,int}^{y}$	$R_{z,int}^{y} = \sum_{g=1}^{G} Q_{z,int,g}^{y} \cdot k_g \cdot T_g$	(4.96)
General linearly integrated component X	$X_{z,int}^{y}$	$X_{z,int}^{y} = \sum_{g=1}^{G} X_{z,int,g}^{y} \cdot k_g \cdot T_g$	(4.97)
Integrated square of current	$A2h_z^y$	$A2h_z^y = \sum_{g=1}^{G} \left(I_{z,g}^{y}\right)^2 \cdot k_g \cdot T_g$	(4.98)

5. CALCULATION OF POWER COMPONENTS IN METERING DEVICES

The authors' works [A9], [A10], [A11] and [A12] concentrate on the algorithms that calculate power- and energy-component quantities inside the signal processing stage of modern meters. A typical metering unit (Fig. 5.1) is organized into five functional layers:

- Analogue acquisition – internal or external current and voltage sensors.
- Measurement analogue front-end – protection circuitry, signal-conditioning stages, anti-aliasing filters and analog-to-digital converters.
- Digital processing and computation core – an FPGA, MCU or DSP (plus RAM and synchronization logic) that executes the power-component algorithms.
- Data storage – non-volatile memory such as EEPROM or removable SD cards.
- Communication and I/O – displays, status LEDs, relay drivers and wired or wireless interfaces [60] - [62].

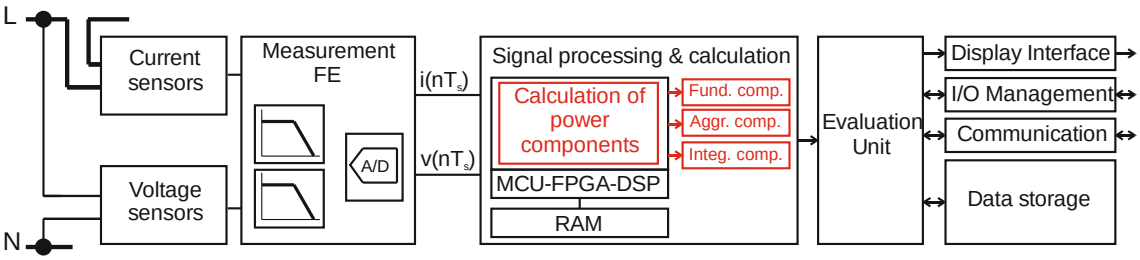

Fig. 5.1: General architecture of a metering device.

Power-component computation resides in the signal-processing stage, where purpose-built algorithms are executed [60]. Although these routines are rooted in the fundamental definitions set out in Section 4, practical implementations often diverge: developers may prioritize either high accuracy or low computational cost—the latter sometimes achieved by accepting a coarser estimation, as with the reactive-power algorithm in [63].

5.1 Dynamic Performance of Algorithms

The following subsections review five alternative algorithms for active power and energy, illustrating how the chosen metric shapes the reported values of both the fundamental component (active power) and its integrated values (imported and exported energy) under fast changes of energy flow [A10],[A11]. The active power measured by the algorithms is in Fig. 5.2, where the blue solid line represents the actual active power alternating with frequency 8.33 Hz. It is obvious that deviations of the active power curves from the reference leads to error, which further propagate to energy registration

especially when distinguishing between imported and exported energy . The detailed description is offered in following subsections.

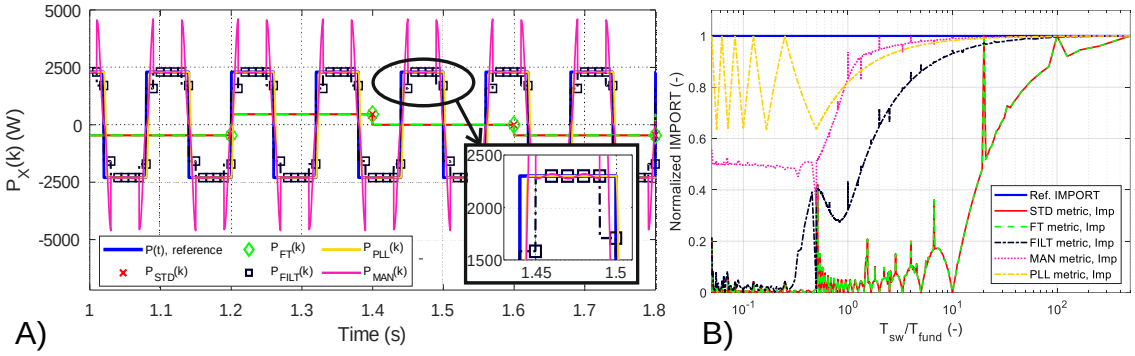

Fig. 5.2: Active power (A) and error of imported energy registration provided by algorithms (B) [A10].

5.1.1 Standard Algorithm (STD)

The straightforward implementation of active power definition (4.23) [18] leads to averaging of instantaneous power in a time period. Practically, the time period is called measuring window (T_{MW}) and length of the measuring window is in range of integer multiples of system half-cycles (~10 ms in 50 Hz system), usually 1 cycle, 10 cycles (~200 ms) or 50 cycles (~1 s) while the beginning of the half-cycles (or full-cycles) might be tracked by various methods (e.g. using detection of voltage zero crossings). The STD is commonly implemented in most electronic revenue (smart) meters, thus it is named "standard" algorithm (STD) with block diagram in Fig. 5.3. The outputs are average active power and increment of energy in the measuring window.

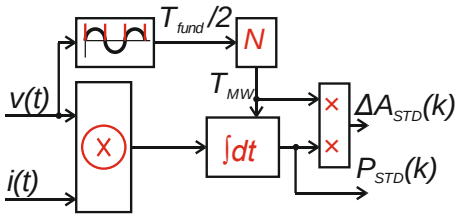

Fig. 5.3: STD algorithm for active power and active energy increment calculation [A11].

The Fig. 5.2 shows, that STD under the energy exchange evidently average the active power in the measurement window, which, for the example, leads to cyclic error with a period of 0.6 s in case of 10 cycle measurement window due to the fact that the measuring window length is not an integer multiple (or divisor) of the period of the cyclic power direction changes.

The measuring window has been further variated in [A11] in length of 50 cycles (typically in RMs [A11]), 10 cycles (power analyzers [23]) and ½ of cycle (STD50p, STD10p, and STD1/2p, respectively) as shows the Fig. 5.4. It is obvious that STD1/2p is relatively accurate, while STD50p measures almost zero active power as a result of its

long averaging window. The consecutive error of registered energy in the exported energy (the same is valid for imported energy) is expressed by means of normalized exported energy related to the true active energy export. The normalized export is quantified in Fig. 5.5 as a function of the ratio of the cyclic power changes period T_{sw} and power system period T_{fund} (see the red curves for the STD parametric variants).

For example, it can be quantified that when T_{sw} = 0.12 s (corresponding to a change frequency of 8.33 Hz) and T_{fund} = 20 ms (for a 50 Hz system), the STD50p registers only 2.4%, STD10p registers 12.8% of the exported energy, while STD1/2p captures up to 100% of the exported energy, depending on time shift between beginning of measuring window and beginning of T_{sw} (discussed further in this section). The same holds for the imported energy, since the duty cycle of the power changes is 0.5.

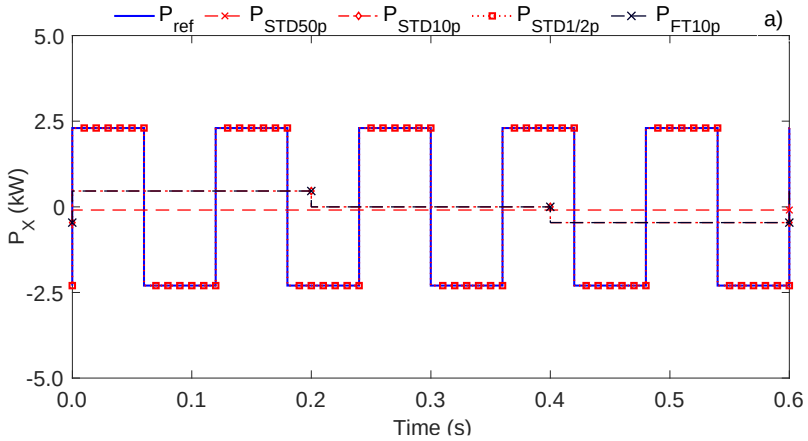

Fig. 5.4: Active power provided by the STD and FT [A11].

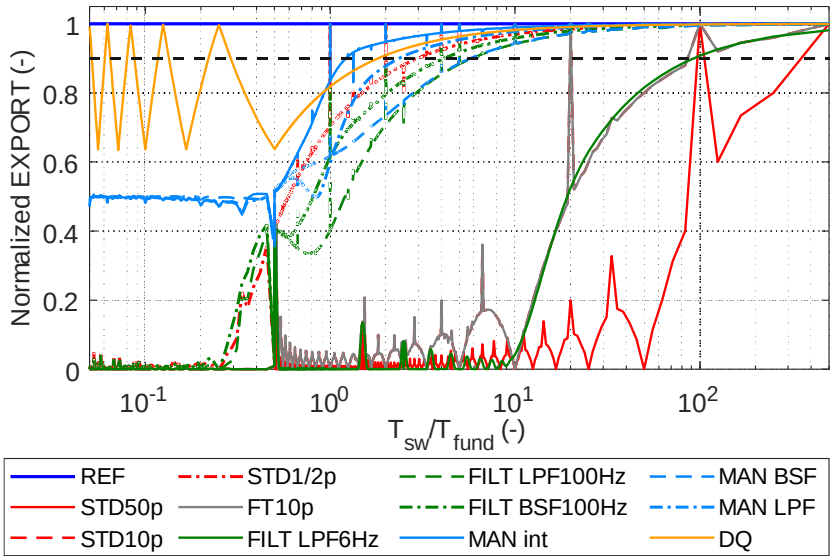

Fig. 5.5: Energy registration provided by algorithms and their parametric variations [A11].

The energy-registration error of the STD algorithm is further affected by specific external circumstances. Fig. 5.5 shows how the normalized energy registered by STD

(STD50p as the example) varies with period of power direction changes T_{sw} in a specific scenario defined by constant factors:

- Import duration T_{imp} within one switching period T_{sw}
- Ratio of exported and imported energy during the T_{sw} ($A_{REF}^{Exp}/A_{REF}^{Imp}$);
- Time shift between the start of the switching cycle T_{sw} and the beginning of the measurement window T_{MW}.

For the parametrized variant STD50, the Fig. 5.6 plots the registered energy for the extreme values of these factors. The results reveal that the range of corresponding error vary significantly with the selected influencing factor. Moreover, the corresponding error is hardly predictable at specific points (see the peaks on the curve). For example, the registered value is in range from 0% to 100% of the true value if T_{sw}/T_{fund} = 100 (i.e. T_{sw} = 2 s at 50 Hz). The uncertainty of the result is practically random as it depends on factor T_{sh}/T_{MW}, which is in real DS nearly impossible to detect as the processes behind the point of measurement (PoM) are generally unknown.

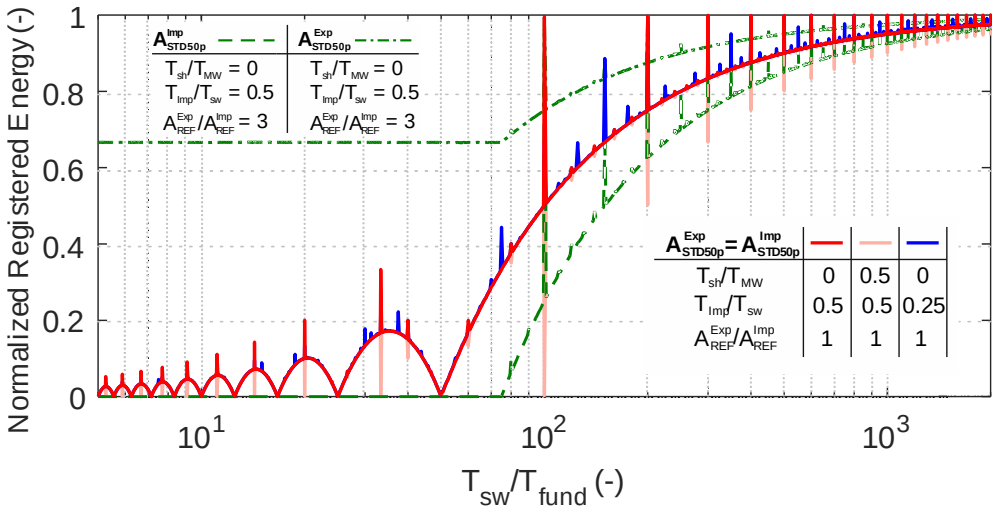

Fig. 5.6: Theoretical error of energy in registers of STD50p under influencing factors [A11].

5.1.2 Fourrier Transform Algorithm (FT)

The FT algorithm (Fig. 5.7) belongs—together with STD—to the class of window-based metrics that use a measurement window T_{MW}. The window length is typically ten cycles (~200 ms in a 50 Hz system), reflecting the standard measurement window of power-quality analyzers [23]; a different length can be selected for energy measurements if required. The FT metric is used e.g. by authors developing of a meter in [17].

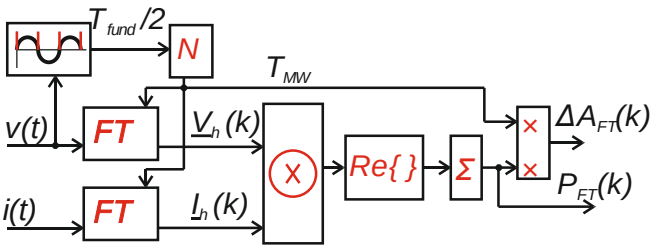

Fig. 5.7: FT algorithm for active power and active energy increment calculation [A11].

Applying the Fourier transform yields a complex spectrum of harmonic components of order *h* in the frequency domain for the voltage $\underline{V}_h^{Lx}$ and current $\underline{I}_h^{Lx}$ in phase *x*. Next, the active power of each observed harmonic *h* is calculated using (5.1); by selecting or arithmetically summing the desired components. One can obtain either the active power of all harmonics up to order *H* (5.2) or the active power of the fundamental component in accordance with (4.23) and (4.24), respectively.

$$P_{FT,h}^{Lx} = Re\left(\underline{V}_h^{Lx} \cdot \underline{I}_h^{Lx}\right) \tag{5.1}$$

$$P_{FT}^{Lx} = \sum_{h=1}^{H} P_h^{Lx} \tag{5.2}$$

The energy increment is obtained by multiplying the power by interval T_{MW}. The error of active power (Fig. 5.4) and deviation of energy-metering (Fig. 5.5 and Fig. 5.6) is influenced by the same external factors identified for the STD method, because both algorithms are fundamentally similar—they rely on a measurement window of fixed length. The authors in [64] investigate the design of weighting functions within the measurement window to improve accuracy under interharmonic distortion. Nevertheless, such parameterization can also be applied to window-based algorithms (FT and STD), since the most significant rapid variations occur in the interharmonic and subharmonic ranges.

5.1.3 Filtration Algorithm (FILT)

The FILT algorithm is based on removing the double-the-fundamental frequency component of instantaneous power (i.e. ~100 Hz for 50 Hz system) using a filter (Fig. 5.8) and optionable averageing in intervals T_{AW} (integer multiples of fundamental half-cycle) in order to eliminate the residual ripple in active power. The energy increment is integral of filtered instantaneous power over T_{AW}.

The pre-processing filter can be implemented in several ways; for example, authors in [A11] discusses variants such as 1) a low-pass filter with cut-off frequencies of 6 Hz and 50 Hz, and 2) a band-stop filter centered at 100 Hz. By default, the FILT algorithm determines active power according to(4.23), i.e. the sum of the active-power contributions of all harmonic components. When an appropriately chosen low-pass filter suppresses higher-order harmonics in the input signals, FILT can instead be configured to evaluate only the active power of the fundamental component, as prescribed by (4.24).

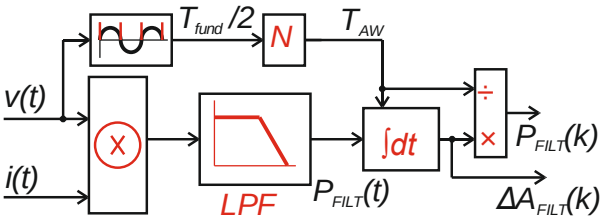

Fig. 5.8: FILT algorithm for active power and active energy increment calculation [A10].

Fig. 5.9 compares the active-power obtained with the various FILT configurations, each averaged over an accumulation window T_{AW} equal to one system half-cycle. The FILT LPF6Hz variant smooths the signal nearly identically to the STD10p and FT10p. In contrast, the FILT LPF50Hz and FILT BSF100Hz versions show similar deviations from the true instantaneous active power, much smaller than FILT LPF6Hz.

The consequences for energy registration are summarized in Fig. 5.5. Within the frequency band of power changes 2.5 Hz – 100 Hz (corresponding to $0.5 \leq T_{sw}/T_{fund} \leq 20$ in a 50 Hz system) the FILT BSF100Hz yields the smallest accumulated-energy error.

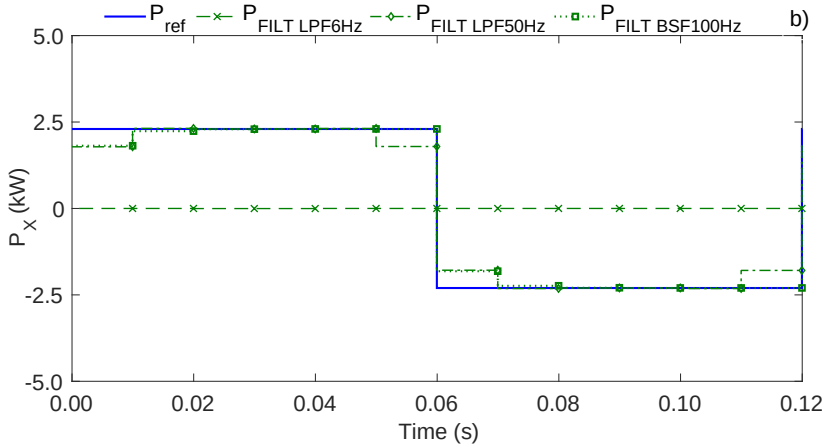

Fig. 5.9: Active power provided by the FILT [A11].

5.1.4 Signal-Manipulation Algorithm (MAN)

The MAN algorithm principally manipulates the input signals, as one of the waveforms is first differentiated, and the second integrated. Consequently, instantaneous power $p(t)$ and component $p'(t)$ are obtained ((5.3),(5.4)) and the resulting active power is computed by (5.5), as illustrated in Fig. 5.10. The algorithm intentionally eliminates the oscillating ~100 Hz component of instantaneous power and the resulting offset component represents instantaneous active power [65].

$$p(t) = v(t) \cdot i(t) \tag{5.3}$$

$$p'(t) = \frac{dv(t)}{dt} \cdot \left[\int_{t(k)}^{t(k)+T_{fund}} i(t)dt - I_{DC}\right]. \tag{5.4}$$

$$P_{MAN}^{Lx} = 1/2 \cdot (p(t) - p'(t)) \tag{5.5}$$

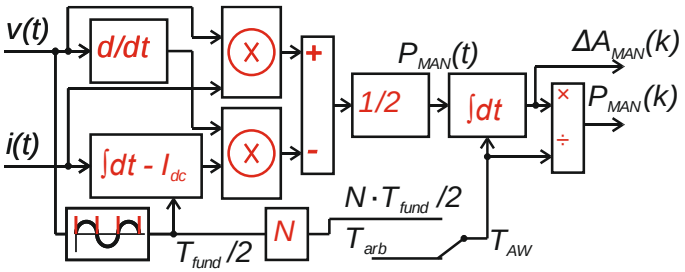

Fig. 5.10: MAN algorithm for active power and active energy increment [A11].

The integration constant I_{DC} embodies the DC component of the integrated signal. Two practicable schemes for its continuous estimation and suppression were examined 1) MAN INT— simple averaging over one fundamental period T_{fund} and 2) Filtering approaches — either a band-stop filter (MAN BSF) or a low-pass filter (MAN LPF).

The Fig. 5.11 shows the difference between the methods based on development of the deviation in active power in time. MAN INT exhibits the largest instantaneous deviations, yet it yields the smallest cumulative error in registered energy—although it still inherits the periodic error spikes characteristic of window-averaging methods such as STD. When the direction of active power changes at frequencies below twice the fundamental, all methods converge to the same 50 % energy error.

Because MAN INT relies on explicit knowledge of the mains period, it must track the fundamental cycle (e.g., via zero-crossing detection). In contrast, the filter-based variants operate without such tracking. Each algorithm provides an instantaneous active-power value at every sampling instant (the discrete form of (5.5)), and the resulting power or incremental energy can subsequently be integrated over any user-defined interval. Fig. 5.11 contrasts the three schemes by plotting the time evolution of their active-power deviation, while the corresponding energy-metering errors appear in Fig. 5.5.

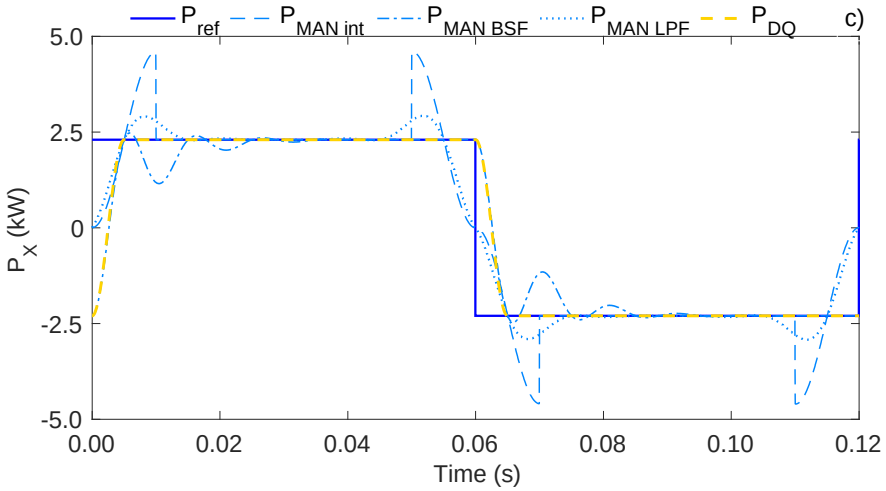

Fig. 5.11: Active power provided by the MAN and DQ [A11].

5.1.5 DQ-domain algorithm (DQ)

A DQ algorithm was developed by adapting a single-phase inverter control scheme as an alternative to the metrics used in practical RMs (Fig. 5.12). A phase-locked loop (PLL) tracks the instantaneous phase angle of the voltage fundamental component; this angle then drives the Park transformation, which projects the measured voltage and current into the synchronously rotating d-q reference frame (v_d, v_q and i_d, i_q, respectively). Consequently, the active power is calculated (5.6) and the active energy increment is calculated by multiplication with arbitrary selected averaging interval T_{AW} in every instant of time, i.e., the sampling interval in a real application.

$$P_{DQ}^{Lx} = \frac{1}{2} \cdot \left(v_d \cdot i_d + v_q \cdot i_q \right) \tag{5.6}$$

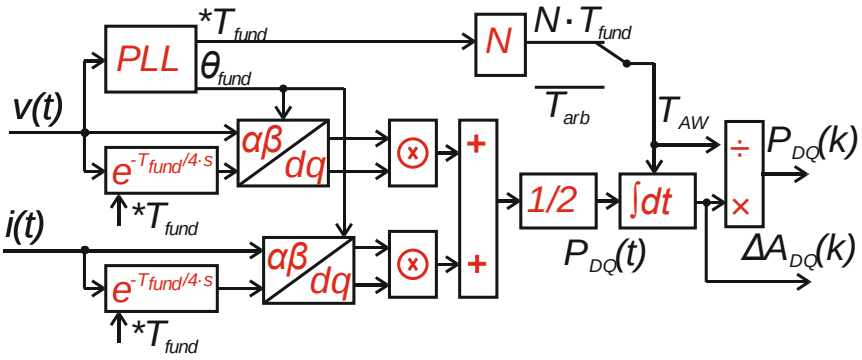

Fig. 5.12: DQ algorithm for active power and active energy increment [A11].

Fig. 5.11 demonstrates that the DQ algorithm exhibits lower active-power overshoot than either MAN group of algorithms. Likewise, Fig. 5.5 indicates that the DQ method achieves the lowest energy-registration error of all the algorithms, except in the short energy exchange cycle—below one fundamental cycle—where MAN INT exhibits a slight advantage.

The performance of the DQ-based algorithm in practice is further influenced by the ability of the particular PLL algorithm to accurately track the grid frequency [66]. Every PLL algorithm exhibits a finite response time when following dynamically varying frequencies, and any desynchronization may introduce additional ripple into the resulting power waveform. Therefore, the key to ensuring the proper functionality of this algorithm lies in employing a robust PLL algorithm—such as one of the variants of the Dual Second-Order Generalized Integrator PLL (DSOGI-PLL) [67],[68]—which is resilient to asymmetric and harmonically distorted supply voltages [69].

5.2 Sorting Algorithms in Three-Phase systems

Measured values of electrical-power and -energy components in the individual phases are usually post-processed into standardized registries—particularly in RMs—to facilitate billing and auditing. The most common sorting separates cumulative active-energy increments (and, by implication, active power) into import and export registers (see also section 4.3).

Publications [A9] and [A12] compare three categorization strategies for active power (Fig. 5.13). Two of them correspond to the methods formalized in [20]:

- Arithmetic, or per-phase, sorting ($RM_{\Sigma 1ph}$), where the sign of each phase's active-power contribution is assessed individually before summation;
- Vectorial, or three-phase, sorting (RM_{3ph}), where the signed per-phase powers are summed first and only the sign of the resulting vector is used to label the increment as import or export.

In addition, the authors introduce an alternative sequence-power approach (RM_{SYM}), which classifies energy on the basis of the positive-sequence active power (4.46), calculated from positive sequence of voltage and current ($|\underline{V}_Y^+|$ a $|\underline{I}_Y^+|$, respectively) [70].

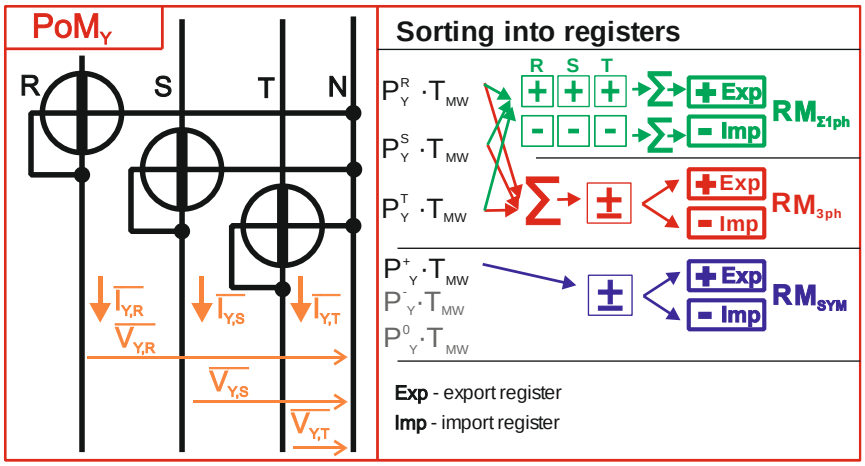

Fig. 5.13: Sorting of active power in three-phase system [A9].

The investigation reported in [A9] evaluates how each categorization algorithm records energy under a set of boundary operating conditions in which the phase-resolved active-power directions differ. One illustrative scenario (Fig. 5.14A) sets two phases to equal-magnitude active powers of opposite sign. Under these conditions the RM_{3ph} produces a net zero reading, because the opposing phase contributions cancel before the sign of the aggregated three-phase vector is determined; the $RM_{\Sigma 1ph}$ registers the opposite flows separately as imported and exported power, which better reflects the physical reality; the RM_{SYM} records only a small export value. It is shown in [A9], that this residual corresponds almost exactly to the loss power incurred by the unbalanced loading of a three-phase, four-wire (3P4W) network, thereby signaling inefficient utilization of the system. From practical point of view, a prosumer is penalized exactly by extent of additional losses which he induces due to unbalanced energy flow.

From the standpoint of energy settlement, the outcome of the RM_{SYM} most closely aligns with RM_{3ph}.

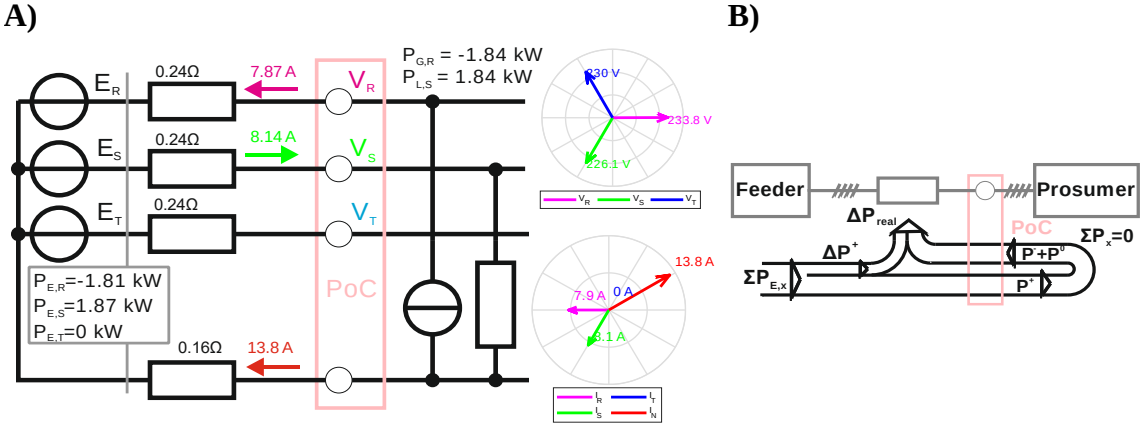

P^{L1} (W)	P^{L2} (W)	P^{L3} (W)	ΔP_{real} (W)	$RM_{\Sigma 1ph}$		RM_{3ph}		RM_{SYM}	
				Imp	Exp	Imp	Exp	Imp	Exp
1840	-1840	0	61.42	1840	-1840	0	0	61.00	0.00

Fig. 5.14: Specific state of energy flow (zero vector sum) in three-phase four-wire system (A), power and loss flow diagram (B) [A9].

5.3 Metrics for Reactive Power

In this section, demonstratively, the following definition of reactive power is selected: the nonactive power produced by the fundamental (first-harmonic) components of current and voltage. This corresponds to definition (4.33). From physical aspect, it is the product of the rms magnitudes of the fundamental-frequency voltage and current that a linear reactive element—an ideal inductor or capacitor—would draw under the excitation by fundamental harmonic voltage. Thus, the quantity practically represents a nonactive power, that is useful for voltage control in AC DSs [A7],[A8].

The quantity can be calculated from the instantaneous waveforms with algorithms that follow the same fundamental principles as the active-power algorithms presented in 5.1 (STD, FT, FILT, MAN, and DQ), however, certain modifications are required. The algorithms must be provided with the input signals, which are pre-processed in accordance with definition (3.33). Specifically, the voltage and current waveforms must be reduced to their fundamental components $v_1^{Lx}(t)$ and $i_1^{Lx}(t)$, e.g. by applying a selective filter that removes all higher harmonics and inter-harmonics. In addition, one of the two fundamental waveforms must be shifted by a quarter of the fundamental cycle so that the current and voltage are in quadrature. This phase shift can be realized by several methods [71]:

- by integrating or differentiating the fundamental (harmonic) waveforms (either $v_1^{Lx}(t)$ or $i_1^{Lx}(t)$),
- by delaying the discrete-time signal by a fixed number of samples corresponding to quarter of the fundamental cycle ($T/4$), or
- by employing a dedicated phase-shifting filter.

For the FT algorithm, a further simplification is possible: instead of shifting the time-domain signals, one may select the imaginary parts of the first-harmonic components of current and voltage (*5.7*), being consistent with definition (3.33).

$$Q_{FT,1}^{Lx} = Im\left(\underline{V}_1^{Lx} \cdot \underline{I}_1^{Lx}\right) \tag{5.7}$$

The DQ algorithm can likewise be adapted by invoking the reactive-power expression formulated in the d-q reference frame. For an individual phase Lx the reactive power is obtained from Eq. (4.9). To comply strictly with definition (3.33), however, only the first-harmonic d- and q-components of current and voltage ($i_1^{Lx}(t)$ a $v_1^{Lx}(t)$, respectively) may be inserted into that relation; all higher-harmonic content must be excluded.

$$Q_1^{Lx} = \frac{1}{2} \cdot \left(v_{1,d}^{Lx} \cdot i_{1,q}^{Lx} - v_{1,q}^{Lx} \cdot i_{1,d}^{Lx}\right) \tag{5.8}$$

Finally, in the case of the MAN algorithm, the initial signal manipulation can be alternatively avoided. By applying a derivative-based phase shift to the current signal (in the context of this section $i_1^{Lx}(t)$), and theoretically exploiting the property of a harmonic signal being shifted by differentiation, one can substitute the signal in expressions (*5.3*) and (*5.4*). This yields alternative instantaneous power waveforms $p_q(t)$ and $p_q{}'(t)$, corresponding to (*5.9*) and (*5.10*), respectively. The resulting reactive power Q_1^{Lx} is then obtained according to (*5.11*). The advantage of this modification is that it eliminates the need for integration, which otherwise requires the calculation of the integration constant, i.e. DC component (see section 5.1.4). Since the differentiation is applied solely to the fundamental harmonic components of the signals, the general drawback of differentiation under distorted waveforms is avoided. Nevertheless, differentiation may still yield large values in the presence of steep signal transitions.

$$p_q(t) = v_1^{Lx}(t) \cdot \frac{di_1^{Lx}(t)}{dt} \tag{5.9}$$

$$p_q'(t) = \frac{dv_1^{Lx}(t)}{dt} \cdot i_1^{Lx}(t) \tag{5.10}$$

$$Q_1^{Lx} = 1/2 \cdot \left(p_q(t) - {p_q}'(t)\right) \tag{5.11}$$

In addition to the signal shifting algorithms listed above, one can adopt a complementary method that exploits the geometric relation between the first-harmonic apparent power S_1^{Lx}, active power P_1^{Lx}, and reactive power Q_1^{Lx} (5.12). Although straightforward, this approach yields only the magnitude of the reactive power—the square-root operation is non-negative—so it provides no information about its sign (inductive or capacitive character).

Adding the sign requires calculation of angle between voltage and current phasors, which is rather problematic in case of distorted waveforms as they consist of multiple harmonics and the phasors angles must be then calculated as a prevalent angle or only the first harmonic angle is assumed ($\underline{V_1}^{Lx}$ and $\underline{I_1}^{Lx}$ respectively). In both cases, however, it requires the calculation of angles, therefore the same computational effort as FT algorithm. Incorporating the sign requires determining the angle between the voltage and current phasors, $\underline{V_1}^{Lx}$ and $\underline{I_1}^{Lx}$ respectively. However, the computation necessitates angle evaluation, implying a computational effort comparable to that of the FT algorithm.

$$Q_1^{Lx} = \sqrt{{S_1^{Lx}}^2 - {P_1^{Lx}}^2} \tag{5.12}$$

The single-phase reactive powers Q_1^{Lx} are further classified into reactive power registers corresponding to quadrants Q1 through Q4, as shown in Fig. 4.2. Several classification methods, corresponding to component groups resulting from aggregations over phases (see Tab. 4.19), might be used. Caution is required, as the vectorial and absolute methods may lead to virtual auto-compensation of reactive power between phases when the reactive power characteristics differ across phases. Only the algebraic method reports the character of the reactive power correctly.

6. OBJECTIVE CRITERIA FOR EVALUATION OF MEASURED QUANTITIES

The physical quantities recorded by a metering unit are subject only to the device's own metrological accuracy and the associated measurement uncertainty. Their interpretation, however, depends on both the formal definition of each power component [72] and the numerical algorithm used to obtain it, and must therefore be assessed in a broader system context. Throughout the thesis and publications, four evaluation criteria are considered (Fig. 6.1).

- Actual, unambiguous, energy flow within the prosumer installation (①)
- Losses induced in upstream DS—expressed either as loss energy or loss power (②).
- Instantaneous energy exchange at the PoC (③).
- The conditioning current that an ideal, virtual power conditioner would inject at the PoC to induce the less losses as possible in the upstream DS while preserving the same active power transfer (④).

Fig. 6.1 illustrates how these criteria apply to a single prosumer equipped with a metering unit at its PoC. Downstream of the meter the installation is composed of 1) an active load (a switching resistive heater that consumes active power), 2) a reactive load (a capacitor or inductor supplying or absorbing reactive power), and 3) a generator (an ideal, loss-free converter delivering solely active power defined at its DC-link input). A virtual current compensator, located conceptually at the PoC, injects a corrective current that enforces the target power-flow condition: in a balanced three-phase DS this corresponds to a harmonic-free, phase-symmetrical currents carrying only active energy.

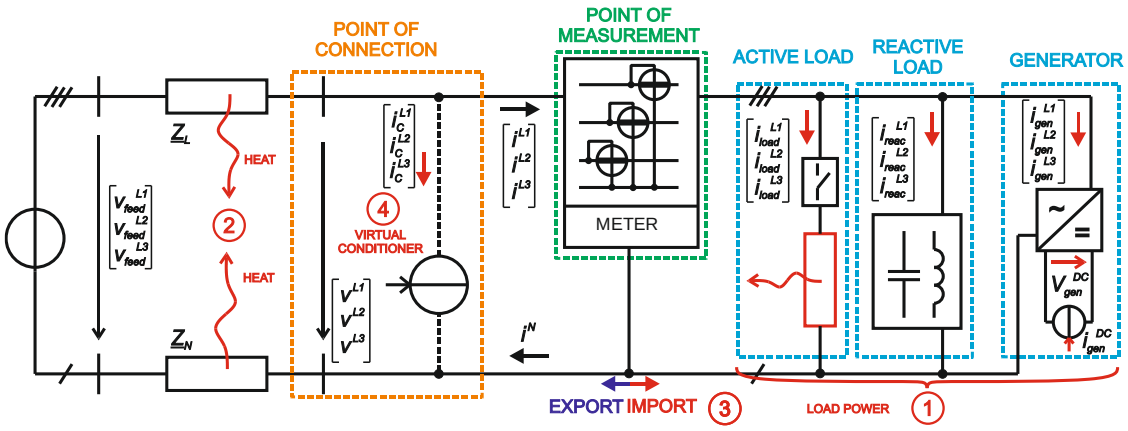

Fig. 6.1: Model of a prosumer connected to a DS and evaluation criteria.

6.1 Real Energy Flow in the System

The term real active-energy flow refers to the portion of electrical energy that is unambiguously converted to—or supplied from—another form of energy inside the consumer's installation, evaluated in real time and resolved at the level of individual components:

- Consumed active power is active power that can be demonstrably transformed into another energy form—heat dissipated by an ideal resistive element in this case.
- Active power (or energy) produced by an ideal generator is the active power delivered to the AC side is inferred from the measured DC-link voltage and current, the AC–DC conversion being treated as ideal at fundamental frequency (i.e. without switching processes) and loss-free (6.1).

$$P_{gen} = P_{gen}^{DC} = v_{gen}^{DC} \cdot i_{gen}^{DC} = P_{gen}^{L1} + P_{gen}^{L2} + P_{gen}^{L3} \tag{6.1}$$

- Reactive load delivering power arising from orthogonal current components at each harmonic, manifesting as bidirectional instantaneous power that do not contribute to active energy transfer.

Fig. 6.2 illustrates the power-flow scenario of the testing system similar to that in Fig. 6.1 but with zero grid impedance (i.e. prosumer connected on ideal voltage feeder). The parametrization is set as follows. The generator injects a sinusoidal current of 10 A in phase L3, delivering a constant active power of 2.3 kW in L3. The instantaneous power of the generator is oscillating unidirectionally with frequency two times higher than fundamental system frequency (Fig. 6.1A). The resistive load is connected to L1 and draws 10 A at 230 V while its switch operates at 5 Hz, so the associated active power (2.3 kW) appears and disappears every 100 ms (Fig. 6.1B). Moreover, the load part has an additional source of current harmonics in L2, steadily emitting 7th current harmonic of magnitude 2 A to phase L2. The instantaneous power of such combined load (in the three-phase system) oscillates unidirectionally 1) due to asymmetrical nature (double the fundamental frequency), 2) due to switching (5 Hz changes) and bidirectionally in stochastic manner due to missing corresponding 7th harmonic component of the voltage (Fig. 6.1B). The reactive load is connected in the phase L1, and it draws a steady inductive current of 5 A at 230 V and the instantaneous current oscillates bidirectionally with double the fundamental frequency (Fig. 6.1C).

The consequent phase currents in PoM are shown in Fig. 6.2D. In L1, the current changes cyclically in range of 5–11.8 A with subharmonic frequency of 5 Hz while the character changes form purely inductive (at 5 A) and resistive-inductive (at 11.8 A). In L2, the current is constant, reaches 2 A and oscillates at 350 Hz (7th harmonic). In L3, the current is constant of magnitude 5 A.

The three-phase instantaneous-power traces p^{L123} describes the quality of instantaneous energy exchange throughout the system; however, the half-period average of p^{L123}—the shortest interval according to the definition (4.23)—is the key indicator for monitoring active energy flow. The active power at PoC oscillates between 2.3 kW and 0 kW at 5 Hz (Fig. 6.2D), precisely following the algebraic sum of the active power generator and the active power of time-modulated resistive load.

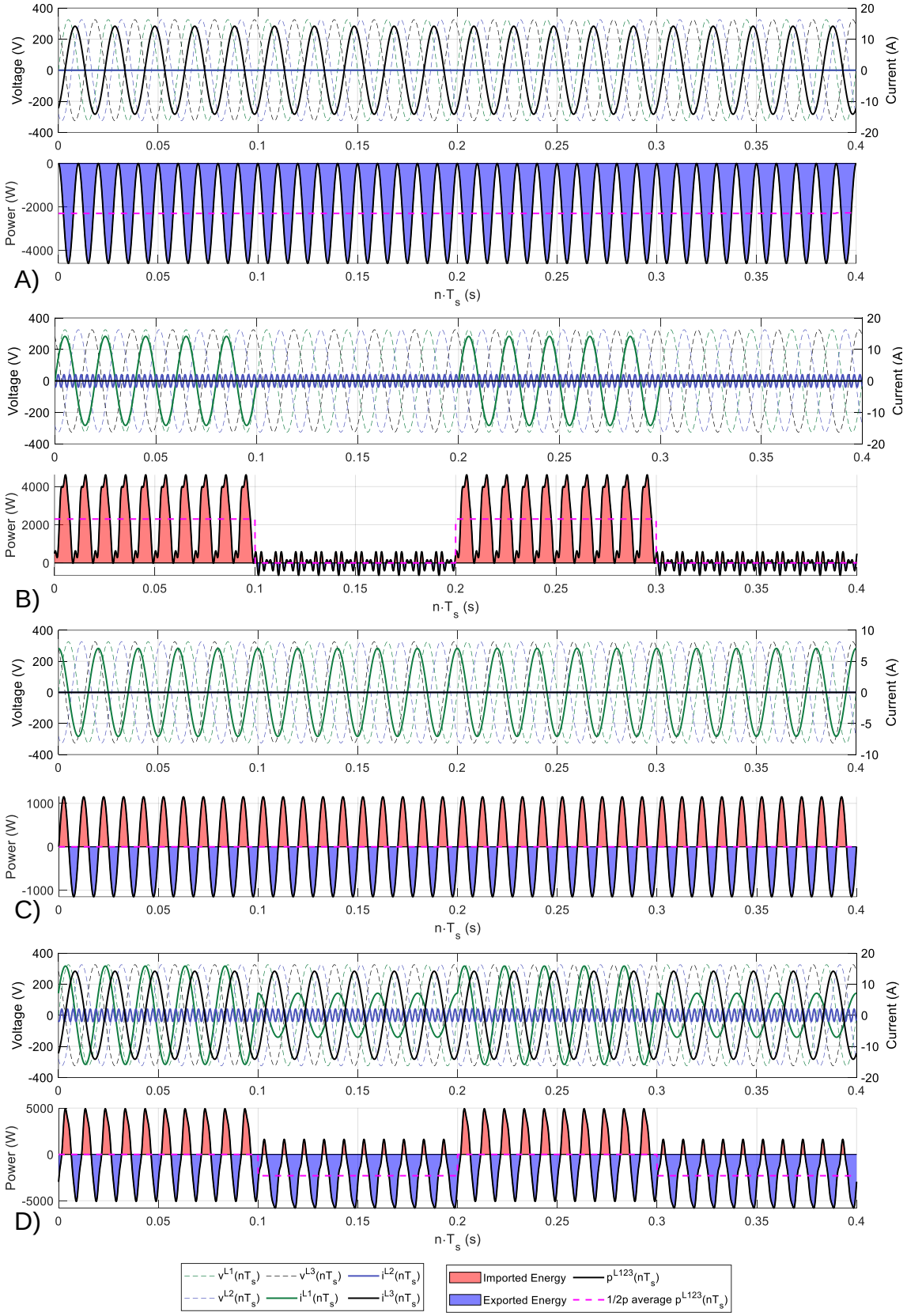

Fig. 6.2: Current, instantaneous power and 1/2p active power of generator (A), resistive load (B), reactive load (C) and at PoC (D).

6.2 Current of Virtual Power Conditioner

A straightforward indicator of how a prosumer's behavior affects the distribution network is the set of reference currents (i_C^{L1}, i_C^{L2} a i_C^{L3} in Fig. 6.1) that an ideal conditioner would inject at the PoC to restore ideal power transfer—that is, perfectly sinusoidal, phase-balanced currents while delivering the same active-power. For three-phase systems these reference currents can be obtained with the instantaneous-power (p-q) theory [74]. In essence, the algorithm removes from the phase currents those components that give rise to ripple in the three-phase instantaneous power at the PoC. Hardware constraints of a real power conditioner are ignored; the resulting currents therefore represent the theoretical optimum.

The phase compensating currents (i_C^{L1}, i_C^{L2} and i_C^{L3}) are obtained at each sampling instant by applying the Clarke transformation (6.2). Their α-β counterparts, (i_C^{α} and i_C^{β}), are derived (6.3) from the reference voltages (v^{α}, v^{β}) together with the instantaneous-power terms defined in p-q theory—namely the instantaneous active power p, instantaneous reactive power q, and zero-sequence power p_0 (*6.5*). The active-power term is split into an oscillatory component $\tilde{p}$, obtained by subtracting the half-cycle mean of p from p, and the DC component of the zero-sequence power $\overline{p_0}$, given by its half-cycle average (6.4). Currents and voltages in the α-β frame are calculated via the Clarke transformation, using the expressions (6.6) and (6.7) appropriate to three-phase (three- or four-wire) systems or, respectively, (6.8) and (6.9) to single-phase (two-wire) systems.

$$\begin{bmatrix} i_C^{L1} \\ i_C^{L2} \\ i_C^{L3} \end{bmatrix} = \sqrt{\frac{2}{3}} \cdot \begin{bmatrix} \frac{1}{\sqrt{2}} & 1 & 0 \\ \frac{1}{\sqrt{2}} & -\frac{1}{2} & \frac{\sqrt{3}}{2} \\ \frac{1}{\sqrt{2}} & -\frac{1}{2} & \frac{-\sqrt{3}}{2} \end{bmatrix} \cdot \begin{bmatrix} -i^0 \\ i_C^{\alpha} \\ i_C^{\beta} \end{bmatrix} \tag{6.2}$$

$$\begin{bmatrix} i_C^{\alpha} \\ i_C^{\beta} \end{bmatrix} = \frac{1}{v^{\alpha 2} + v^{\beta 2}} \cdot \begin{bmatrix} v^{\alpha} & v^{\beta} \\ v^{\beta} & -v^{\alpha} \end{bmatrix} \cdot \begin{bmatrix} -\tilde{p} + \overline{p_0} \\ -q \end{bmatrix} \tag{6.3}$$

$$\overline{p_0} = \frac{2}{T} \int_{\tau}^{\tau + \frac{T}{2}} p^0(t) \cdot dt$$
$$\tilde{p}(t) = p(t) - \frac{2}{T} \int_{\tau}^{\tau + \frac{T}{2}} p(t) \cdot dt \tag{6.4}$$

$$\begin{bmatrix} p^0 \\ p \\ q \end{bmatrix} = \begin{bmatrix} v^0 & 0 & 0 \\ 0 & v^{\alpha} & v^{\beta} \\ 0 & v^{\beta} & -v^{\alpha} \end{bmatrix} \cdot \begin{bmatrix} i^0 \\ i^{\alpha} \\ i^{\beta} \end{bmatrix} \tag{6.5}$$

$$\begin{bmatrix} v^0 \\ v^{\alpha} \\ v^{\beta} \end{bmatrix} = \sqrt{\frac{2}{3}} \cdot \begin{bmatrix} \frac{1}{\sqrt{2}} & \frac{1}{\sqrt{2}} & \frac{1}{\sqrt{2}} \\ 1 & -\frac{1}{2} & -\frac{1}{2} \\ 0 & \frac{\sqrt{3}}{2} & \frac{-\sqrt{3}}{2} \end{bmatrix} \cdot \begin{bmatrix} v^{L1} \\ v^{L2} \\ v^{L3} \end{bmatrix} \text{ for 3P4W system} \tag{6.6}$$

$$\begin{bmatrix} i^0 \\ i^\alpha \\ i^\beta \end{bmatrix} = \sqrt{\frac{2}{3}} \cdot \begin{bmatrix} \frac{1}{\sqrt{2}} & \frac{1}{\sqrt{2}} & \frac{1}{\sqrt{2}} \\ 1 & -\frac{1}{2} & -\frac{1}{2} \\ 0 & \frac{\sqrt{3}}{2} & \frac{-\sqrt{3}}{2} \end{bmatrix} \cdot \begin{bmatrix} i^{L1} \\ i^{L2} \\ i^{L3} \end{bmatrix} \text{ for 3P4W system} \quad (6.7)$$

$$\begin{bmatrix} v^0 \\ v^\alpha \\ v^\beta \end{bmatrix} = \begin{bmatrix} 0 \\ v^{L1}(\omega t) \\ v^{L1}\left(\omega t - \frac{\pi}{2}\right) \end{bmatrix} \text{ for 1P2W system} \quad (6.8)$$

$$\begin{bmatrix} i^0 \\ i^\alpha \\ i^\beta \end{bmatrix} = \begin{bmatrix} 0 \\ i^{L1}(\omega t) \\ i^{L1}\left(\omega t - \frac{\pi}{2}\right) \end{bmatrix} \text{ for 1P2W system} \quad (6.9)$$

Fig. 6.3A reproduces the current and instantaneous-power waveforms at the PoC (already shown in Fig. 5.2D). Fig. 6.3B displays the corresponding current and instantaneous power of the virtual conditioner. Note that the conditioner's power is of the nonactive type: the half-cycle average of the instantaneous power remains zero, so the conditioner neither delivers nor absorbs active energy (it compensates only currents causing power fluctuations and is loss-less). What it does provide is an exchange of instantaneous energy within each half-cycle—both within a phase in time and among phases.

After the virtual compensation, the PoC quantities would appear as in Fig. 6.3C: the instantaneous power now coincides with the active-power curve, while the phase currents are perfectly sinusoidal and mutually balanced. This represents the ideal operating point that preserves the same transfer of active energy as the original state in Fig. 6.3A but eliminates all parasitic power oscillations.

In Fig. 6.3B, within t = 0-0.1 s, the current loading of the virtual conditioner is non-zero (11.18 A in phase L1) despite zero active-power transfer. In other words, in the absence of the conditioner, the prosumer would impose a current load on the network even though the transferred active energy is zero. In t = 0.1-0.2 s, the conditioner current is several times higher (6.67 A in phase L3) than the current associated with an ideal active-power transfer (3.33 A per phase). In both intervals, the compensating current exceeds the current required for ideal active energy transfer. The computation of compensating current of a virtual conditioner enables one to:

- determine how the network would be utilized in the absence of the conditioner,
- distinguish upstream DS utilization due to ideal transfer from that due to inefficient transfer and
- specify sizing requirements for prospective conditioner hardware.

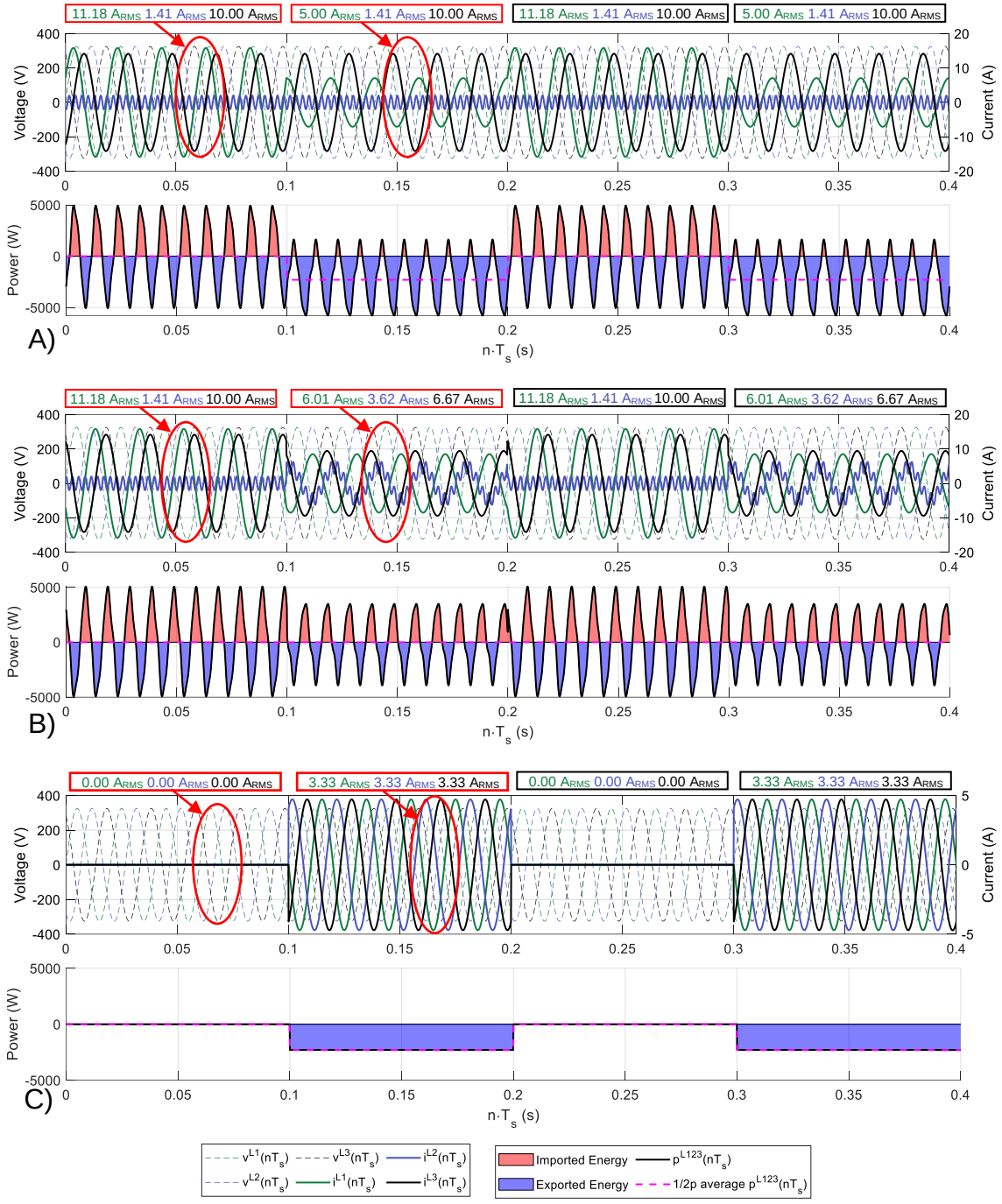

Fig. 6.3: Current, instantaneous power and 1/2p active power at PoC before compensation (A), of virtual conditioner (B) and PoC at after virtual compensation (C).

6.2.1 Parametrization of the Conditioner Algorithm

From eqs. (6.2) – (6.9) it follows that, in a three-phase network, the compensating currents cannot be computed without measuring or estimating the fundamental frequency (6.4); e.g. phase-locked loop. Moreover, in a single-phase system the voltage and current must be shifted by $\pi/2$ (one quarter of the fundamental cycle) to obtain their α–β components, as implied by (6.8) and (6.9). Any of the phase-shifting techniques reviewed

in section 5.3 may be used for this purpose, all of which rely—explicitly or implicitly—on estimating the fundamental period.

In practice, the components $\tilde{p}$ and $\overline{p_0}$ of the instantaneous power need not be obtained by half-cycle averaging as in (6.4); they can instead be extracted with a high-pass/low-pass filter pair (6.10). When the filters are designed appropriately, this approach eliminates the need for an explicit phase-locked loop, allowing the compensating currents in a three-phase system to be computed without real-time knowledge of the fundamental frequency.

Applying the filter-based implementation of (6.10) to the same voltage- and current waveforms used in Fig. 6.3A yields the compensator currents and power shown in Fig. 6.4A and the post-compensation PoC currents in Fig. 6.4B (the plots start after the initial filter transient, thus avoiding the current overshoot). The filters were tuned for a 50 Hz network, assuming frequency excursions within the statutory limits of EN 50160:

- Low-pass filter (LPF): pass-band ≤ 25 Hz, stop-band ≥ 75 Hz
- High-pass filter (HPF): pass-band ≥ 75 Hz, stop-band ≤ 25 Hz

A comparison of Fig. 6.3B-C with Fig. 6.4A-B shows that the quasi-steady one-cycle rms values of the phase compensator currents are almost identical. The transient behavior, however, differs: the filter-based approach exhibits a slower response to power changes and a residual ripple in the quasi-steady state. Because the filter characteristics strongly influence the computed currents, half-period averaging remains preferable for analytical studies, where numerical transparency is critical. For real-time control of a hardware compensator, by contrast, computational speed and smoothness may take precedence, making the filter-based method more attractive despite its parameter sensitivity.

$$\begin{aligned} \overline{p_0} &= (\mathcal{L}^{-1}\{F_{LPF,50Hz}(s)\} * p^0) \\ \tilde{p} &= (\mathcal{L}^{-1}\{F_{HPF,50Hz}(s)\} * p) \end{aligned} \tag{6.10}$$

This subsection presents a type of deviation that may be introduced by realistic parameterization of the compensating current calculation algorithm. A comparison of conditioning using a realistically parameterized algorithm (Fig. 6.4B) and an ideally parameterized one (Fig. 6.3C) reveals deviation of realistically parametrized one by 0.16 A at t = 0.24-0.26 s (corresponding to the state at t = 0-0.1 s in Fig. 6.3C) and by 0.07 A at t = 0.34-0.36 s (corresponding to the state at t = 0.1-0.2 s in Fig. 6.3C) when compared with the ideally parameterized algorithm.

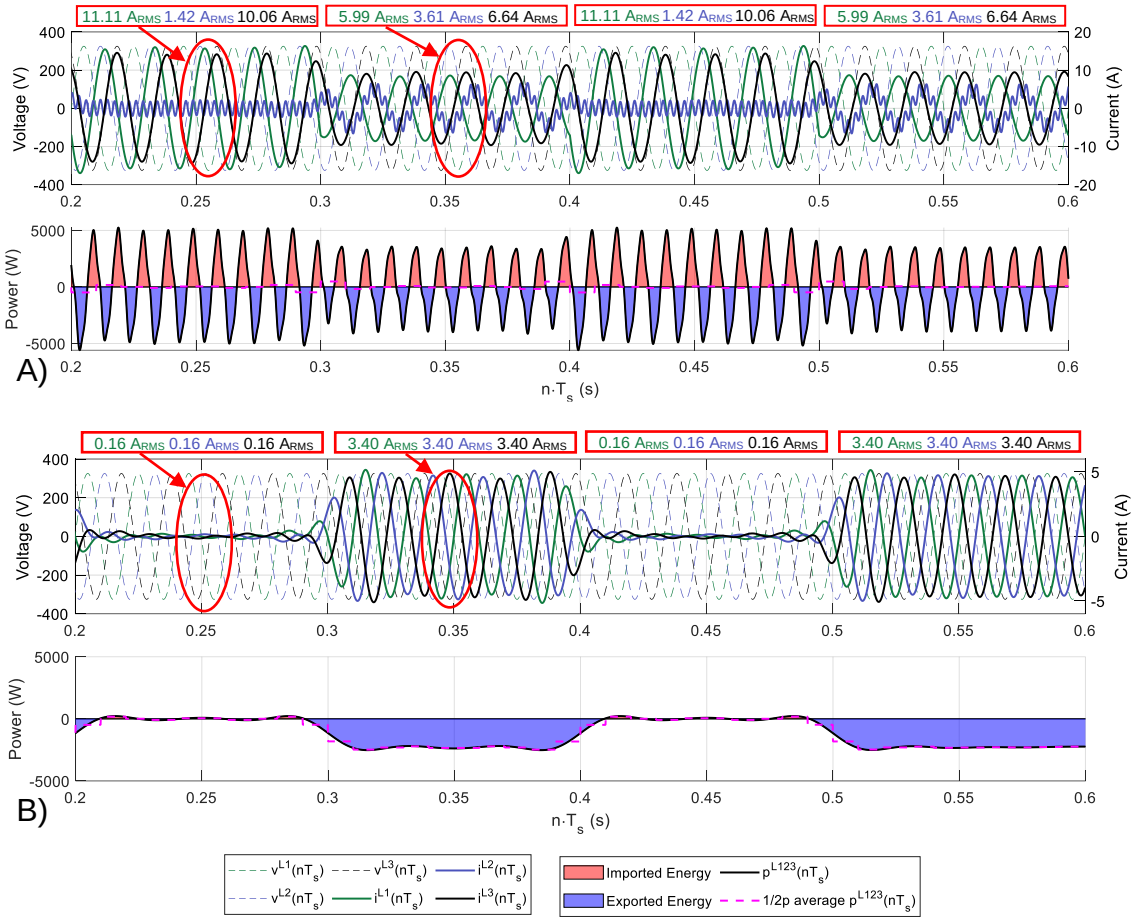

Fig. 6.4: Current, instantaneous power and 1/2p active power injected by compensator (A) and at PoC after virtual compensation (B).

6.3 Total Energy Exchange at PoC

The three-phase instantaneous-power waveforms p^{L123} in Fig. 6.2 quantify the instantaneous energy exchange throughout the installation and reveal how efficiently active power is transferred (calculated as a half-period average of p^{L123}). Whenever the polarity of the instantaneous power oscillates while the average (active) value remains constant, the transfer is inefficient; the detrimental impact of such power oscillations on equipment ageing and network stability is reviewed in [73].

In a three-phase system, bidirectional oscillations of instantaneous power can arise through several mechanisms.

- Reactive currents drawn by inductive or capacitive loads (Fig. 6.2C).
- Simultaneously operating load and generator connected to different phases (e.g., 0.0–0.1 s and 0.2–0.3 s in Fig. 6.2D, where combined with reactive load current).

- Non-linear loads, which inject harmonic currents and generate instantaneous power pulsations at frequencies above twice the fundamental (visible in 0.1–0.2 s and 0.3–0.4 s in Fig. 6.2B).
- Fluctuations in the power of simultaneously operating load and generators, which results in fast bidirectional active-energy flow.

The last category is examined in detail in [A10] and [A11] as part of an evaluation of active-energy algorithms. In [A10] the polarity-reversal frequency is varied by periodically switching a resistive load in a reduced version of the Fig. 6.1 test set-up (only the generator and switched resistive load, see Fig. 6.5), allowing the sensitivity of different active power algorithms to fast power oscillations to be quantified.

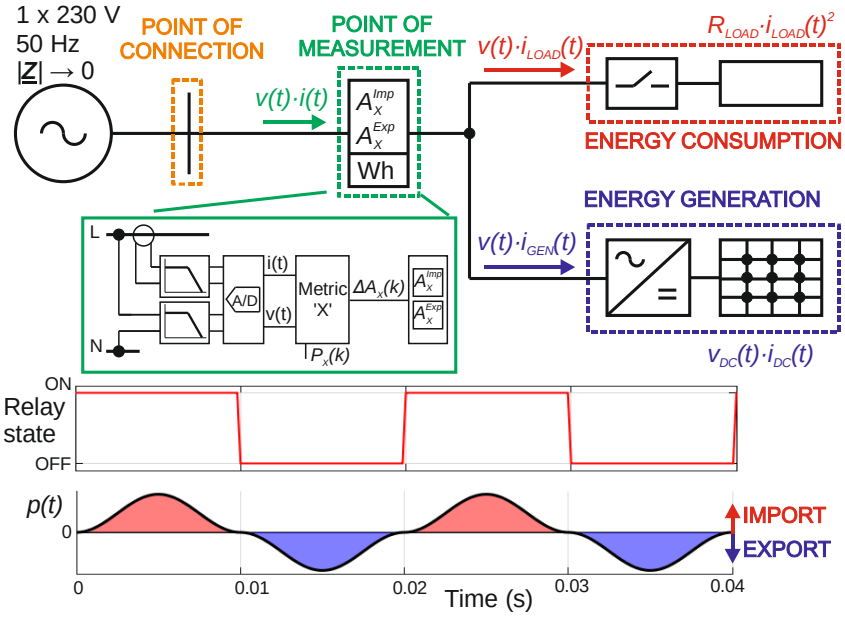

Fig. 6.5: Single line diagram of a prosumer with a generator and switching load causing periodic and fast changes in the active power direction at the PoC [A10].

When the active-power changes polarity with 100 Hz (Fig. 6.6A), the polarity of the instantaneous power reverses as rapidly as it does for a purely reactive load (Fig. 6.2C); from the standpoint of the instantaneous power, the two situations are therefore equivalent. They are not equivalent, however, in terms of current wave-shapes. At 100 Hz and higher (Fig. 6.6B), a measurement at the PoC offers no clear indication of whether the observed power oscillations arise from rapid active-power changes or nonactive power—power pulsations associated with non-linear loads, harmonic or inter-harmonic distortion, or other high-frequency disturbances. The ambiguity reflects a limitation of the active-power definition in (4.23), which leaves the averaging interval T unspecified. In AC systems the shortest unambiguous averaging window is one half of the mains period, i.e. ~10 ms in a 50 Hz network.

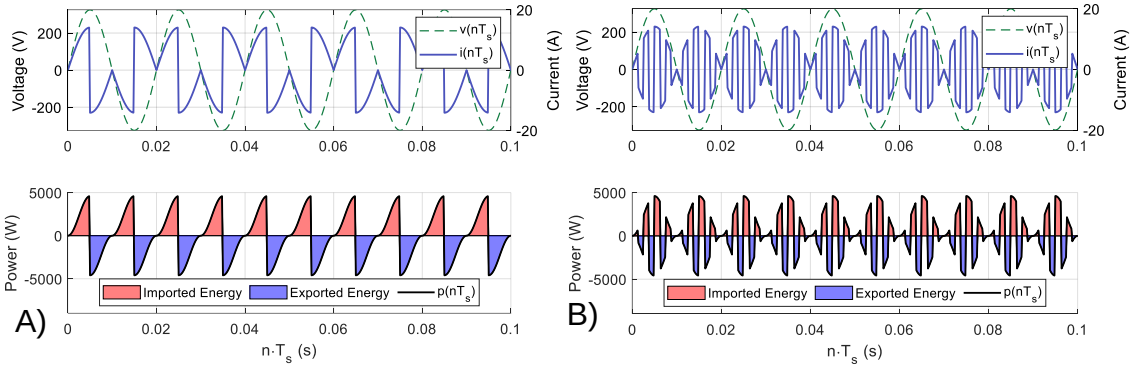

Fig. 6.6: Current and instantaneous power at PoC of a system with generator and switched resistive load, switched with frequency of 100 Hz (A) and 400 Hz (B) [A10].

Quantifying active-power variations above 100 Hz lies primarily within the scope of electromagnetic-compatibility (EMC) analysis; nevertheless, the associated imported and exported energy can be relevant for advanced power-quality assessments. Because conventional consecutive-window algorithms used in power-quality instruments report zero energy whenever the average power over the evaluation window is zero [A10], it might be advantageous to complement the standard PQ indices with a direct integration of the instantaneous-power waveform at the PoC, imported instantaneous energy (6.11) and exported instantaneous energy (6.12). Energy exchange can therefore be characterized by the areas above and under the instantaneous-power curve—an approach that captures high-frequency power pulsations even if the half-period average is zero.

$$E_{imp} = \begin{matrix} \int_{-\infty}^{\infty} p(n \cdot T_s) \cdot dt & if\ p(n \cdot T_s) \geq 0 \\ 0 & if\ p(n \cdot T_s) < 0 \end{matrix} \tag{6.11}$$

$$E_{exp} = \begin{matrix} \int_{-\infty}^{\infty} p(n \cdot T_s) \cdot dt & if\ p(n \cdot T_s) < 0 \\ 0 & if\ p(n \cdot T_s) \geq 0 \end{matrix} \tag{6.12}$$

Applying the (6.11) and (6.12) on the instantaneous power waveforms in Fig. 6.3, from system in Fig. 6.1 the energy throughput is calculated. The Tab. 6.1 shows the energy throughput at PoM (before the virtual conditioning, Fig. 6.3A), at PoC (after the virtual conditioning, Fig. 6.3C) and at the terminals of virtual conditioner (Fig. 6.3B).

Tab. 6.1. Energy throughput at PoM, PoC and virtual conditioner.

Objective criterion	Energy throughput		
	PoM (before VC*)	Virtual conditioner	PoC (after VC*)
E_{imp} (Ws)	504	753	0
E_{exp} (Ws)	1194	753	690
$\lvert E_{imp} - E_{exp} \rvert$ (Ws)	**690**	**0**	**690**

* VC – Virtual Conditioning

It is evident that, after the application of virtual conditioning, the considered grid user solely exports energy, as E_{imp} = 0 at the PoC, while E_{exp} = 690Ws. In contrast, without virtual conditioning, the PoC both imports and exports energy (E_{imp} = 504 and E_{exp} = 1194), although the net saldo $\left|E_{imp} - E_{exp}\right|$ equals 690 , corresponding to the exported energy after conditioning. It can further be observed that the imported and exported energies of the virtual conditioner are identical, 753 Ws (representing a lossless ideal conditioner), and the value exceeds the exported energy after conditioning. Hence, the evaluation of energy throughput in this case reveals that the combined effects of generation and load in different phases, together with reactive and nonlinear load, cause an exchange of energy across the PoC that is nominally greater than the useful (active) energy exported to the upstream DS.

Although calculating energy throughput from instantaneous power describes the actual exchange of energy at the PoC, this approach does not enable identification of the underlying cause of the exchange. From a physical perspective, it is not possible, for instance, to distinguish which portion of the transferred energy arises from unbalanced generation and consumption and which portion originates from reactive load. This differentiation is actually the purpose of power components definitions.

6.4 Loss Energy and Loss Power

Another evaluation aspect for any power-component definition or computational algorithm is its ability to reflect the user's utilization of the distribution network. As an objective criterion we adopt the customer's contribution to upstream DS losses.

Publications [A9] and [A12] pursue this idea by comparing import-/export-sorting algorithms—as well as the sequence-component measurements introduced in section 5.2—on their ability to describe how intensely a prosumer "uses" the grid. Building on that motivation, the same studies explore whether the symmetrical power components can quantify the extra loss power incurred in the upstream DS when customers inject phase-unbalanced flows into a three-phase network [56].

Fig. 6.7 summarizes the interpretation of power exchanges and associated losses—derived from the numerical results in Tab. 6.2 (Case 1, Case 3, Case 5 and Case 6)—for the algorithms described in section 5.2. The diagram highlights how the behavior of a single prosumer at its PoC (PRO2,PoC) translates into losses in the DS [56].

The power flow diagram (Fig. 6.7) is the outcome of losses tracking in the upstream distribution system, and it clearly illustrates the useful energy flows, power losses, and their decomposition into the defined components. Combining with the component quantification in Tab. 6.2, a complete description of the system power flow is obtained. For instance, Fig. 6.7B presents the case of unidirectional unbalanced import (3680 W in Case 3), where the component P_Y^+ = 3767 W penalizes the prosumer for unbalanced consumption by including an additional loss power caused by the unbalance,

ΔP_{add} = 87.85 W. In the context of symmetrical components, this additional loss is represented by the sum of the negative-sequence (P_Y^-) and zero-sequence (P_Y^0) components. The diagram further highlights the relationship to the vectorial power (denoted as ΣP_Y^X in Fig. 6.3), which does not account for these losses.

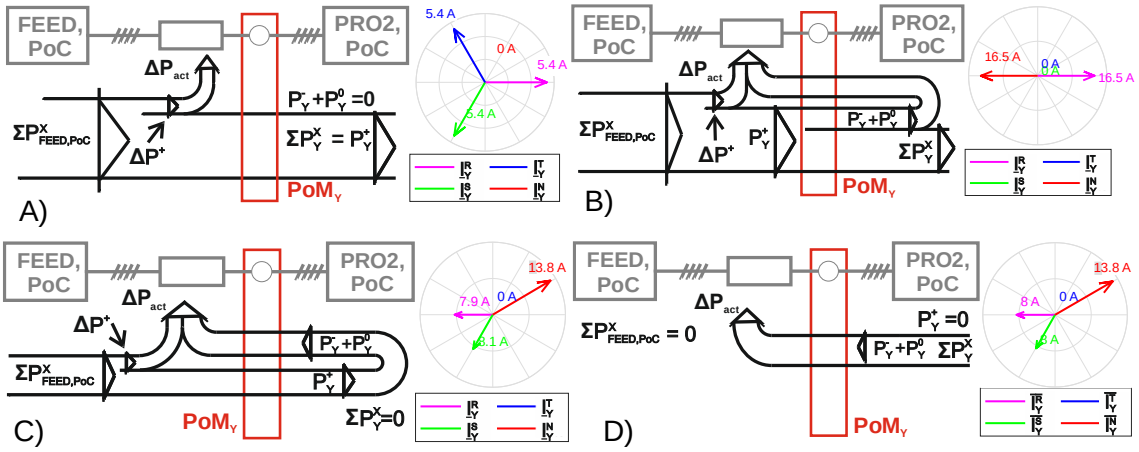

Fig. 6.7: Power and loss power flow diagram, balanced consumption – Case 1 (A), unbalanced consumption – Case 3 (B), zero net power – Case 5 (C), zero positive sequence power – Case 6 (C)[A12].

In another example of bidirectional unbalanced import and export (P_Y^R = 1840 W and P_Y^S = -1840 W in Case 3), it is numerically demonstrated that P_Y^+ is nearly equal to the sum $|P_Y^- + P_Y^0|$. The diagram in Fig. 6.7C clearly illustrates that, despite the zero vectorial power ΣP_Y^X, a loss-generating energy exchange occurs at the PoM.

Tab. 6.2. Specific states of system with single prosumer.

		Case 1 (BC)	Case 2 (BG)	Case 3 (UC)	Case 4 (UG)	Case 5 ($CB_{\Sigma 0}$)	Case 6 (CB_{POS0})
P_Y^R (W)		1227	-1227	3680	0	1840	1810
P_Y^S (W)		1227	-1227	0	-3680	-1840	-1870
P_Y^T (W)		1227	-1227	0	0	0	0
P_Y^+ (W)		3680.0	-3680.0	3766.9	-3602.3	60.8	0.0
P_Y^- (W)		0.0	0.0	-21.7	-19.4	-15.5	-15.5
P_Y^0 (W)		0.0	0.0	-65.1	-58.3	-45.3	-45.3
ΔP_{act} (W)		20.71	20.26	108.57	97.10	60.78	60.71
ΔP_{bal} (W)		20.71	20.26	20.71	20.26	0.00	0.01
ΔP_{add} (W)		0.00	0.00	87.85	76.84	60.78	60.70
$P_Y^{\Sigma 1ph}$ (W)	Exp	3680	0	3680	0	1840	1810
	Imp	0	-3680	0	-3680	-1840	-1870
P_Y^{3ph} (W)	Exp	3680	0	3680	0	0	0
	Imp	0	-3680	0	-3680	0	-61
P_Y^{SYM} (W)	Exp	3680	0	3767	0	61	0
	Imp	0	-3680	0	-3602	0	0

7. ESTIMATION OF DISTRIBUTION SYSTEM LOSSES

References [A9] and [A12] examine in detail how to estimate the loss power caused by prosumers causing asymmetrical energy flows in a distribution network (modelled in Fig. 7.1). The authors demonstrate that this unbalance loss, when added to the ohmic losses that would arise under an ideal, perfectly symmetrical transfer of the same power, yields the network's total loss power. Such estimation is made possible by measuring the symmetrical (positive-, negative-, and zero-sequence) components of power.

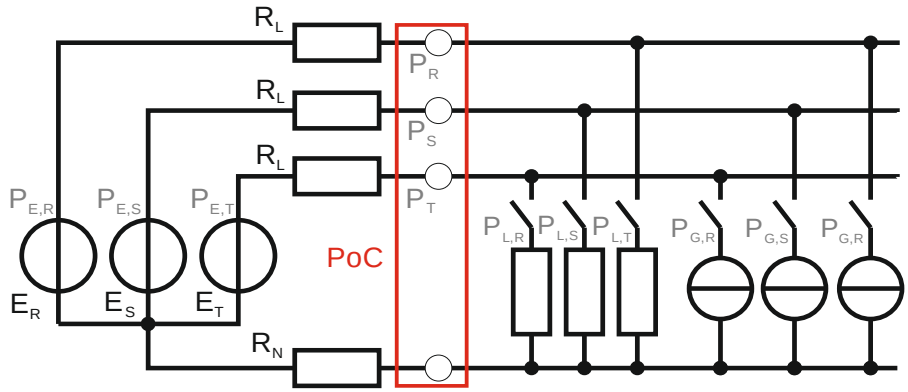

Fig. 7.1: Testing model of a prosumer [A9].

The feasibility of estimating this loss term was first validated on a set of deliberately chosen operating scenarios. Analytical derivation [A9] shows that the incremental loss power produced by unbalanced phase flow (denoted $\Delta P_{1,add}$) can be approximated by (7.1).

$$\Delta P_{1,add} = \left(|P_1{}^{-}| + |P_1{}^{0}|\right) \cdot K_{PI} \tag{7.1}$$

The $P_1{}^{-}$ and $P_1{}^{0}$ are the negative- and zero-sequence active-power components measured at PoC, and K_{PI} is a dimensionless correction factor. Further analysis shows that the correction factor K_{PI} is required to capture hidden losses (7.2). These hidden losses depend on:

- the positive-, negative-, and zero-sequence currents measured at the PoC (I_1^+, I_1^- and I_1^0, respectively);
- the positive-sequence current that would flow in an equivalent balanced state ($I_{1,bal}^+$); and
- the ratio of the neutral-conductor resistance (R_N) to the phase-conductor resistance (R_L).

$$K_{PI} = 1 + \frac{|(I_1^+)^2 - I_{1,bal}^{+\,2}|}{(I_1^-)^2 + (I_1^0)^2\left(1 + 3\frac{R_N}{R_L}\right)} \tag{7.2}$$

However, determining K_{PI} in the practice is far from trivial because it requires detailed knowledge of the local distribution network—phase impedances. Reference [A9] therefore investigates the realistic range of K_{PI} that may arise in typical European low-voltage DSs. First, the active power of each phase was swept in discrete steps (black dots in Fig. 7.2A) from –9.2 kW to +9.2 kW. This interval covers the plausible export/consumption limits for prosumers in Czech, German, and Italian LV networks. For all power triplets the corresponding sequence currents were calculated with realistic phase and neutral line resistance values (80th percentile of connection impedances in Czechia, Austria, Germany and Switzerland and reference impedance from IEC TR 60 725), and equation (8.2) was evaluated to obtain K_{PI}. The resulting distribution of K_{PI} values is plotted in Fig. 7.2B. To define the operating conditions at the PoC by single parameter, the authors introduce a prosumity index *PI* (7.3).

$$PI = \frac{P_1^+}{|P_1^+|+|P_1^-|+|P_1^0|} \tag{7.3}$$

Fig. 7.2B shows a range of the calculated K_{PI} values with their empirical probability density. The results indicate that K_{PI} can, in extreme cases, approach 1.10, yet 90% of all simulated operating points (90th percentile) fall between 1.00 and 1.05. Consequently, adopting a fixed correction factor of K_{PI} = 1.05 yields a deliberately conservative—but still realistic—estimate of hidden losses for the vast majority of practical scenarios in European LV feeders.

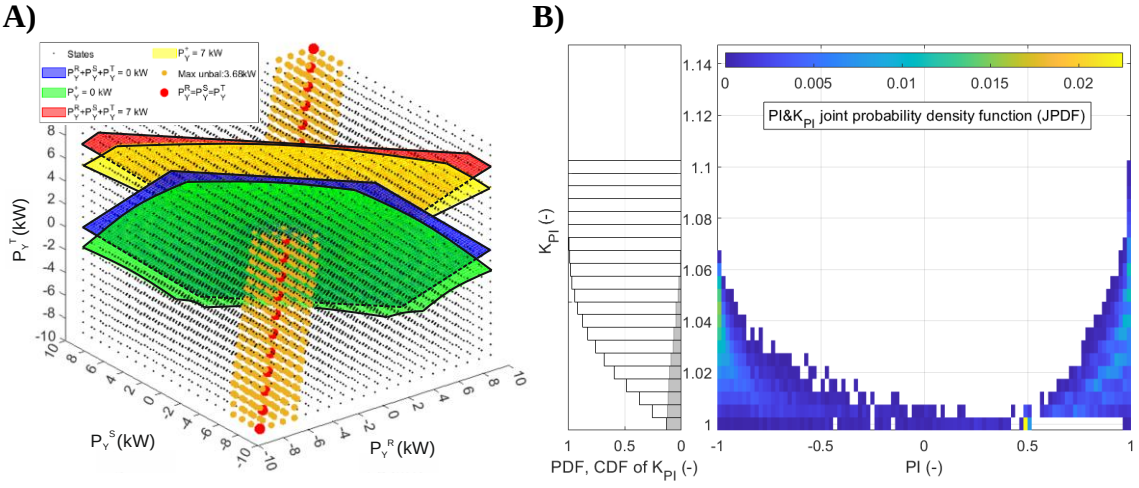

Fig. 7.2: Testing states of PoC defined by active power in phases (A) and distribution of K_{PI} in the test network (B) [A12].

In Fig. 7.2A, visualizing the situation in reference phase and neutral line resistance values (0.24 Ω and 0.16 Ω, respectively), several characteristic operating subsets are emphasized:

- Perfectly balanced states (red dots on the cube's main diagonal), where the three phase powers are identical; under such conditions every allocation algorithm yields the same result.

- States (orange dots forming a cylindrical envelope around the diagonal) in which the power difference between any two phases is below 3.68 kW.
- Points with a fixed algebraic three-phase sum of 7 kW (red plane) and those for which the positive-sequence active power equals 7 kW (yellow plane).
- Points with a zero algebraic sum (blue plane) and those for which the positive-sequence active power is zero (green plane).

Inspection of the blue-versus-green and red-versus-yellow planes reveals that the phase-sum and the positive-sequence power agree only when the PoC operates in a perfectly symmetrical condition, i.e., along the central diagonal.

Since the additional losses due to power imbalance can—neglecting the hidden losses—be quantified by the sum of the negative- and zero-sequence active-power components, reference [A9] introduces the approximate relationship given in (7.4).

$$P_1^+ = \left(\sum_{x=L1,L2,L3} P_1^x \right) - (P_1^- + P_1^0) \tag{7.4}$$

Every operating point located on the red (or blue) plane can be mapped to a unique counterpart on the yellow (or green) plane by dropping a perpendicular from the red (blue) plane until it intersects the yellow (green) surface. Because the algebraic three-phase sum appearing in (7.4) is, by definition, the quantity recorded by the RM_{3ph} sorting algorithm (section 5.2), the normal (Euclidean) distance between each pair of points represents an approximation of the unbalance-related losses that RM_{3ph} does not register.

For completeness, the $RM_{\Sigma 1ph}$ sorting algorithm likewise omits these losses, yet it still records the sign of the active power in each phase separately—i.e., it respects the phase-wise coordinates of the black dots along the individual axes.

From a practical standpoint, the losses attributable to phase-unbalanced power can be estimated with satisfactory accuracy as $P_1^- + P_1^0$ (neglecting the hidden-loss). This means by simply taking the difference between the energy values reported by the RM_{3ph} and RM_{SYM} algorithms, as indicated in (7.4). However, in order to conservatively regard the hidden losses, the value might be multiplied by the factor 1.05 as calculated above.

7.1 Relationship to Voltage Quality

Section 5.2 compared several allocation algorithms—$RM_{\Sigma 1ph}$, $RM_{3\mathrm{ph}}$ and RM_{SYM}—and showed how each treats situations in which adjacent phases export and import energy simultaneously. The previous subsection then demonstrated that the symmetrical-component measurement available at the PoC can be exploited to estimate the additional losses caused by power unbalance in phases. Fig. 7.3 extends this idea by linking the loss-estimation concept to two long-standing regulatory approaches for limiting the unbalanced operation: 1) limiting the maximum power difference between phases, and 2) restricting the emission of voltage unbalance.

Fig. 7.3 was generated from Fig. 7.2A by rotating the original coordinate frame by 54.74 °, such that the body diagonal highlighted in Fig. 7.2A becomes the vertical axis of Fig. 7.3. This rotation enables geometric symmetry, but it also means that the new x-, y-, and z-coordinates no longer map directly to the per-phase powers, even though the axes retain kilowatt units.

The colored surfaces in Fig. 7.3 thus play the same explanatory role as their counterparts in Fig. 7.2A:

- The grey surface groups operating points for which the algebraic sum of the three phase powers is zero.
- The red surface groups points where the positive-sequence active power is zero, calculated for a phase-conductor impedance of (0.24+j0.16) Ω and a neutral-to-phase impedance ratio of R_N/R_L=2/3 (reference impedance).

For comparison, additional surfaces are plotted for positive-sequence power equal to zero when the PoC impedances correspond to the 80th-percentile values observed in European LV feeders:

- green surface: (0.41+j0.16) Ω (typical of Czech and Austrian networks); and
- pink surface: (0.13+j0.09) Ω (typical of Swiss networks).

These surfaces make the impact of phase-power imbalance on loss power immediately visible: the farther an operating point lies from the grey plane (zero algebraic sum), the larger the extra losses, and the magnitude of that offset clearly depends on the local connection impedance.

Because the loss power increases with the PoC impedance, customers located at the remote ends of long LV feeders may appear "worse" simply due to their location—a potentially discriminatory outcome. A straightforward correction might be to introduce an individual correction factor K_{corr} that scales the estimated loss according to the customer's individual PoC impedance (7.5). With K_{corr} derived from a coarse impedance matrix of the LV network the loss estimate is normalized so that all PoCs share a common, "unified" limit surface (Fig. 7.3), while the underlying principle—penalizing excessive asymmetry—remains intact and the total losses can be equitably apportioned among the connected customers.

$$P_1^+ = \left(\sum_{x=L1,L2,L3} P_1^x \right) - K_{corr} \cdot (P_1^- + P_1^0) \tag{7.5}$$

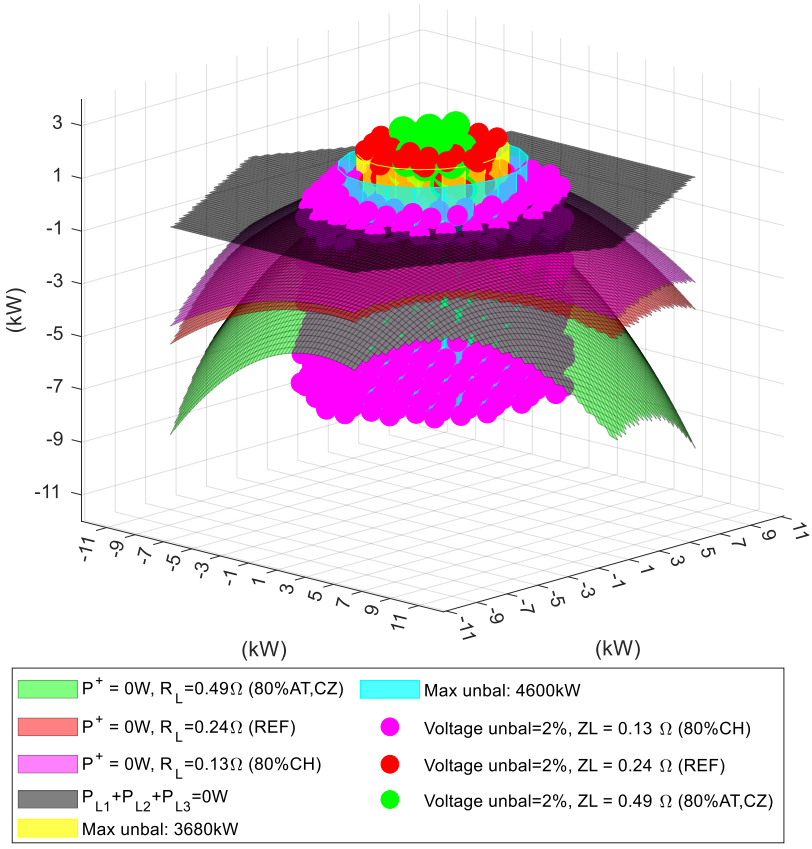

Fig. 7.3: Losses and voltage unbalance during unbalanced energy flow at PoC in typical European low voltage distribution grids.

In Fig. 7.3 several additional operating boundaries are super-imposed on the previously discussed surfaces.

- A yellow and a blue cylindrical surface enclose the continuous set of points for which the maximum phase-to-phase power difference equals 3.68 kW and 4.60 kW, respectively. These cylinders therefore delimit the region that the PoC could occupy if a limit of 3.68 kW (or 4.60 kW) on inter-phase power imbalance was applied.
- The figure also marks operating points that keep the resulting voltage unbalance contribution below 2 %. The color coding reflects realistic LV impedances: green points correspond to the 80th-percentile impedances found in Czech and Austrian feeders, red to the reference impedance, and pink to Swiss feeders.

A comparison of these colored surfaces shows that coordinating 1) a limit on the phase-power difference and 2) a constraint on voltage unbalance may essentially select the same subset of PoC states.

It is evident that, in order to guarantee the voltage unbalance using a phase-power difference limit, the threshold must be defined such that all theoretical PoC states

satisfying the given power limit constitute a subset of the states complying with the unbalance limit. However, it is desirable that the set of states fulfilling the voltage unbalance limit be broader, since the power limit is defined for a single PoC, whereas the voltage unbalance limit is composed of contributions from all PoCs in the DS. The difference between these sets of states should therefore be determined by the assumed simultaneity, where, in defining the overlap, simultaneity may be considered analogously to the assessment of individual disturbance contributions as in [57]. Finally, restricting voltage unbalance automatically curtails the additional losses associated with unbalanced power flow, and vice-versa.

The imposed limits also shrink the discrepancy between the $RM_{3\mathrm{ph}}$ and RM_{SYM} algorithms, because the admissible operating points remain close to the vertical axis, where both algorithms coincide. Although $RM_{\Sigma 1ph}$ still resolves the individual phase powers—as shown in Fig. 7.2A —it differs from $RM_{3\mathrm{ph}}$ in far fewer cases, since many of the extreme asymmetric states are excluded by the defined limits.

8. MICROGRIDS

Publications [A11] and [A12] extend the discussion to multi-prosumer environments presented as shared networks—physical or virtual micro-grids that interface with the public DS through a single PoC. This setting captures both local private grids and community-energy schemes and therefore places the findings of sections 5.1 and 5.2 in a realistic distribution-system context.

- Reference [A11] investigates time-domain bi-directional energy flow: how each allocation algorithm reacts when the net power at the PoC oscillates between import and export.
- Reference [A12] focuses on phase-domain bi-directional energy flow: situations in which different phases simultaneously import and export energy. A realistically parameterized LV micro-grid is simulated for one year of prosumer profiles. The results moreover quantify the additional system losses induced by prosumers behavior

Together, these studies demonstrate that both fast directional changes and inter-phase asymmetry materially influence billing accuracy and loss allocation in shared prosumer networks—reinforcing the need for the enhanced algorithms and loss-estimation techniques introduced earlier.

8.1 Asymmetrical Energy Flow in a Microgrid

Asymmetric power flows are analyzed in [A12] using the micro-grid configuration shown in Fig. 8.1A, which may be regarded as a minimal example of an energy community. Three revenue-class meters are installed 1) at the points of common coupling of the two prosumers (PRO1,PoC and PRO2,PoC), and 2) at the point where the micro-grid connects to the public DS (FEED, PCC). Each meter simultaneously implements the three allocation algorithms $RM_{\Sigma 1ph}$, RM_{3ph} and RM_{SYM}.

Mathematically, the micro-grid is represented by the network model in Fig. 8.1B. Steady-state operating points are specified by the power outputs of the individual members (modelled as controlled current sources) and by the voltage of the upstream feeder (modelled as ideal voltage sources). The line impedances inside the micro-grid are scaled fractions of the reference low-voltage impedance in LV public distribution networks.

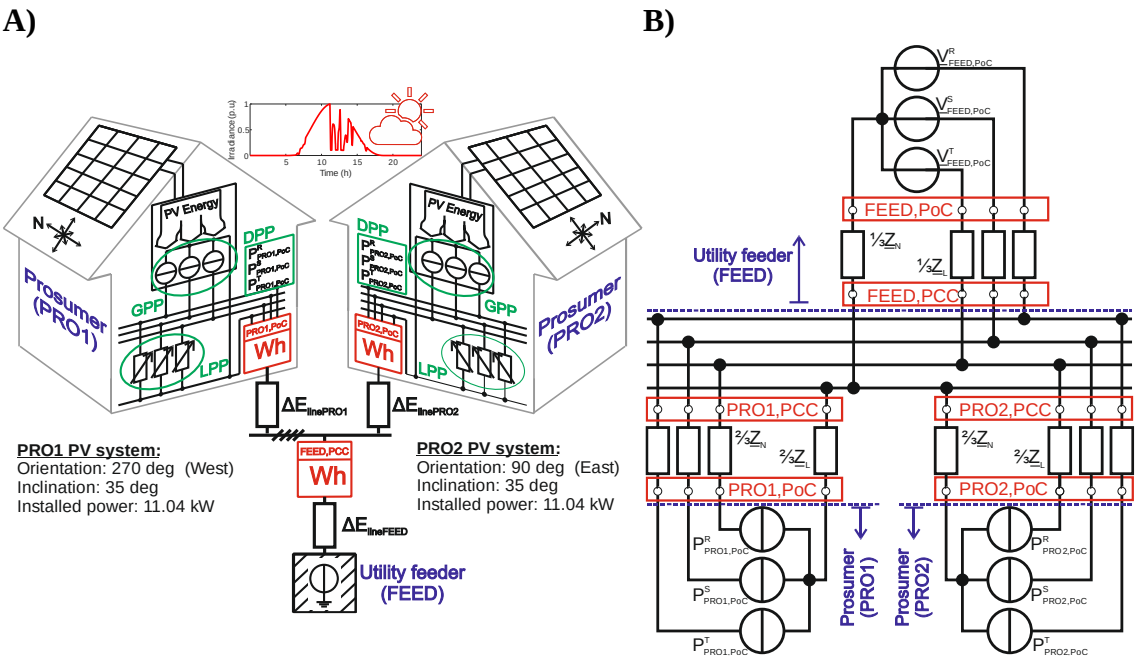

Fig. 8.1: Low-voltage three-phase four-wire testing microgrid with two prosumers connected to DS via single PoC, realistic use-case (A) and electrical scheme (B) [A12].

8.1.1 Specific Steady-states

The network of Fig 9.2 was simulated under a set of steady-state operating points that represent different energy-sharing scenarios among the micro-grid members (Tab. 8.1). Beyond the findings already documented in [A12], the additional observations follow:

- Case 7 – Fully symmetric sharing. All three metering algorithms ($M_{\Sigma 1ph}$, RM_{3ph} and RM_{SYM}.) record identical active-power values at every measurement point. At FEED,PCC the registered power equals the total ohmic losses of the micro-grid, ΔP_{act}.
- Case 8 – Asymmetric sharing in the same phase. At FEED,PCC every algorithm again records ΔP_{act}, but the loss power is now more than four times higher than in Case 7 for the same sharing power. Inside the community, RM_{SYM} registers the positive-sequence power; its magnitude exceeds (import) or falls short of (export) the arithmetic sum by exactly the negative- plus zero-sequence components.
- Case 9 – Asymmetric sharing in different phases. The three algorithms diverge at FEED, PCC. The difference between the import and export registers of RM_{3ph} and $RM_{\Sigma 1ph}$ is the same (136.6 W), whereas the difference in case of RM_{SYM} equals the total system losses. Compared to RM_{3ph}, the $RM_{\Sigma 1ph}$ additionally records simultaneous import and export, revealing that the public grid is providing a balancing service. Within the community, the sum of the negative- and zero-sequence powers (190.3 W) matches the loss power due to asymmetrical power, while the overall loss power ΔP_{act} are given by this

value plus the equivalent balanced-state loss power, which is actually the Case 7 (27.3 W).

- Case 10 – Individual PoC imbalance with phase-coherent sharing. All algorithms report the same power at FEED, PCC, equal to the total micro-grid loss power, similarly as in Case 7. At the individual PoCs, RM_{3ph} records zero, $RM_{\Sigma 1ph}$ separates power import and export, and RM_{SYM} assigns each prosumer an almost equal share of the loss power (the 0.6 W difference is matter of further study).
- Case 11 – Voltage unbalance propagated through the feeder. An unbalanced flow from one prosumer produces a voltage unbalance at FEED, PCC that, in turn, forces an otherwise symmetric three-phase resistive load of another prosumer to draw unbalanced currents. None of the three metrics, however, penalizes this second prosumer: at its PoC every algorithm reports the sum of the power in the phases.

In all the Cases 7–9 one community member is a pure exporter, the other a pure importer, and the exchanged active power is fixed at 3.68 kW. A comparison of network losses reveals a clear hierarchy of efficiency:

- Case 7 (phase-balanced exchange) produces the lowest loss.
- Case 8 (identical phase unbalance for both members) incurs higher—but still moderate—losses.
- Case 9 (different phase unbalance at each member) is the least efficient; the dissipated active power is almost eight-times that of the symmetric benchmark (Case 7).

Thus, a mismatch between the members' asymmetric phase powers causes losses to an order of magnitude (order of eight times higher in this particular analysis) above the symmetrical case. Despite this, the metering algorithms RM_{3ph} and $RM_{\Sigma 1ph}$ record the same import/export figures in all three scenarios; they therefore provide no incentive for participants to phase-symmetrize their power at the PoC and, by extension, no encouragement to adopt the loss-minimizing sharing.

Tab. 8.1 Specific states of two-member energy community.

		Case 7	Case 8	Case 9	Case 10	Case 11
PoM		***Y* = PRO1,PoC (Prosumer 1)**				
P_Y^R (W)		1226.7	3680.0	3680.0	1840.0	1840.0
P_Y^S (W)		1226.7	0.0	0.0	-1840.0	-1840.0
P_Y^T (W)		1226.7	0.0	0.0	0.0	0.0
P_Y^+ (W)		3680.1	3738.2	3772.3	40.7	60.9
$P_Y^- + P_Y^0$ (W)		0.0	-58.2	-92.3	-40.7	-60.9
$P_Y^{\Sigma 1ph}$ (W)	Imp	3680.1	3680.0	3680.0	1840.0	1840.0
	Exp	0.0	0.0	0.0	-1840.0	-1840.0
P_Y^{3ph} (W)	Imp	3680.1	3680.0	3680.0	0.0	0.0
	Exp	0.0	0.0	0.0	0.0	0.0
P_Y^{SYM} (W)	Imp	3680.1	3738.2	3772.3	40.7	60.9
	Exp	0.0	0.0	0.0	0.0	0.0
PoM		***Y* = PRO2,PoC (Prosumer 2)**				
P_Y^R (W)		-1226.7	-3680.0	0.0	-1840.0	1201.8
P_Y^S (W)		-1226.7	0.0	-3680.0	1840.0	1228.8
P_Y^T (W)		-1226.7	0.0	0.0	0.0	1208.6
P_Y^+ (W)		-3680.1	-3628.7	-3582.0	41.3	3639.1
$P_Y^- + P_Y^0$ (W)		0.0	-51.3	-98.0	-41.3	0.1
$P_Y^{\Sigma 1ph}$ (W)	Imp	0.0	0.0	0.0	1840.0	3639.2
	Exp	-3680.1	-3680.0	-3680.0	-1840.0	0.0
P_Y^{3ph} (W)	Imp	0.0	0.0	0.0	0.0	3639.2
	Exp	-3680.1	-3680.0	-3680.0	0.0	0.0
P_Y^{SYM} (W)	Imp	0.0	0.0	0.0	41.3	3639.1
	Exp	-3680.1	-3628.7	-3582.0	0.0	0.0
PoM		***Y* = FEED,PCC (Utility feeder)**				
$P_Y^{\Sigma 1ph}$ (W)	Imp	27.3	136.9	3752.3	82.0	4276.5
	Exp	0.0	0.0	-3615.8	0.0	-583.1
P_Y^{3ph} (W)	Imp	27.3	136.9	136.6	82.0	3693.4
	Exp	0.0	0.0	0.0	0.0	0.0
P_Y^{SYM} (W)	Imp	27.3	137.0	217.6	82.0	3713.6
	Exp	0.0	0.0	0.0	0.0	0.0
ΔP_{act} (W)		27.3	137.0	217.6	82.0	81.3

8.1.1 Daily Power Profile

The configuration of Fig. 8.1 was further subjected in [A12] to a time-series simulation consisting of consecutive 1-s steady-state states that jointly emulate a full-day power profile. Two sets of curves are examined:

- Baseline scenario (Fig. 8.2A). The traces represent the natural 24-h variation of active power at the points of common coupling of the micro-grid members (Prosumer 1 - PRO1,PoC and Prosumer 2 - PRO2,PoC) as well as at the interface with the public DS (FEED,PCC). Both members possess generation

and demand, so the power at PoC powers can swing between import and export over the day.

- Controlled-load scenario (Fig. 8.2B). Here Prosumer 2 employs an energy diverter—typically a water-heating element—to absorb surplus PV output and thereby prevent export at its PoC. The additional load is connected to only one phase, and the control signal is derived from the RM_{3ph} algorithm, simulating the behaviour of commercially available single-phase diverters [75].

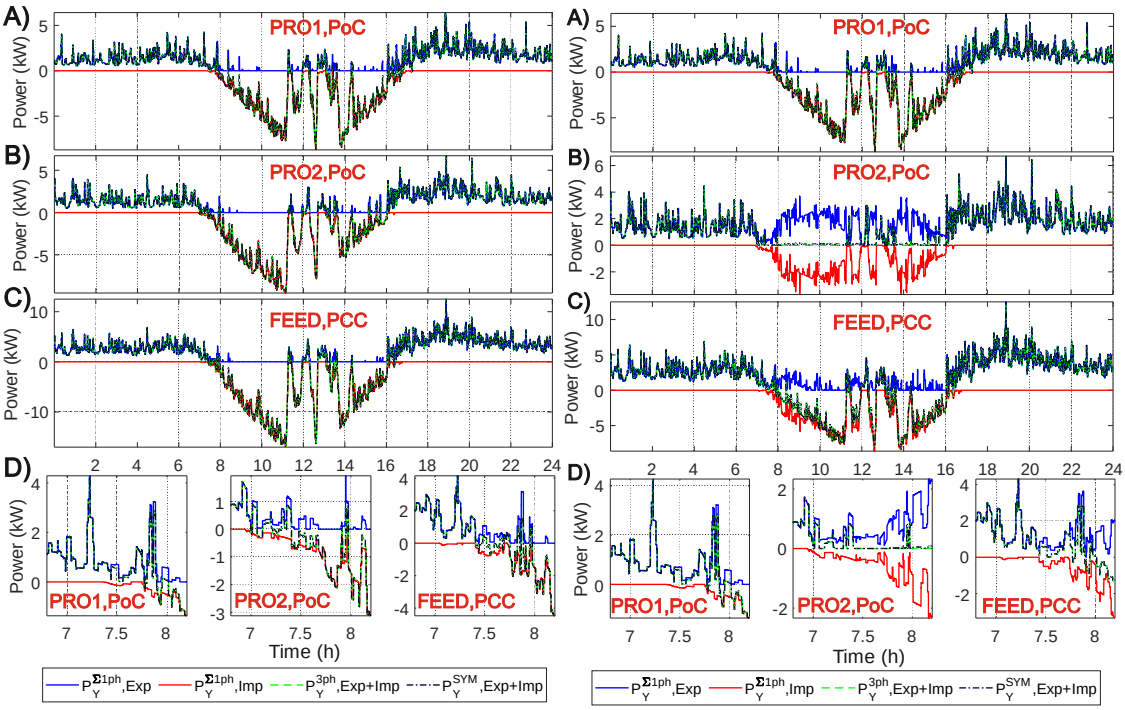

Fig. 8.2: 1-second power profiles in a microgrids without active diverting (left) and with deployment of commercial energy diverter (right) [A12].

Fig. 8.3A compares the total energy recorded during the simulation (Fig. 8.2A) by the three metering algorithms— $RM_{\Sigma 1ph}$, RM_{3ph} and RM_{SYM}—at each monitoring point of the micro-grid model in Fig. 8.1B. All values are normalized to the energy registered by $RM_{\Sigma 1ph}$ (taken as 100 %).

- $RM_{\Sigma 1ph}$ consistently registers the largest energy total at every location.
- Readings from RM_{SYM} and RM_{3ph} are ~2–4 % lower than those of $RM_{\Sigma 1ph}$.
- RM_{SYM} shifts a fraction of energy from the export to the import register relative to RM_{SYM}—thus it records less exported and more imported energy.

Analysis of Fig. 8.3B yields following findings:

- At each prosumer PoC, the difference between the energies registered by RM_{SYM} and RM_{3ph} exactly matches the additional loss power generated by asymmetrical power (ΔE_{add}).

- Under the baseline scenario—prosumers operating without any active power-diverting—this imbalance loss ΔE_{add} accounts for ~25 % of the total active losses in the micro-grid (ΔE_{act}).

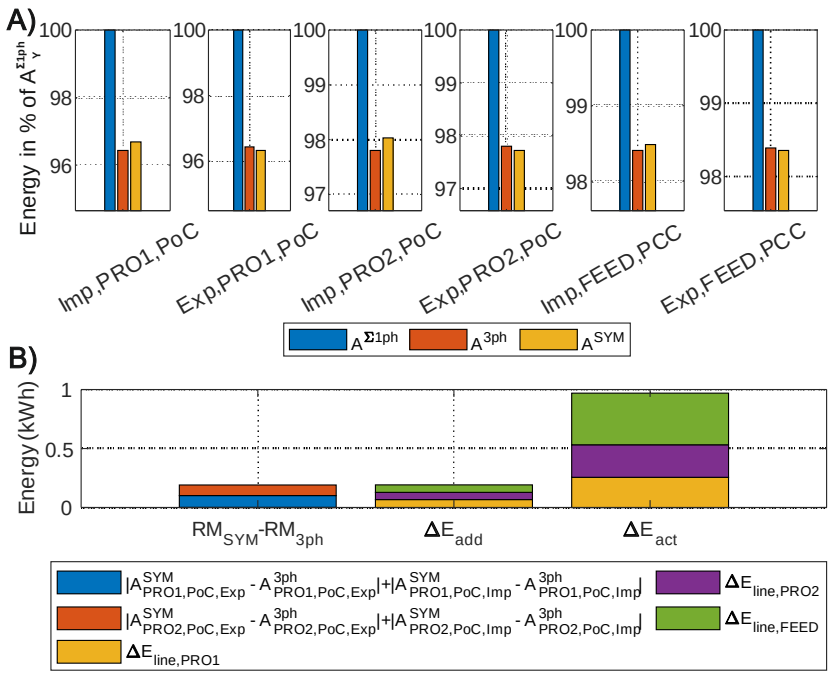

Fig. 8.3: Registered energy (A) and energy losses (B) in the system, controlled-load scenario [A12].

Fig. 8.4A shows the registered energy, if a micro-grid member (Prosumer 2) employs a single-phase energy diverter in order to eliminate the energy export. The Fig. 8.4A shows:

- At the PoC of non-diverting micro-grid member (Prosumer 1), RM_{SYM} and RM_{3ph} deviate from $RM_{\Sigma 1ph}$ by ~4 %, as the probability opposite-direction phase imbalances is given only the natural behavior of the member.
- At the PoC of actively diverting micro-grid member (Prosumer 2), the same algorithms diverge by ~30 % in the import register and ~100 % in the export register, due to higher incidence of counter-directional power in phases caused by the diverter.
- At the measuring point between micro-grid and public DS, the difference between algorithm rises to ~7 % (import) and ~15 % (export), showing that phase-selective control of a member causes asymmetrical counter-directional power states even in the micro-grid.

Fig. 8.4B documents following findings:

- At each prosumer PoC, the difference between the energies registered by RM_{SYM} and RM_{3ph} exactly matches the additional loss power generated by asymmetrical power (ΔE_{add}).

- In diverting scenario, the imbalance loss ΔE_{add} accounts for ~50 % of the total active losses in the micro-grid (ΔE_{act}), which is double the share observed in the baseline scenario.

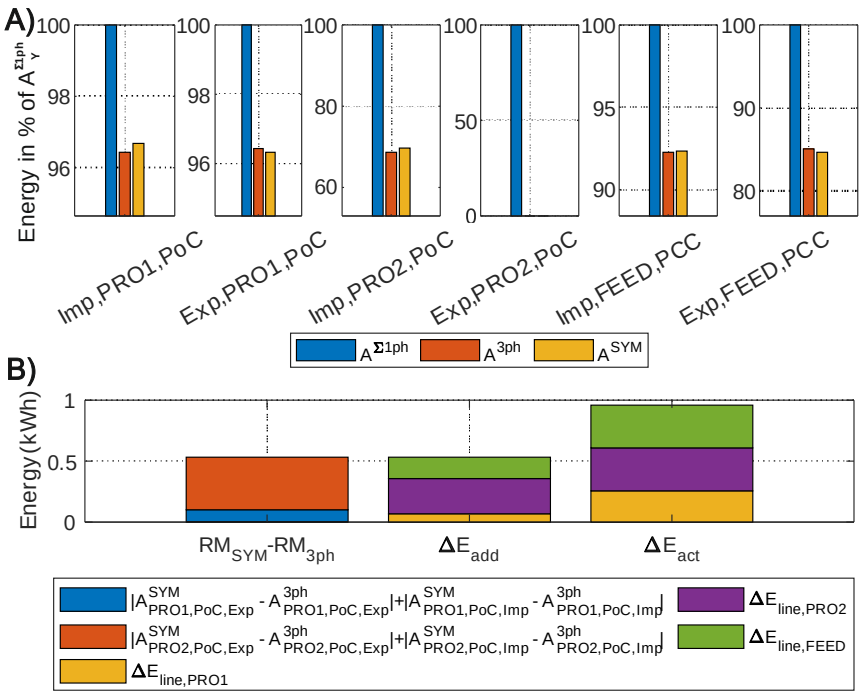

Fig. 8.4: Registered energy (A) and energy losses (B) in the system, power diverting scenario [A12].

By comparing the columns of total losses ΔE_{act} in Fig. 8.3B and Fig. 8.4B, the following conclusions can be drawn:

- the overall magnitude of losses in the entire system remains unchanged (~1 kWh) when the active energy diverter for energy self-sufficiency is applied,
- although losses in the upstream DS are reduced through active diverting (green part, $\Delta E_{line,FEED}$, by ~0.1 kWh), this reduction is offset by an increase in losses within the DS section between prosumers (LV DS or microgrid), most prominently diverting prosumer's section $\Delta E_{line,PRO2}$ (shown in violet).

In practical terms, this use-case analysis demonstrates that active diverting for the purpose of energy self-sufficiency does not necessarily lead to a reduction in DS utilization by prosumers (defined by reduction of energy losses in DS) if the diverting is targeted at a power component assuming simplifying assumptions in its definition, which fail to account for the actual energy exchange across the PoM in all phases.

8.2 Dynamic Changes of Power Direction in a Microgrid

This section investigates how the discrepancies among the active-power algorithms listed in Section 5.1 influence observability and energy accounting within a micro-grid under dynamically varying operating conditions [A11].

Experimental set-up (Fig. 8.5), set in a laboratory, represents a single-phase micro-grid connected to the public DS and hosts two members at their respective PoC:

- CON (upper end-user in Fig. 8.5) – a pure consumer represented by a 1 kW, 230 V resistive load.
- PRO (lower end-user in Fig. 8.5) – a prosumer equipped with 1) photovoltaic inverter supplied by a programmable DC source, and 2) a 4 kW, 230 V resistive load switched by a soli d-state relay that switches at the voltage zero-crossing. The relay is pulse-width regulated with a fixed cycle (5 s in Fig. 8.5), intended to produce a dynamic export profile.

Measurement points are placed at both members' PoCs (PoC,CON and PoC,PRO) and at the interface of the micro-grid and the public network (PoC, FEED). At each point:

- Instantaneous voltage and current waveforms are recorded by a high-speed data logger, which are used for a calculation of a reference active-energy (REF, green) and allowing post-process calculation using selected algorithms from Section 5.1 (STD50 p, STD10 p, STD1/2 p, grey).
- A commercial revenue meter (Real RM, black) is installed. The FEED meter provides separate import and export registers as well as pulse outputs (metallic contacts PO+ for import and PO– for export, and an optical LED).
- The registered energy readings are logged in 56.88 min test while all the parameters (power, voltage, etc.) has been kept constant.
- Further details of the hardware implementation are given in [A11].

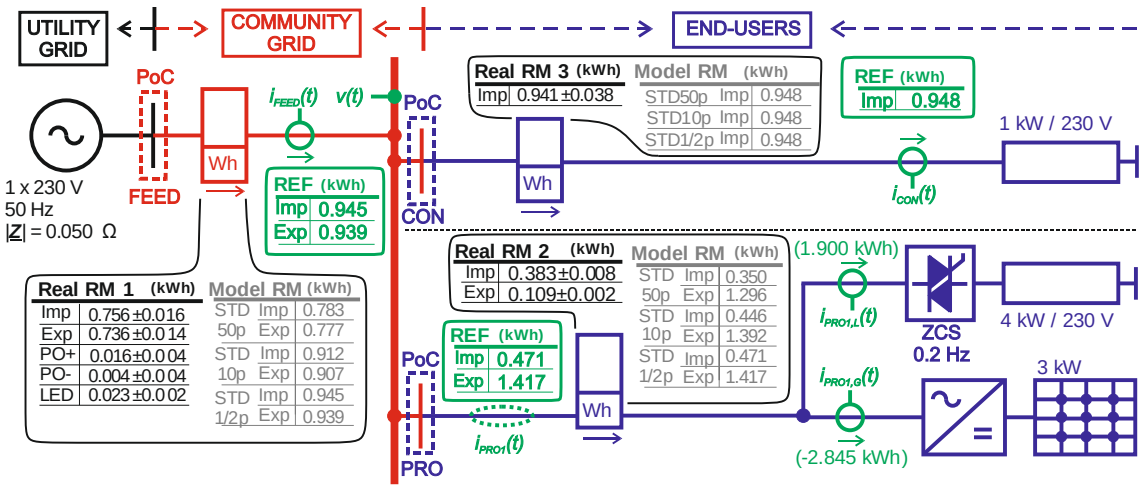

Fig. 8.5: Low-voltage testing microgrid with a prosumer and consumer, connected to DS via single PoC [A11].

Fig. 8.5 shows the active-energy increments registered in the import and export registers of the meters installed at each monitoring point. The observations are summarized below.

- The variations of active power in the testing micro-grid correspond to the periodic switching of the prosumer's 4 kW resistive load, confirming that the test scenario tests the meters with rapidly changing of active power.
- A comparison of the commercial meter (Real RM) with the model meter implementing algorithm STD-50p in all the measurement points shows agreement in both import and export registers. This indicates that all commercial meters in the set employ the STD-50p algorithm.
- The real meter located at the PoC, FEED calculates different values at its outputs indicating that the manufacturer has embedded different algorithms for individual outputs (cumulative registers – pulse outputs (metallic) – LED) inside the same meter.
- Whenever economic or regulatory meanings are assigned to the two registers independently—e.g. 1) differential tariffs for imported versus exported energy, 2) verification whether the average importing/exporting power over a billing interval remains below a contracted limit or 3) allocation of shared generation within a physical or virtual energy community—the result, however, directly depends on the implemented algorithm. Moreover, the deviations of the algorithms might be amplified by external factors such as poor time-alignment between the meter's evaluation window and rapid load changes (see Fig. 5.6).
- If the registered values are used to calculate the system energy balance, obtained by summing all import registers and subtracting all export registers (8.1), the net-balance (SALDO) is invariant with respect to the particular algorithm parametrization used in the meters. Tab. 8.2 confirms that the energy balance computed from STD50p, STD10p, or STD1/2p is numerically identical. However, the identical algorithm and its parametrization must be applied on import and export registers in single PoM.
- If the registered values are used to calculate the total energy entering A_{IN} (8.2) and leaving A_{OUT} (8.3) the microgrid, the results are variant with respect to the used algorithm, as shown in Tab. 8.2. Therefore, the calculation of the total energy, that the microgrid has transmitted, is ambiguous (see the red-marked values). However, the difference $|A_{IN} - A_{OUT}|$, representing energy loss in the system (generally non-measured loads), is invariant with respect to the used algorithm (0.004 kWh).

$$SALDO = A_{X,PROS}^{Imp} + A_{X,CON}^{Imp} + A_{X,FEED}^{Imp} - A_{X,PROS}^{Exp} - A_{X,FEED}^{Exp} \quad (8.1)$$

$$A_{IN} = A_{X,PROS}^{Exp} + A_{X,FEED}^{Imp} \quad (8.2)$$

$$A_{OUT} = A_{X,PROS}^{Imp} + A_{X,CON}^{Imp} + A_{X,FEED}^{Exp} \quad (8.3)$$

Tab. 8.2 Total SALDO values in the micro-grid for RMs implementing different calculation algorithms.

RM at PoC FEED	RM at PoC PRO	RM at PoC CON	SALDO (kWh)	A_{IN} (kWh)	A_{OUT} (kWh)	$\lvert A_{IN} - A_{OUT} \rvert$ (kWh)
REF	**REF**	**REF**	**0.008**	**2.362**	**2.358**	**0.004**
STD50p	STD50p	STD50p	0.008	2.079	2.075	0.004
STD1/2p	STD1/2p	STD1/2p	0.008	2.362	2.358	0.004
STD50p	STD1/2p	STD50p	0.008	2.200	2.196	0.004

8.3 Energy sharing in an Energy Community

An energy community is a socio-legal construct that enhance 1) collective ownership of generation assets or and the equitable distribution of the resulting benefits or 2) sharing the generated energy from a private generation asset on point-to-point basis, while still relying on the public distribution grid. Consequently, the geographical proximity is not a mandatory prerequisite for participation. The Czech regulatory framework, for example, recognizes three operational sharing modes [76]:

1. Community sharing – a legally constituted Energy Community of up to 1 000 customers drawn from no more than three administrative regions (with regional restriction).
2. Peer-to-peer (P2P) sharing – nationwide exchange among clusters of ≤ 11 customers, each customer able to draw from up to five generating units (without regional restriction).
3. Sharing behind single cable-box – highly localized sharing (e.g. within a multi-dwelling building) involving up to 1 000 customers, typically accompanied by reduced distribution charges.

Moreover, the communities might be further classified by their physical position in the grid [77]:

- Type A – all members located within one building;
- Type B – customers connected to the same MV/LV substation;
- Type C – MV and LV customers supplied by a common HV/MV substation;
- Type D – MV and LV customers fed from different HV/MV substations.

Although the primary objective of this taxonomy is to assign differentiated distribution- and transmission-fee discounts, it implicitly traces the electrical path taken by the shared energy and reflects the ownership boundaries of the distribution infrastructure. The present study concentrates on Type A communities (equivalent of 3rd group in Czech Republic), which frequently own the internal LV network that facilitates sharing. Such communities are typically equipped with a dedicated RM at the PoC,

intended for precise registration of the net energy exchange between the community and the public DS.

A use-case is conducted in order to examine the disturbing impacts on the allocation of the generated energy to the consumers within the energy community. The aspects considered in this use-case study, leading to deviations between real and allocated energy flow in energy community, are:

- selection of allocation key (AK),
- aggregation window length of RMs,
- missing measurements of energy flow (typically energy losses, auxiliary load consumption).

8.3.1 Model of the Residential Building Community

Fig. 8.6 shows the electrical circuit diagram of example energy community in residential building, consisting of PV generator exporting power P_{PV}, two consumers importing powers P_{conA}, P_{conB}, auxiliary loads importing power P_{aux} and grid feeder inherently maintaining the power balance (8.4) in the system by power P_{grid}.

$$P_{conA} + P_{conB} + P_{aux} = P_{DS} + P_{PV} \tag{8.4}$$

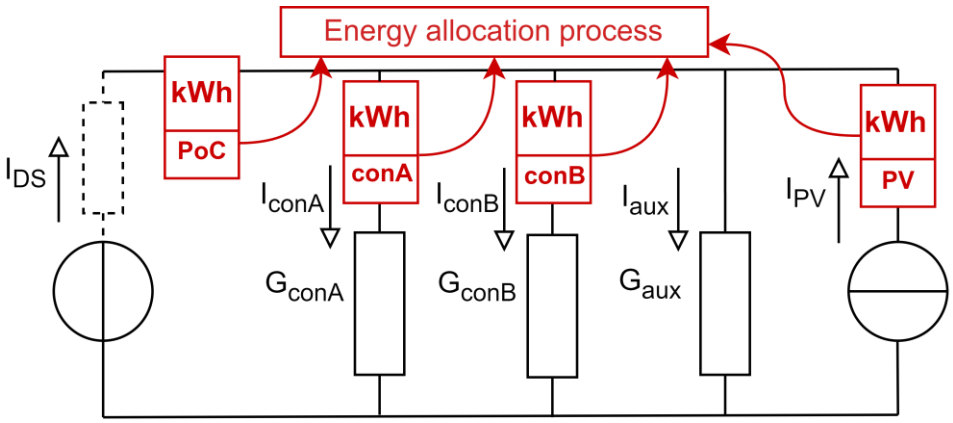

Fig. 8.6. Electrical circuit diagram of example energy community in residential building.

The PV generator is modelled as current source delivering current I_{PV}, the consumers and auxiliary load are modelled as conductance consuming current I_{conA} (consumer A), I_{conB} (consumer B), I_{aux} (auxiliary load) and the DS delivers current I_{DS}. The current equation for the circuit is (8.5).

$$I_{conA} + I_{conB} + I_{aux} = I_{DS} + I_{PV} \tag{8.5}$$

In absence of the DS, the PV generator would supply the loads according to the equation of current divider (8.6).

$$I_{PV-k} = I_{PV} \cdot \frac{G_k}{\sum_k G_k}, k = \{con1, con2, aux\} \tag{8.6}$$

The DS serves as an implicit power balancer, thus delivers the current into the loads (8.7).

$$I_{DS-k} = V \cdot G_k - I_{PV-k} \tag{8.7}$$

The residential building system is simplified, assuming that all the members (consumers, PV generator, auxiliary load and DS) are connected on single busbar (i.e. the voltage V is the same) and the model is single-phase equivalent.

8.3.2 Deviation due to Allocation Keys

An allocation key (AK) specifies how the energy generated within a community during a metering interval is apportioned to individual consumers. Three AK classes are commonly recognized: static, dynamic, and hybrid.

Because allocation is executed at each measurement interval, the AK partitions the photovoltaic power in the interval is P_{PV} among the participating members. To reflect the actual current paths, the AK should be derived from (8.6). If one further assumes 1) that only the active-current component is relevant and 2) that mutual impedances between consumers are negligible, the portion of PV power delivered to member *k*, (P_{PV-k}), is given by (8.8); this expression therefore serves as the reference dynamic AK. The grid power attributed to the same member under this dynamic AK, P_{DS-k}^{dyn}, follows (8.9).

$$P_{PV-k}^{dyn} = P_{PV} \cdot \frac{P_k}{\sum_k P_k} \tag{8.8}$$

$$P_{DS-k}^{dyn} = P_k - P_{PV-k}^{dyn} \tag{8.9}$$

Conversely, an allocation key may not reflect the physical flow of electricity; it can be designed to satisfy explicit sharing- or trading-objectives. To that end, static and hybrid AKs are defined [78].

A static AK allocates the community's generation in each metering interval according to fixed coefficients K_k specified a priori by the members. The static allocation runs in iterations, where in each iteration i the P_{PV}^i (Fig. 8.6) is allocated to members consuming power P_k^i. In the first iteration, the $P_{PV}^i = P_{PV}$ and $P_k^i = P_k$. The reserved power for k-th consumer ($P_{PV-k}^{res,i}$) is calculated as (8.10). The allocated power is then minimum of P_k^i and P_{PV-k}^{res} (8.11). After the first iteration, the P_{PV} is updated to P_{PV}^{i+1} (8.12) and P_k to P_k^{i+1} (8.13). The (8.10) - (8.11) are repeated in next iteration with the updated values. Finally, the final P_{PV-k}^{stat} is a sum of the allocated power in the N iterations (8.14). The power consumed from the grid according to the static allocation key P_{grid-k}^{stat} is calculated as (8.15).

$$P_{PV-k}^{res,i} = P_{PV}^i \cdot K_k \tag{8.10}$$

$$P_{PV-k}^{stat,i} = \min\left(P_{PV-k}^{res,i}, P_k^i\right) \tag{8.11}$$

$$P_{PV}^{i+1} = P_{PV}^i - \sum_k P_{PV-k}^{stat,i} \tag{8.12}$$

$$P_k^{i+1} = P_k^i - P_{PV-k}^{stat,i} \tag{8.13}$$

$$P_{PV-k}^{stat} = \sum_i^N P_{PV-k}^{stat,i} \tag{8.14}$$

$$P_{DS-k}^{stat} = P_k - P_{PV-k}^{stat} \tag{8.15}$$

A hybrid AK combines the advantages of the dynamic and static schemes—simultaneously respecting the physical power flow while honoring the contractual preferences of community members. As an illustrative case, consider a hybrid rule that first serves an auxiliary (house-service) load and then distributes any residual PV output among the remaining participants in proportion to their demand.

In the first step, the allocated power to the auxiliary load (P_{PV-aux}^{hyb}) is minimum of the P_{PV} and P_{aux} (8.16). Then, the unallocated generator power is allocated to the consumers as in case of dynamic AK (8.17). The power consumed from the grid according to hybrid allocation key P_{grid-k}^{hyb} is calculated as (8.18).

$$P_{PV-aux}^{hyb} = \min(P_{PV}, P_{aux}) \tag{8.16}$$

$$P_{PV-k}^{hyb} = (P_{PV} - P_{PV-aux}^{hyb}) \cdot \frac{P_k}{\sum_k P_k} \tag{8.17}$$

$$P_{DS-k}^{hyb} = P_k - P_{PV-k}^{hyb} \tag{8.18}$$

The community's net import from the DS and its export back to the grid—calculated under each AK ($m = \{dyn, stat, hyb\}$) —are obtained from (8.19) and (8.20).

$$P_{DS-com}^{m} = \sum_k P_{DS-k}^{m} \tag{8.19}$$

$$P_{com-DS}^{m} = P_{PV-DS}^{m} = P_{PV} - \sum_k P_{PV-k}^{m} \tag{8.20}$$

The performance of the three AKs—dynamic, static, and hybrid—was evaluated through a time-domain simulation of a residential community (Fig. 8.6). Fig. 8.8 depicts the individual load and generation profiles used in the study.

- Photovoltaic source. The PV-generation profile $P_{PV}(t)$ (blue line in Fig. 8.8 and normalized to maximal power in Fig. 8.7) represents an ideal clear-sky irradiance pattern modulated by stochastic cloud cover, yielding a daily energy output of 4.56 kWh over the 24-h horizon.
- Consumers A and B. Each consumer's demand $P_{conA}(t)$ and $P_{conB}(t)$ combines 1) a 200 W baseload and 2) a set of resistive appliances whose on/off states follow a Poisson distribution. Appliance powers range from 5 W to 3.48 kW, with switch-on times inversely proportional to rated power. The aggregate daily energies are 6.08 kWh for Consumer A and 3.75 kWh for Consumer B.
- Load-profile shaping. Appliance-switching intensities are moreover weighted by hourly normalized load-profile vectors: LP1 (Consumer A) mirrors a standard nationwide residential profile, whereas LP2 (Consumer B) is biased toward periods of peak solar production (Fig. 8.7).

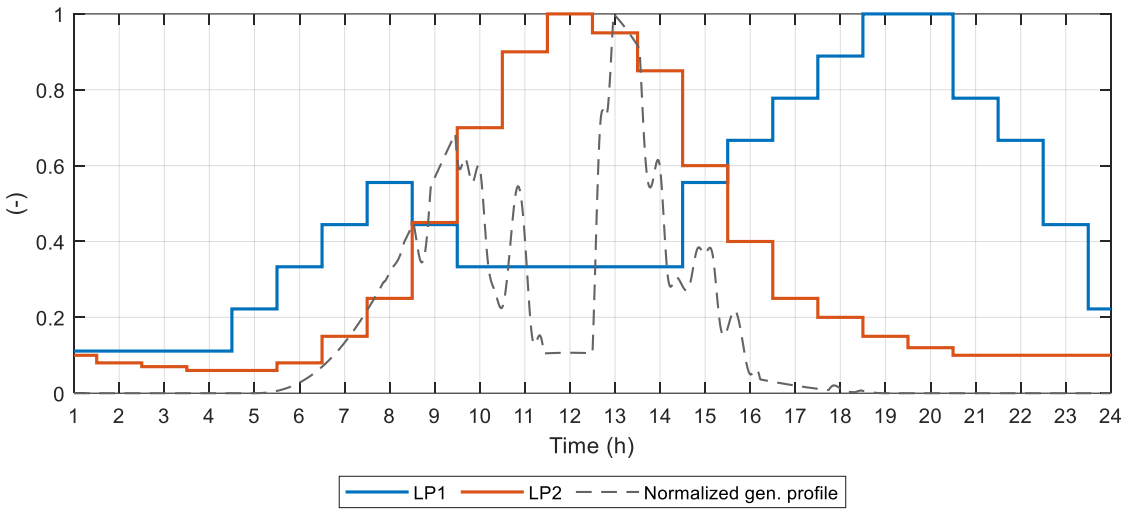

Fig. 8.7. Normalized 24-hour load profiles of the consumers.

The auxiliary power profile $P_{aux}(t)$ is composed of 0.8 kW power pulses with duration of 2 min and repeated every single hour (consumed energy 1.28 kWh in 24 h). The power at PoC P_{PoC} is sum of the abovementioned power profiles.

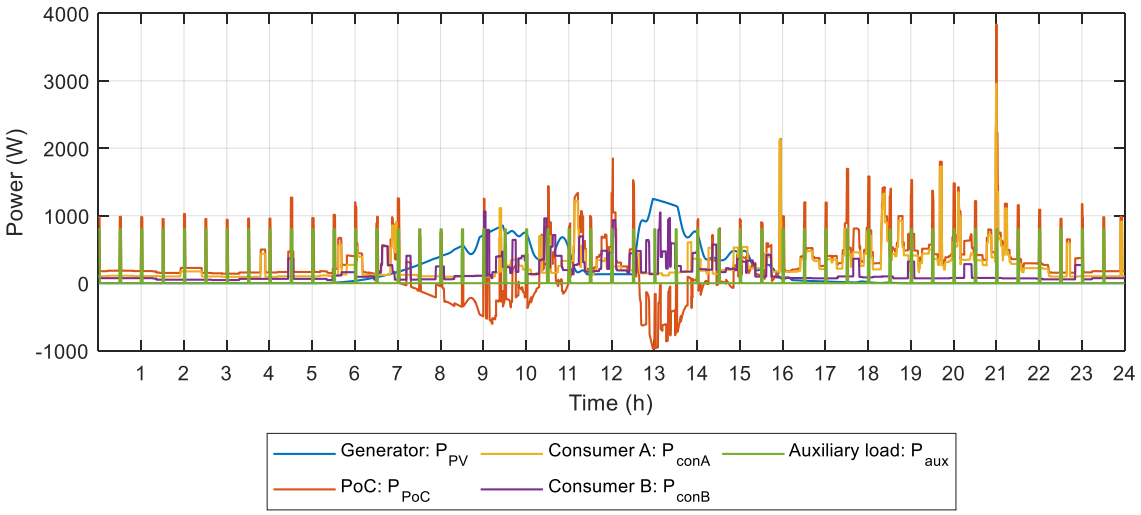

Fig. 8.8. Realistic 24-h power profiles of the community members, resolution of 1 s.

Tab. 8.3 reports the energies apportioned to each community member by the respective AKs. Every entry was computed with the general relation (8.21): the total energy equals the sum of the elemental increments ΔA_b (8.22) taken over all sub-intervals b with duration Δt_b, in which the allocated power P_b is constant.

$$A = \sum_b^B \Delta A_b \tag{8.21}$$

$$\Delta A_b = P_b \cdot \Delta t_b \tag{8.22}$$

Tab. 8.3 contrasts the energy shares assigned by four allocation keys: the dynamic AK, the hybrid AK, and two variants of the static AK—1) with a priori arbitrary

coefficients (Static 1) and 2) with coefficients proportional to the participants' annual consumption (Static 2).

The results in Tab. 8.3 confirm that the dynamic AK, being derived from real energy flow, distributes energy in strict accordance with the physical flow inside the community. Consequently, the community's net import and export calculated under this key exactly match the energy recorded by the RM at the PoC.

Tab. 8.3 Energy allocation within the community using different allocation keys (allocation on 1s basis).

Allocation key	PV ↓ ConA	PV ↓ ConB	PV ↓ Aux	PV ↓ DS	Grid ↓ ConA	Grid ↓ ConB	Grid ↓ Aux	Comm ↓ Grid (AK)	Grid ↓ Comm (AK)	Import at PoC (RM)	Export at PoC (RM)
(kWh)											
Real energy flow	1.460	1.650	0.198	1.248	4.625	2.101	1.082	1.248	7.808	7.808	1.248
Dynamic	1.460	1.650	0.198	1.248	4.625	2.101	1.082	1.248	7.808		
Static 1*	1.457	1.699	0.048	1.352	4.628	2.052	1.232	1.352	7.912		
Static 2**	1.567	1.534	0.055	1.399	4.517	2.217	1.225	1.399	7.959		
Hybrid	1.419	1.607	0.283	1.248	4.666	2.145	0.997	1.248	7.808		
Deviation from real energy flow (%)											
Dynamic	0.00	0.00	0.00	0.00	0.00	0.00	0.00	0.00	0.00	--	--
Static 1*	-0.19	2.99	-75.75	8.31	0.06	-2.35	13.89	8.31	1.33		
Static 2**	7.39	-7.01	-72.13	12.09	-2.33	5.51	13.23	12.09	1.93		
Hybrid	-2.81	-2.63	42.49	0.00	0.89	2.06	-7.79	0.00	0.00		

* Arbitral sharing coefficients: $K_{conA}:K_{conB}:K_{aux}$ = 45:45:10.

** Sharing coefficients based on annual consumption: $K_{conA}:K_{conB}:K_{aux}$ = 547:338:115.

By contrast, the static AKs deviate from the physical flows. The variant with arbitrary coefficients (Static 1) yields smaller allocation errors than the variant scaled to annual consumption (Static 2); moreover, the error changes polarity for different members. This outcome illustrates that tailoring static coefficients to long-term energy use does not necessarily bring the allocation closer to real-time power flows. The magnitude and sign of the error depend mainly on how the real load ratio in every evaluation interval (15 min in this case) differs from the chosen static coefficients. In the present case, Consumer B—whose total daily demand is lower than Consumer A's—receives a smaller static share, yet its demand peaks coincide with PV production (Fig. 8.7), amplifying the misallocation. The import/export inferred from the static AKs diverge from the meter at PoC by 8.33 %/1.33 % (Static 1) and 12.18 %/1.93 % (Static 2), respectively.

The hybrid AK does not replicate the intra-community power flow, because its initial steps apply an arbitrary priority rule. Nevertheless, its final balancing step enforces the proportional rule of (8.6), so the community-level energy import and export exactly coincide with the PoC meter. Hence a hybrid AK that combines contractual priorities with a real flow-consistent principle preserves the community energy balance even though the energy allocated inside the community differ from the real energy flow.

8.3.3 Deviation due to Meter-Aggregation Interval

To isolate the influence of meter-aggregation (evaluation) interval, the residential community of Fig. 8.6 was resimulated with aggregation interval set to 1 s (reference), 1 min, 5 min, 10 min, and 15 min. A dynamic AK was retained throughout so that any deviation would stem solely from temporal aggregation, not from the AK itself.

Tab. 8.4 and Tab. 8.5 reveal a clear trend: the longer the aggregation window (and thus the evaluation period), the larger the discrepancy between the allocated energies and the physical energy flows. As the aggregation interval increases, each AK (dynamic or static) allocates progressively more PV energy to the consumers (positive percentage bias) and progressively less grid energy (negative bias). Consequently, the total energy recorded as imported from the DS—and, symmetrically, the energy exported to it—declines with increasing aggregation interval. The net effect is that the community appears more self-sufficient when longer metering intervals are used.

In the presented case, extending aggregation interval from 1 s to 15 min induces an error of +22.9 % / +25.8 % in the community total exported energy and –3.65 % / –4.41 % in the community total imported energy for the Dynamic / Static 1 AK, respectively.

It is clear from the results in Tab. 8.4 and Tab. 8.5, that the deviation of allocated energy from real energy flow (1s basis) increases with increasing length of the aggregation interval. The expectable deviation is evaluated for a testing system with a single set of power profiles and may be both positive and negative. The deviation is, however, dependent on 1) ratios of produced and consumed energy within the community and 2) correlation of consumption profiles and generation profiles. Since the abovementioned parameters may vary, the simulation of typical communities is matter of further study.

Tab. 8.4 Energy allocation in community in different allocation intervals (AK Dynamic).

Allocation interval	PV ↓ ConA	PV ↓ ConB	PV ↓ Aux	PV ↓ DS	Grid ↓ ConA	Grid ↓ ConB	Grid ↓ Aux	Comm ↓ Grid (AK)	Grid ↓ Comm (AK)
(kWh)									
1s	1.460	1.650	0.198	1.082	4.625	2.101	1.082	1.248	7.808
1min	1.465	1.659	0.198	1.082	4.620	2.093	1.082	1.234	7.794
5min	1.468	1.673	0.291	0.989	4.617	2.078	0.989	1.123	7.683
10min	1.494	1.688	0.342	0.938	4.591	2.063	0.938	1.031	7.591
15min	1.518	1.713	0.362	0.918	4.566	2.038	0.918	0.963	7.523
Deviation from 1s (%)									
1min	0.37	0.53	0.00	-1.11	-0.12	-0.41	0.00	-1.11	-0.18
5min	0.57	1.41	46.88	-9.98	-0.18	-1.10	-8.60	-9.98	-1.60
10min	2.35	2.33	72.57	-17.37	-0.74	-1.83	-13.31	-17.37	-2.78
15min	4.01	3.81	82.50	-22.85	-1.27	-2.99	-15.13	-22.85	-3.65

Tab. 8.5 Energy allocation in community in different allocation intervals (AK Static 1).

Allocation interval	PV ↓ ConA	PV ↓ ConB	PV ↓ Aux	PV ↓ DS	Grid ↓ ConA	Grid ↓ ConB	Grid ↓ Aux	Comm ↓ Grid (AK)	Grid ↓ Comm (AK)
(kWh)									
1s	1.457	1.699	0.048	1.352	4.628	2.052	1.232	1.352	7.912
1min	1.460	1.715	0.048	1.333	4.624	2.037	1.232	1.333	7.893
5min	1.479	1.750	0.117	1.210	4.606	2.001	1.163	1.210	7.770
10min	1.490	1.751	0.203	1.112	4.595	2.001	1.077	1.112	7.672
15min	1.500	1.782	0.270	1.003	4.584	1.969	1.010	1.003	7.563
Deviation from 1s (%)									
1min	0.25	0.90	0.00	-1.38	-0.08	-0.74	0.00	-1.38	-0.24
5min	1.52	3.01	142.61	-10.50	-0.48	-2.50	-5.57	-10.50	-1.79
10min	2.28	3.03	323.01	-17.76	-0.72	-2.51	-12.61	-17.76	-3.03
15min	3.00	4.88	462.33	-25.82	-0.95	-4.04	-18.05	-25.82	-4.41

8.3.4 Deviation Due to the Active Energy Calculation Algorithms

In addition to deviations arising from the choice of allocation key (AK) and aggregation interval, allocation may also inherit deviations introduced by the definitions of power components and the algorithms used for their calculation (see sections 8.1 and 8.2). An illustrative example is provided in Fig. 8.5. It can be observed that parametric variants of the STD algorithm (STD50p, STD10p, STD1/2p) register varying amounts of energy at the level of individual PoMs (FEED, CON, PRO). Although the computation of the overall energy balance is independent of the selected algorithm (see partial conclusions in section 8.2), within the context of the allocation process the deviations manifest, as export and import registers are applied separately. In the presented example, it is evident that the amount of energy exported by the prosumer (PRO) depends on the algorithm employed (STD50p – 1.296 kWh, STD10p – 1.392 kWh, STD1/2p – 1.417 kWh). This ambiguity is problematic for the allocation process in terms of correctness, since in practice the deviation of allocated energy is random as it depends on the actual commercial model, whose algorithms are not typically specified by manufacturers. It should be emphasized that all RMs implementing these respective algorithms are considered equivalent under existing requirements and metering test procedures (section 3.1).

8.3.5 Auxiliary Load

An objective in apartment-block energy communities might be to allocate as much on-site generation as possible into the building's own (shared) loads—for example corridor lighting, mechanical ventilation, rain-water conditioning, small wastewater treatment, or even energy losses in the installation.

In this section, unlike the preceding analyses, this house-service demand is considered as not measured directly. Instead, it is inferred from the meters of the individual community members (ConA and ConB), PV generator meter and meter at PoC, as expressed in (8.23). Energy from the community generator and from the public DS is then allocated according to the same allocation keys (AKs) used in the earlier sections.

$$P_{aux} = P_{DS} + P_{PV} - P_{conA} - P_{conB} \tag{8.23}$$

Tab. 8.6 summarizes the energy allocated to the auxiliary (house-service) load under each AK for progressively coarser metering intervals. The total auxiliary demand—1.28 kWh over the 24-h horizon (Aux)—is preserved in every case, yet the split between PV and grid energy varies markedly with both the interval length and the selected AK.

For the dynamic AK at 1 s, 1 min, 5 min, 10 min and 15 min, and for all AKs at 1 s resolution, the allocations replicate the values already reported in Tab. 8.3 a Tab. 8.4. When every meter in the system delivers data with the same granularity, (8.23) yields an auxiliary-load estimate whose uncertainty is limited only by the accuracy class of the meters; the allocation errors are identical to those obtained when the auxiliary load is metered directly. This equivalence, however, presupposes strict time synchronization; offsets up to 5 s—observed in commercial smart-meter fleets [23]—introduce an additional source of error which may impact the result.

A specific scenario—labelled "15 min & 1 min"—assumes a 15-min aggregation meter at the PoC, while the PV, Consumer A and Consumer B meters report at 1-min resolution. Despite the finer data from three of the four devices, the combined allocation error exceeds that of the uniform 15-min case even assign negative PV energy to the auxiliary load.

Tab. 8.6 Calculation and allocation of the auxiliary load in the community.

		Dynamic		Static 1		Static 2		Hybrid	
(kWh)									
1s	PV to Aux / DS to Aux	0.198	1.082	0.048	1.232	0.055	1.225	0.283	0.997
	Aux	1.280		1.280		1.280		1.280	
1 min	PV to Aux / DS to Aux	0.198	1.082	0.048	1.232	0.055	1.225	0.283	0.997
	Aux	1.280		1.280		1.280		1.280	
5 min	PV to Aux / DS to Aux	0.291	0.989	0.117	1.163	0.134	1.146	0.451	0.829
	Aux	1.280		1.280		1.280		1.280	
10 min	PV to Aux / DS to Aux	0.342	0.938	0.203	1.077	0.228	1.052	0.523	0.757
	Aux	1.280		1.280		1.280		1.280	
15 min	PV to Aux / DS to Aux	0.362	0.918	0.270	1.010	0.303	0.977	0.558	0.722
	Aux	1.280		1.280		1.280		1.280	
15 min & 1 min	PV to Aux / DS to Aux	0.385	0.895	-0.405	1.685	-0.363	1.643	-0.070	1.350
	Aux	1.280		1.280		1.280		1.280	
Deviation from 1s (%)									
1 min	PV to Aux / DS to Aux	-0.13	0.02	-0.40	0.02	-0.33	0.02	0.00	0.00
	Aux	0.0		0.0		0.0		0.0	
5 min	PV to Aux / DS to Aux	46.9	-8.6	142.6	-5.6	143.2	-6.5	59.5	-16.9
	Aux	0.0		0.0		0.0		0.0	
10 min	PV to Aux / DS to Aux	72.6	-13.3	323.0	-12.6	312.0	-14.1	84.9	-24.1
	Aux	0.0		0.0		0.0		0.0	
15 min	PV to Aux / DS to Aux	82.5	-15.1	462.3	-18.1	447.4	-20.2	97.4	-27.6
	Aux	0.0		0.0		0.0		0.0	
15 min & 1 min	PV to Aux / DS to Aux	93.9	-17.2	-941.4	36.8	-755.9	34.1	-124.8	35.4
	Aux	0.0		0.0		0.0		0.0	

The outcomes of this subsection can be summarized as follows:

- The allocation of energy produced by the generator and the allocation of energy drawn from the DS to unmetered consumption exhibit the smallest deviations from the actual energy flow when a dynamic AK is applied. The largest deviations occur with static AKs.

- The deviation of allocated energy for unmetered loads increases with the length of the aggregation interval, and in the case of static AKs deviations may even exceed 100%.
- Deploying only a subset of meters with shorter aggregation intervals and thus shortening the allocation period does not improve the allocation accuracy; on the contrary, the magnitude of deviations increases.
- In all cases, the total consumed energy is determined correctly (sum of energy allocated from the PV and from the DS, 1.28 kWh).

9. POWER DEFINITIONS IN ACTIVE ENERGY DIVERTERS

For active customers (prosumers), it is a common practice to actively control (divert) active electrical energy in order to achieve the desired energy balance at the PoC. Formally, however, this corresponds to achieving the required value of that component of electric power or energy under which the energy balance is evaluated. In most cases, this is determined by the RM. This practically should imply an adaptation of the control algorithms in the active device to national metering regulations, vectorial or algebraic increments of active energy in this context.

In [A5], using a model example of a prosumer with a generating plant, uncontrolled and actively controlled resistive loads (Fig. 9.1A), a numerical analysis is presented with fundamental question: What active power and active energy will be measured by RMs registering different power components (i.e. different classification algorithms, Section 5.3) when applying diverters with control algorithms derived from these components.

The diverter of the positive-sequence power component ("P+") is shown in Fig. 9.1B, the diverter of vectorial power ("P∑") is in Fig. 9.1C, and the diverter of algebraic power ("Pph") is in Fig. 9.1D. All diverters employ feedback control targeting a specific three-phase active-power component. For measurements associated with "P∑" and "Pph", the STD algorithm is applied in sliding window (updated every 1.25 ms) to determine the active power in each individual phase, after which the respective three-phase component is calculated. For "P+", the positive-sequence active power is calculated according to (4.46), where the positive-sequence voltage and current are obtained using Fourier and Fortescue transforms, applied on sliding window (updated every 1.25 ms). On the other hand, the measurement of active energy in all phases by the RMs $RM_{\Sigma 1ph}$ and RM_{3ph} is carried out using the STD algorithm with a consecutive 50-period window (STD50p, see Section 5.1.1), followed by the application of the relevant sorting algorithms (see section 5.2). The positive-sequence active power is determined according to (4.46), where the fundamental voltage and current components are extracted via a Fourier transform applied over the same 50-period window (1 s at 50 Hz). The measurement windows of the diverters and RMs are synchronized, while the diverter control is updated at a much higher rate (800 times) to minimize deviations registered in the RM caused by the diverter's finite response time.

The diverters in Fig. 9.1B–D differ not only in the controlled quantity but also in the minimum hardware requirements: in the case of "P+" and "P∑" a continuously controllable converter is required in only one phase (e.g. a full-bridge converter with an active front-end or a dedicated AC–AC converter [A4]), whereas in other phases less complex switches (e.g., mechanical or solid-state relays) are sufficient. In the case of "Pph" continuously controllable converters are required in every phase, making it evident

that the portability of diverters across regions with different legislative frameworks for measurement may not be feasible.

The above-described model was subjected to a numerical simulation in the PSCAD software environment. A test power profile of the generating plant was created (Fig. 9.2A) together with the profile of the uncontrolled load (Fig. 9.2B). It should be noted that the switching of the uncontrolled load is synchronized with integer-second intervals, ensuring alignment of power variations with the measurement process (both in diverter feedback measurement and in RM) and thereby avoiding additional uncertainty of registration error in RMs arising from desynchronization between energy flow changes and measurement (see Fig. 5.6 section 5.1.1).

The resulting power at the PoC was then subject of control by the models of the respective diverters, diverting the surplus energy into controlled loads, thus ensuring that no generated power is injected (exported) into the DS. Publication [A5], furthermore, presents the design of the control algorithms for all diverters as well as a detailed analysis of the resulting power at the PoC when each diverter is deployed.

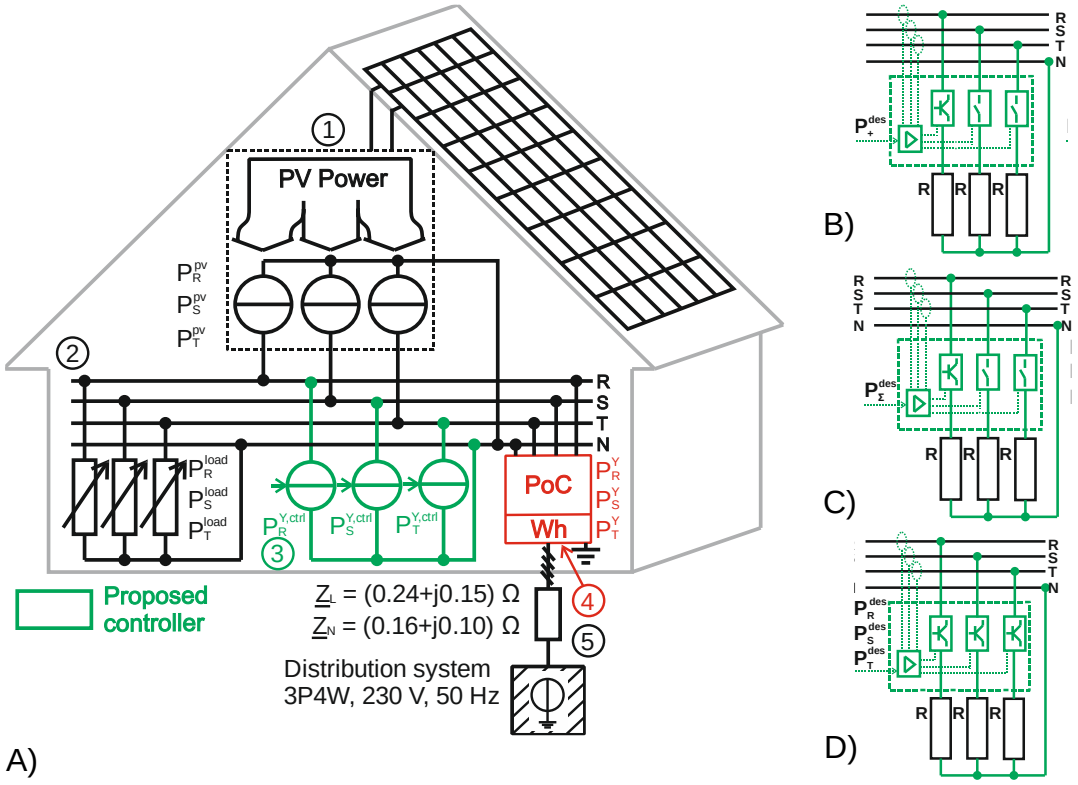

Fig. 9.1. Model of a single prosumer equipped with energy diverter connected to DS (A) and minimal hardware for positive sequence diverter (B), vectorial power diverter (C) and algebraic power diverter (D).

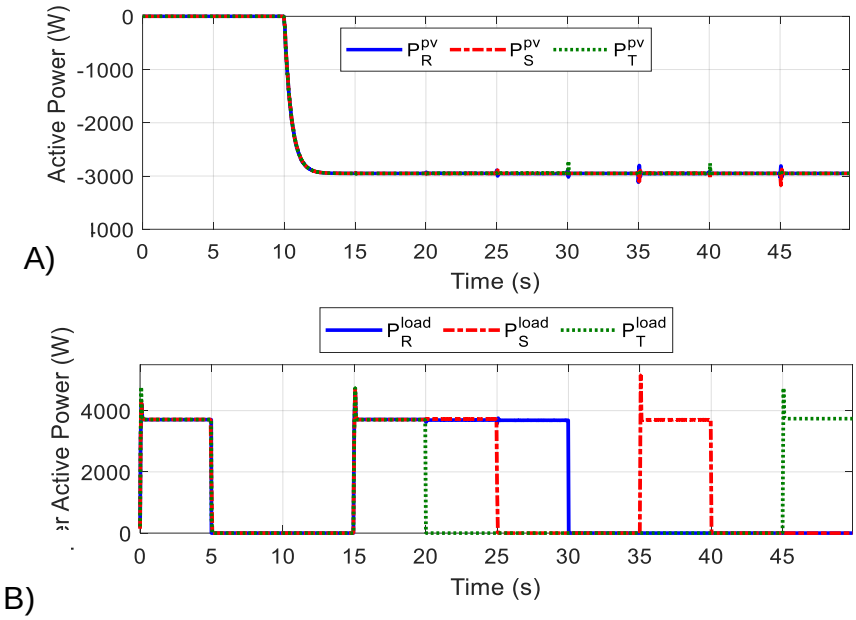

Fig. 9.2. Tested active power profiles of the generating plant (A) and uncontrolled load (B).

The resulting energy flows during the simulation are summarized in Tab. 9.1. It is shown that in all cases the generating plant supplied the same amount of energy (①), and the uncontrolled loads consumed nearly the same amount of energy (②). However, it can be observed that the loads controlled by the individual diverters consumed different amounts of energy, with the lowest value for the "P+" diverter, followed by "P∑" and the highest for "Pph." It can therefore be stated that under regulation with "Pph," the controlled loads consume the largest share of the total energy (③), and the overall saldo (import direction) of energy of the prosumers system (②+③–①) is also the highest. On the other hand, $RM_{\Sigma 1ph}$ registers the actual imported and exported power, and from the perspective of network utilization, regulation with "Pph" imposes the least burden on the grid (energy export is not zero due to the finite response time of the regulation in the dynamic simulation). Finally, it can be observed that only in the case of "Pph" regulation the exported power recorded in all meter components is minimized.

Tab. 9.1 Energy throughput and energy registered by algorithms in revenue meters.

Controller			**"P+"**	**"P∑"**	**"Pph"**
Registers of revenue meters (kWs)	**$RM_{\Sigma 1ph}$**	**Imp**	119.44	120.22	86.67
		Exp	54.58	53.72	**0.261**
	RM_{3ph}	**Imp**	67.25	67.25	86.60
		Exp	2.38	**0.75**	0.19
	RM_{SYM}	**Imp**	67.20	68.65	86.46
		Exp	**0.74**	0.52	0.17
① Generated energy (kWs)			369.7	369.7	369.7
② Cons. energy in uncontrolled loads (kWs)			204.0	204.0	204.6
③ Cons. energy in controlled loads (kWs)			210.6	212.2	**231.5**
② + ③ - ① SALDO (kWs)			64.8	66.5	**86.4**

The study in this section yields the following conclusions:

- The diverting objective is achieved only when the control algorithm corresponds to the respective definition of power component in the RM (see the green-highlighted diagonal in Tab. 9.1)
- Only the control algorithm that diverts active energy continuously and independently in each phase ("Pph") achieves the highest degree of energy self-sufficiency (i.e., no energy exported to the upstream DS), regardless of the RM, although it leads to the highest total imported active energy from the grid among phases (largest positive SALDO).
- The "Pph" control algorithm produces, in comparison with "P+" and "P∑", the smallest discrepancies among the components registered by the individual meters ($RM_{\Sigma 1ph}$, RM_{3ph}, RM_{SYM}).
- No control algorithm achieves infinitely fast control action; therefore, the exported energy is non-zero in all cases.

10. CONTRIBUTIONS AND DISCUSSION

Throughout the research a conceptual framework of knowledge and interrelations has been developed. This framework is visualized in the diagram in Fig. 8.5, which methodologically introduces the central objective of this thesis. The objective is further decomposed into four main thematic areas representing the key domains to which this work aims to contribute. Each publication is linked to specific research questions from which it originally stemmed. Furthermore, each publication is associated with the predominant methodological approach it applies.

Specifically, the applied methodologies can be summarized as follows:

- all publications include a literature review focused on the specific topic; the thesis itself provides a more comprehensive and overarching review,
- all publications and the thesis involve theoretical modeling and simulation,
- publications [A5], [A8], [A9], [A10] and [A12] and the thesis apply analytical methods,
- publications [A5], [A7], [A8], [A9], [A10], [A11], [A12] and the thesis involve numerical analysis,
- publications [A1], [A2], [A3] and [A6] include experimental investigations.

In terms of content, publications [A1] through [A6] explore, in various contexts, the current state of active power control technologies and their effects on voltage quality and metering in DS. Thus they primarily contribute to the 1st, 2nd and 3rd topic presented in Fig. 8.5. The following conclusions can be drawn:

- Diverters operating with pulse-width regulation (PWR), when combined with a generator, induce rapid and cyclic changes of energy flow, which in metering devices lead to deviations of the recorded values from the actual transferred active energy.
- Cyclic variations may also arise from non-standard behavior of the control loops implemented in commercial electrical storage systems.
- Active energy diverters exist which, in combination with a generator, cause different directions of energy flow among phases, thereby producing deviations of the measured values from the actual transferred energy.
- The influence on measurements in metering units should be examined in a broader context—for example, in relation to associated impacts on voltage quality or control algorithms in active devices.
- In the context of rapid active power changes, publication [A1] presents measurements and commentary on control strategies implemented in energy diverters. It outlines algorithms used in commercial devices and describes the design process of a prototype diverter compliant with EMC emission requirements.

Publications [A6] to [A8] primarily address voltage regulation using reactive power injection. However, in this thesis, particular attention is paid to sections describing the physical phenomena and implications of reactive power flows in DS.

Publications [A10] and [A11] focus on algorithms for active power calculation under conditions of rapid power direction changes. These works compare not only different algorithms but also selected parameter settings, highlighting their specific characteristics and providing commentary relevant to practical implementation. These insights enable informed selection of algorithms in real-world applications, based on their strengths and limitations and primarily contribute to the 2nd and 4th topic presented in Fig. 8.5. The following phenomena have been identified and further elaborated:

- Errors in the registration of active energy depend not only on the applied computational algorithm and its parameterization but also on external factors beyond the the metering device, which must nevertheless be considered (e.g., the rate of energy flow changes or the synchronization of changes cycles and the measurement cycles).
- Such registration errors introduce deviations into energy registers, and these deviations may assume values that are difficult to define in practice as they depend on manufacturers of commercial metering devices. The deviations, however, have significant implications for subsequent calculations based on the measured values, such as energy allocation within energy communities or monitoring of energy flows transferred across DS sections and microgrids.
- It is recommended to implement measures for eliminating, or at least standardizing, these deviations. This necessarily entails either updating the existing tests for metering devices or, alternatively, adopting a uniform measurement algorithm, at least within a single microgrid or energy community.

Publications [A9] and [A12] address asymmetrical and bidirectional energy flows. They assess selected three-phase power definitions of active energy, derived from classification into import and export registers and analyze the impact of unbalanced flows on distribution networks, as well as ability of power components to account for these effects. Publications primarily contribute to the 3rd and 4th topic in Fig. 8.5 and the main identified and further elaborated phenomena are listed below:

- Algebraic, vectorial, and positive-sequence power components yield different values under bidirectional and unbalanced energy flows. However, by combining these components, the actual energy flows can be retrospectively tracked through post-process analysis.
- Ability of sequence power components to estimate the additional losses induced in the DS due to unbalanced energy flow. Practically, the estimate

might be quantified using registering of energy carried by vectorial and positive sequence power components

- Active diverters that systematically induce unbalanced bidirectional energy flows among phases in order to increase energy self-sufficiency do not contribute to reducing the overall losses in the distribution system; they merely shift losses from the upstream DS into the microgrid.
- Publication [A5] builds upon this by linking metering and sorting algorithms with active power diverter control algorithms, while also specifying minimal hardware requirements. This is particularly relevant for engineering practice, where evaluating the applicability and impact of algorithms on distribution networks is essential for technology selection.

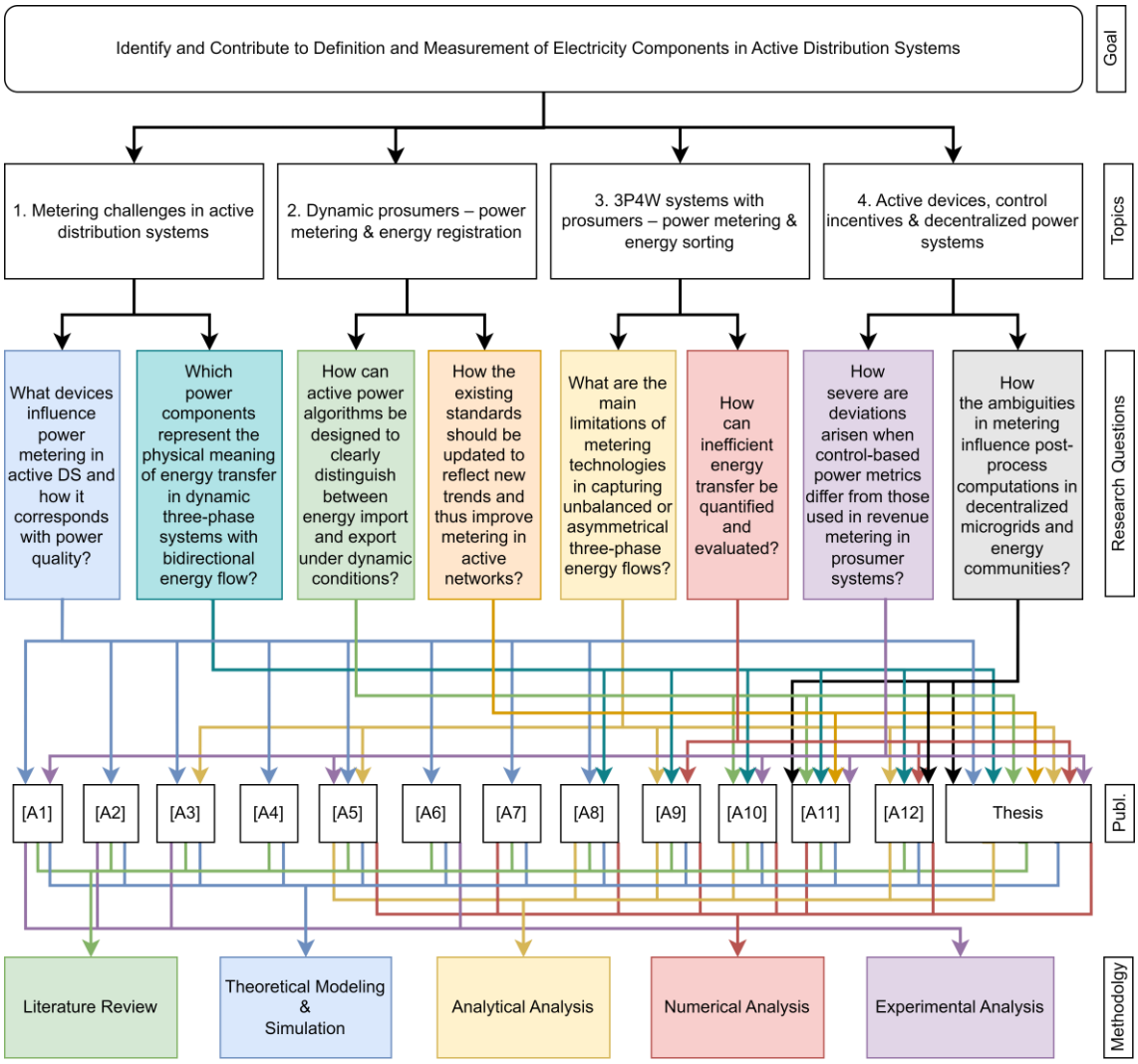

Fig. 10.1. Methodological diagram of the thesis.

In following subsections, selected contributions of the thesis are discussed in more details.

10.1 Recommendation for Standardized Testing

The publication [A11], based on observed discrepancies in the registration of imported and exported active energy by various algorithms, proposes a modification to the testing procedure specified in the current version of the IEC 62052-11 standard (2020). The standard defines a testing procedure (①) for evaluating meter accuracy under dynamic load conditions. Publication [A11] also considers the theoretical error arising from the classification of energy as imported and exported (see Fig. 5.6) and therefore proposes that the polarity of power (i.e., import vs. export) be alternated during the dynamic changes, rather than remaining unipolar.

The proposed test procedure accounts for the fact that a significant proportion of RMs implement a standard window-based measurement algorithm with a measuring window length of 1 second (referred to as STD50p/FT50p according to section 5.1.1). This is reflected in the design of the test, where the frequency of power changes is deliberately chosen such that the theoretical error reaches two-thirds of the theoretical maximum permissible uncertainty for Class 2/A meters, i.e., 1.33%. At the same time, the period of change is selected to avoid being an integer multiple of the fundamental measurement window.

Publication [A11] further introduces additional testing procedures designed to test the coherence of all outputs of a single device (typically registers, LED indicators, and metallic pulse outputs):

1. a procedure with a shorter period of power changes (②), and
2. a procedure with asymmetric energy distribution between the import and export registers (③).

All proposed procedures and supplementary criteria were applied to three samples of commercial electricity meters. The results indicate the following:

- Procedure ① does not disqualify any algorithms that may be realistically implemented in practice.
- Procedures ② and ③ reveal inconsistencies when different outputs of a single device yield divergent results.
- There exist meters that distinguish between import and export energy flows across all their outputs. However, not all tested devices exhibit this behavior. Therefore, it is recommended that this capability be included as a requirement in future revisions of the standard.

The detailed descriptions of the proposed testing procedures and their evaluation are thoroughly presented in [A11].

10.2 System Loss Estimation

The section 6.4 demonstrates, that the energy registered through the zero- and negative-sequence power components provides a satisfactory estimate of the additional losses

induced by unbalances in the DS, even in operating conditions where conventional sorting methods indicate zero energy. This observation has led the authors to propose a method for estimating losses associated with asymmetrical energy flows by means of measuring the symmetrical components in the distribution network. To verify this concept, the difference between estimated and actual losses was evaluated across all possible unbalanced states of prosumers connected to low-voltage distribution networks with internal impedances representative of European systems. The results indicate that the concept cannot capture losses under perfectly balanced operating conditions. On the other hand, it was demonstrated on the example of a realistic European network that the losses under symmetrical energy transfer are relatively small, remaining below 1%.

When estimating loss power by means of the negative- and zero-sequence components of power, a so-called hidden power arises. However, as demonstrated in section 6.4 (and the related author's publications), this term can be neglected from a practical perspective. Consequently, the losses due to asymmetrical power flow can be determined with satisfactory accuracy—by disregarding the hidden losses—as the sum $P_1^- + P_1^0$. In practice, this corresponds to the difference between the values obtained using the RM_{3ph} a RM_{SYM}, as expressed in relation (7.4).

The results of this work, including the supporting literature review, are consistent with the well-established fact that non-ideal current waveforms in three-phase (four-wire) networks—whether asymmetrical, harmonic-distorted, or temporal unevenness —lead to relatively inefficient energy transfer. In the case of asymmetry, this inefficiency has been quantified in the present work using a model test network (see section 6.4). Moreover, such conditions adversely affect voltage quality, resulting in voltage unbalance, harmonic and interharmonic distortion, or voltage fluctuations and flicker [A4]. It can therefore be concluded that by quantifying the inefficiency of energy transfer (for instance, through the loss power demonstrably induced in the upstream DS at the PoC), it is also possible to quantify the degree of contribution to voltage unbalance. Moreover, it is shown that by introducing and intentional setting of the phase-power difference limit at the individual PoCs (customers), the maximal contribution to voltage unbalance is set simultaneously. Coordinated setting of the limits is a promising tool for keeping the voltage unbalance in permissible limits.

10.3 Calculations in Microgrids and Energy Communities

Section 8 presents deviations between the active energy measured by metering units—employing different parametrizations of computational algorithms describing the energy flow—and the actual physical energy transfer. This is demonstrated on a simplified microgrid model with participants who both generate and consume active energy. Section 8.1 quantifies the deviations observed in selected three-phase algorithms when the three-phase network is systematically utilized inefficiently as a consequence of active prosumer

behavior. The results are expressed numerically and can be interpreted both at the level of individual metering devices and in the broader microgrid context. The main outcome of the analysis can be formulated as follows: although losses in the upstream DS are reduced through active energy diverting, equivalent losses may arise within the microgrid, particularly when the resulting energy flow is bidirectional among phases.

Section 8.2 evaluates the deviations of single-phase algorithms under intentional dynamic energy flow, in which the direction of energy flow alternates. The outcomes quantify the deviations in active energy measurements at the level of individual metering units for selected algorithms, specifically in the process of separating active energy into import and export registers. At the microgrid level, the results reveal an important finding.

- When import and export values are used in a combined form—such as for evaluating the overall energy balance of the microgrid or community (energy saldo)—the selection and parametrization of algorithms at the level of individual devices has no significant impact.
- When import and export energy values are treated separately—for example, 1) quantification of shared portion of energy inside the community or 2) evaluation of total energy entering and leaving the community—the resulting values depend on the choice of computational algorithm. Since these algorithms are not standardized, the measured values may differ depending on the implementation.
- It is therefore recommended to use RMs implementing the same algorithms in all measuring points of the community in order to avoid ambiguous results.

It is further demonstrated that deviations in the interpretation of measurements may also arise at the level of subsequent calculations, in which the measured components from metering units are applied. One example is provided by allocation algorithms used for energy sharing in energy communities. The allocation of energy within such communities is primarily motivated by socio-economic considerations. When a so-called static allocation key is applied, it does not necessarily correspond to the physical energy flow within the community. On the other hand, it is possible to design allocation keys that preserve the overall community energy balance while at the same time allowing the allocation of energy according to non-physical principles, such as a hybrid allocation key. This, at least, enables the quantification of the total energy demand of the community.

Section 8.3 provides a quantification of the discrepancy between energy transfers derived from allocation keys and the real energy flow. The section also quantifies the influence of the time granularity of the allocation process, which practically follows the aggregation interval in metering devices. The following recommendations can be formulated:

- The allocation process can be affected more adversely when it follows the shorter aggregation intervals of a minority of meters than when it is based on the longest aggregation interval across all meters.

- In general, the shorter the aggregation interval (and thus the allocation interval), the smaller the deviation from the actual energy flow. However, it is shown that aggregation into 1-minute values already results in deviations below 2%, which corresponds to the required measurement uncertainty of standard RMs.
- To avoid ambiguities in measurement, it is recommended that RMs within an energy community register the same components using identical algorithms.

10.3.1 Recommendation for Further Study

It is evident form the study, that using short aggregation window (~1min and shorter) and dynamic AK leads to the lowest deviations. However, it should be also regarded, that energy communities have already started to evolve and aggregation intervals (typically 15 min) and AKs have been established in relevant legislative rules. Therefore, one of the contribution of this work is to propose a survey not only to point out the bottlenecks for following upgrades but also to quantify the deviations so the results of existing rules might be interpreted correctly.

To quantify the deviation due to selection of AK and aggregation interval and even more realistically on larger subset of situations of typical community members, it would be desirable to conduct a larger set of simulations using realistic input data. Fig. 10.2 presents a proposed flow diagram which, based on realistic inputs—such as load and generation profiles obtained from measurements and typical parameter ranges—can provide an estimate of the realistically expected deviation.

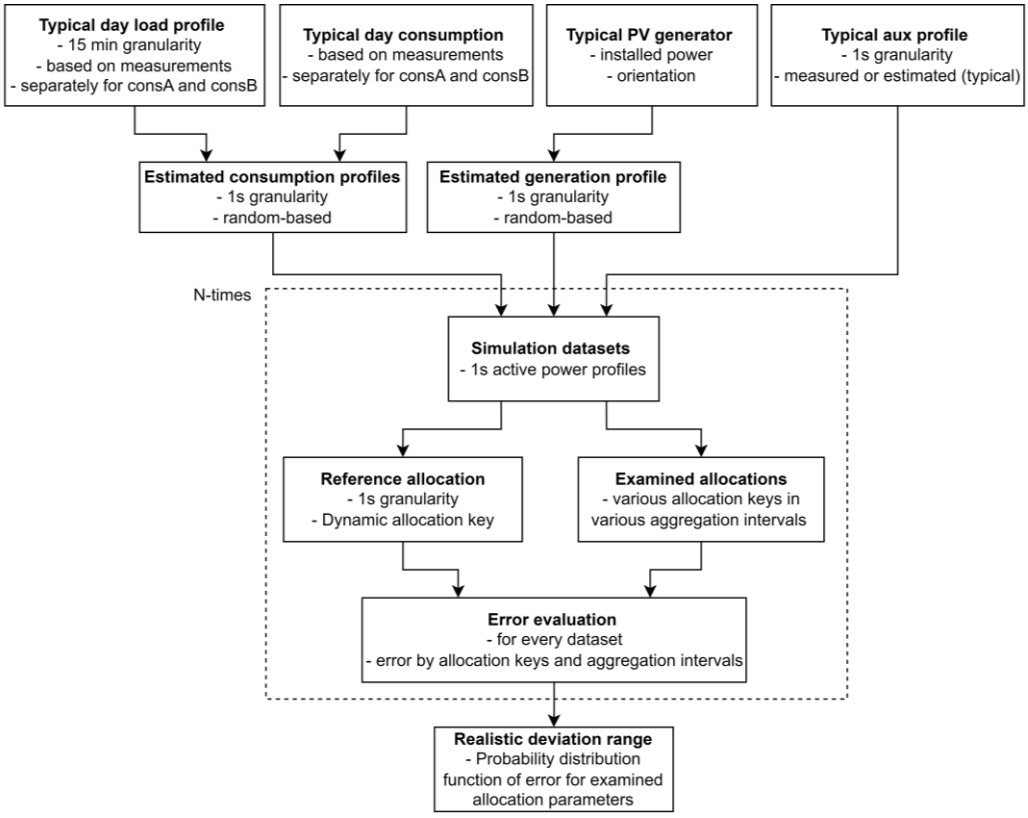

Fig. 10.2. Flow diagram of further work.

Beyond the influence of the allocation key and aggregation granularity, several additional factors are identified that may contribute to deviations in energy allocation within communities. To capture and quantify the realistic impact of these factors, a dedicated set of simulations is required. The key factors are listed below.

- The selection of the three-phase power component (e.g., vectorial or algebraic component, positive-sequence component), as discussed in Section 7.1.
- The selection of the single-phase power component and the parametrization of the computational algorithm, as addressed in Section 7.2.
- The possible desynchronization of aggregation windows among individual metering devices in time.

10.4 Discussion about Active Power Definition

The p–q theory [74] is capable of determining the compensating current in such a way that the ideal energy transfer is achieved at every instant of time. On the other hand, the outcome depends on the parametrization of the algorithm—specifically on the method used to extract the average active power (see section 6.2.1)—and may therefore lead to different results. By modifying the computational approach and its parametrization, it is possible to define the ideal power trajectory for various applications. In the context of metering, this enables the establishment of a benchmark in the form of specific

parameters, effectively constituting a metric. Hence, the definition of ideal energy transfer can be extended: in addition to harmonic and balanced current, the ideal current may also be characterized as one that varies smoothly over time with defined rate, without causing frequent changes in power magnitude or even in its direction. Thus, the temporal unevenness (see 4.4.1) is regarded.

Closely related to this is the specific definition of the computational interval of active power (kT in (4.23) and (4.24)), which could become a subject of further discussion and, ideally, be incorporated into the relevant standardization framework. In the context of modern distribution networks, where billing measurements are inherently linked with active control of energy flows, the selected computational interval should adequately reflect the realities of regulatory processes. A systematic mapping of this issue would merit further investigation. It is problematic to approach the question from a single perspective. For instance, the authors in [79] propose a measurement window of 3 s in the context of interharmonic components (specifically subharmonics) and the accuracy of window-based algorithms. While such a choice may yield optimal accuracy with respect to subharmonic variations, under conditions of rapidly changing energy flow directions—as reported in [A10] and [A11]—the deviation margin for distinguishing between import and export power would increase, as evident from extrapolation of the comparison between the algorithms STD50p and STD10p in Fig. 5.5.

11. CONCLUSIONS

This dissertation establishes the interrelation between the definition of electrical energy components, the algorithms used for their determination, and their relevance in the contexts of electricity trading and sharing, distribution, as well as analysis and control. It connects the motivations and objectives of active participants in DSs with the regulatory framework that governs their operation—requirements which are in practice defined by billing and evaluation measurements—and links these with the physical nature of energy transfers in DSs, while also considering the hardware for energy flow control that is currently available on the market. Specific use cases were identified and analyzed from multiple perspectives, initially defined through a practice-oriented approach, to demonstrate the consequences of active behavior with respect to the efficiency of energy transfer. Based on the results, it is possible to infer how the motivations driving active control align—or conflict—with the intended objectives.

This work demonstrates that the currently applied approach to billing measurement requirements—defined primarily through testing procedures and verification of tolerance limits—allows for the implementation of different algorithms that may produce divergent results. In practice, this can lead to ambiguity in the consequences for the involved stakeholders. From the perspective of requirement design, a recommendation can therefore be formulated towards the unified implementation of algorithms. The microgrid examples further illustrate that for the purpose of unambiguous evaluation of energy flows, determination of their direction (import vs. export), and, secondarily, for reliable network analysis based on the widespread deployment of metering units, a consistent algorithmic implementation is necessary, even though deviations from the real energy flow may occur at the level of an individual metering unit. These deviations can, in specific cases, be mapped—as also demonstrated in this work—and their consequences mitigated, for example by measuring auxiliary components or by implementing alternative computational algorithms. The dissertation thus provides a knowledge base for shaping future concepts of energy measurement and the evaluation of electricity flows for diverse applications.

An integral part of this dissertation is the mapping of the behavior of individual algorithms. The work summarizes a portfolio of algorithms and definitions which, although primarily applied in specialized use cases, can also serve as auxiliary tools for quantifying real energy flows in situations where standard (and primarily employed) algorithms fail. In addition to the enumeration of algorithms for power component measurement, the dissertation further elaborates on the circumstances of algorithm parametrization and highlights requirements for measurement processes and metering hardware. In this way, it establishes a knowledge base for the design and prototyping of future metering devices.

11.1 Further development

Future progress of this research can be is projected along several lines. First, the development of a test model for evaluating the deployment of different algorithms and definitions of power components in realistic networks under specific participant behaviors would enable broader utilization of the data. Typical applications include estimation-based analytical tools for network load monitoring, algorithms for energy allocation in energy communities, and the identification of suitable complementary definitions and algorithms. Such investigations can be carried out through dynamic modeling of algorithmic calculation chains in simulation environments such as PSCAD or Simulink.

Second, the design and realization of a prototype of versatile metering device implementing parameterizable algorithms for the definition of power components is suggested. The aim would be to analyze the technical impact of the entire signal measurement chain—covering sensing, data digitization, and relevant acquisition processing—on the overall quantification results, to describe and quantify the associated effects, and to propose mitigation measures. To support this, the prototype should be equipped with a reference set of algorithms for the power components (i.e. metrics), that should be defined first. Moreover, the prototype should be resilient to the external electromagnetic fields coming from both the measured circuit and general environment [80], [81].

Multiple prototypes should be deployed in a representative microgrid, additionally incorporating allocation algorithms of energy communities. The objective is to practically validate the significance of measurement deviations under real microgrid operation and energy community management during a long-term test, involving various user types—consumers, producers, prosumers, and even community devices. The microgrid should therefore feature a topology at least comparable to the models described in sections 8.1 and 8.2, with all user connection points equipped with the proposed prototype, including the points of interconnection between the microgrid and the upstream DS.

Finally, further work should also address the study of external influences of the calculation process, such us the robustness of sensors and metering systems (e.g., Aron’s measuring system as a practical application of Blondel’s theorem) under real operational conditions of power networks. This includes the analysis of disturbances such as DC components in the signals, ground faults, or electromagnetic interference, which are critical for ensuring reliable performance of metering systems in practice.

LITERATURE

[1] SANDULEAC, M., CHIMIREL, C., EREMIA, M., TOMA, L. a MARTINS, J. Supporting market solutions by calculating ancillary services and quality of service with metrology meters. In: *2016 IEEE PES Innovative Smart Grid Technologies Conference Europe (ISGT-Europe)*. IEEE, 2016, s. 1–6. DOI 10.1109/ISGTEurope.2016.7856190.

[2] OLIVERO, S., GHIANI, E. a ROSETTI, G. L. The first Italian Renewable Energy Community of Magliano Alpi. In: *2021 IEEE 15th International Conference on Compatibility, Power Electronics and Power Engineering (CPE-POWERENG)*. IEEE, 2021, s. 1–6. DOI 10.1109/CPE-POWERENG50821.2021.9501073.

[3] ATZARAKIS, N., KOUVELIOTIS-LYSIKATOS, I., PALAIOGIANIS, F., VASILAKIS, A., TSEKERIS, D. a HATZIARGYRIOU, N. SMART energy communities: a case study for Greece. In: *CIRED 2020 Berlin Workshop (CIRED 2020)*. IET, 2020, s. 136–139. DOI 10.1049/oap-cired.2021.0289.

[4] HALA, T. a DRÁPELA, J. On Stabilization of Voltage in LV Distribution System Employing MV/LV OLTC Transformer with Control Based on Smart Metering. In: *2019 20th International Scientific Conference on Electric Power Engineering (EPE)*. IEEE, 2019, s. 1–6. DOI 10.1109/EPE.2019.8778012.

[5] CIRED WG 2019-5. Monitoring and Control of LV Networks. Final Report. Brussels: CIRED – International Conference on Electricity Distribution, září 2021.

[6] SĂNDULEAC, M., CIORNEI, I., TOMA, L., PLĂMNESCU, R., DUMITRESCU, A.-M. a ALBU, M. M. High Reporting Rate Smart Metering Data for Enhanced Grid Monitoring and Services for Energy Communities. *IEEE Transactions on Industrial Informatics*. 2022, roč. 18, č. 6, s. 4039–4048. DOI 10.1109/TII.2021.3095101.

[7] CIGRE/CIRED JWG C6/B5.25/CIRED. Control and Automation Systems for Electricity Distribution Networks (EDN) of the Future. Paris: CIGRE/CIRED, 2017. 67 s. ISBN 978-2-85873-413-9.

[8] HAVE, B. t., HARTMAN, T., MOONEN, N. a LEFERINK, F. Inclination of Fast Changing Currents Effect the Readings of Static Energy Meters. In: *2019 International Symposium on Electromagnetic Compatibility – EMC Europe*. IEEE, 2019, s. 208–213. DOI 10.1109/EMCEurope.2019.8871982.

[9] DRÁPELA, J. *Electricity metering by means of static revenue meters deployed in active distribution systems*. Brno: Brno University of Technology, VUTIUM, 2020. ISBN 978-80-214-5900-7. (in Czech).

[10] MORÁVEK, J., DRÁPELA, J., WASSERBAUER, V. a MASTNÝ, P. Power quality issues related to power flow control in systems with renewable energy micro sources. In: *2016 17th International Scientific Conference on Electric Power Engineering (EPE)*. IEEE, 2016, s. 1–6. DOI 10.1109/EPE.2016.7521784.

[11] MATHEW, R. T., THATTAT, S., ANIRUDH, K. V., ADITHYA, V. P. K. a PRASAD, G. Intelligent Energy Meter with Home Automation. In: *2018 3rd International Conference for Convergence in Technology (I2CT)*. IEEE, 2018. DOI 10.1109/I2CT.2018.8529702.

[12] DAVIDSON, E. A. Induction-type watt-hour meters. *Transactions of the American Institute of Electrical Engineers*. 1929, roč. 48, č. 2, s. 547–560.

[13] SHERBURNE, R. R. Driving Torque Equations for the Watthour Meter Based on the Ferraris Principle. *IEEE Transactions on Power Apparatus and Systems*. 1971, roč. PAS-90, č. 1, s. 325–330. DOI 10.1109/TPAS.1971.293008.

[14] EDISON ELECTRIC INSTITUTE. *Handbook for Electricity Metering*. 10. vyd. Washington, D.C., 2002. 604 s. ISBN 0-931032-52-0.

[15] FREIBURG, M., SCHMIDT, M., GUO, X., CHRIST, L., HACKELOEER, F. a ABRAHAM, R. Accuracy of Electricity Metering and Monitoring Devices Under Industry-Typical Operating Conditions. In: *2024 IEEE 14th International Workshop on Applied Measurements for Power Systems (AMPS)*. Caserta: IEEE, 2024, s. 1–6. DOI 10.1109/AMPS62611.2024.10706684.

[16] TOLEDO, F. *Smart metering handbook*. Tulsa: PennWell, 2013. 320 s. ISBN 978-1-59370-298-4.

[17] MORELLO, R., DE CAPUA, C., FULCO, G. a MUKHOPADHYAY, S. C. A Smart Power Meter to Monitor Energy Flow in Smart Grids: The Role of Advanced Sensing and IoT in the Electric Grid of the Future. *IEEE Sensors Journal*. 2017, roč. 17, č. 23, s. 7828–7837. DOI 10.1109/JSEN.2017.2760014.

[18] IEEE. *IEEE Standard Definitions for the Measurement of Electric Power Quantities Under Sinusoidal, Nonsinusoidal, Balanced, or Unbalanced Conditions*. IEEE Std 1459-2010. New York: IEEE, 2010.

[19] IEC. *IEC 61557-12:2018 Electrical safety in low voltage distribution systems up to 1 000 V a.c. and 1 500 V d.c. – Equipment for testing, measuring or monitoring of protective measures – Part 12: Power metering and monitoring devices (PMD)*. 2. vyd. Geneva: International Electrotechnical Commission, 2018.

[20] IEC. *IEC 62052-41:2022 Electricity metering equipment – General requirements, tests and test conditions – Part 41: Energy registration systems*. Geneva: International Electrotechnical Commission, 2022.

[21] IEC. *IEC 61000-4-7:2009 Electromagnetic compatibility (EMC) – Part 4-7: Testing and measurement techniques – General guide on harmonics and interharmonics measurements and instrumentation, for power supply systems and equipment connected thereto*. Ed. 2.1. Geneva: International Electrotechnical Commission, 2009.

[22] IEC. *IEC 61000-4-15:2010 Electromagnetic compatibility (EMC) – Part 4-15: Testing and measurement techniques – Flickermeter – Functional and design specifications*. Ed. 2.0. Geneva: International Electrotechnical Commission, 2010.

[23] IEC. *IEC 61000-4-30:2015 Electromagnetic compatibility (EMC) – Part 4-30: Testing and measurement techniques – Power quality measurement methods*. Ed. 3.0. Geneva: International Electrotechnical Commission, 2015.

[24] IEC. *IEC 62053-21:2003 Electricity metering equipment (a.c.) – Particular requirements – Part 21: Static meters for active energy (classes 1 and 2)*. Ed. 1.0. Geneva: International Electrotechnical Commission, 2003.

[25] IEC. *IEC 62053-22:2003 Electricity metering equipment (a.c.) – Particular requirements – Part 22: Static meters for active energy (classes 0.2S and 0.5S)*. Ed. 1.0. Geneva: International Electrotechnical Commission, 2003.

[26] IEC. *IEC 62053-23:2020 Electricity metering equipment (a.c.) – Particular requirements – Part 23: Static meters for reactive energy (classes 2 and 3)*. Geneva: International Electrotechnical Commission, 2020.

[27] IEC. *IEC 62053-24:2015 Electricity metering equipment (a.c.) – Particular requirements – Part 24: Static meters for reactive energy (class 0.5)*. Ed. 1.0. Geneva: International Electrotechnical Commission, 2015.

[28] IEC. *IEC 62053-41:2022 Electricity metering equipment – Particular requirements – Part 41: Stand-alone meter – Static meter for active energy with integral test output*. Ed. 1.0. Geneva: International Electrotechnical Commission, 2022.

[29] IEC. *IEC 62052-11:2003 Electricity metering equipment (a.c.) – General requirements, tests and test conditions – Part 11: Metering equipment*. Ed. 1.0. Geneva: International Electrotechnical Commission, 2003.

[30] EUROPEAN PARLIAMENT and COUNCIL. *Directive 2014/32/EU of the European Parliament and of the Council on the harmonisation of the laws of the Member States relating to the making available on the market of measuring instruments (Measuring Instruments Directive – MID)*. *Official Journal of the European Union*. 2014.

[31] CENELEC. *EN 50470-1:2006 Electricity metering equipment (a.c.) – Part 1: General requirements, tests and test conditions – Metering equipment (class indexes A, B and C)*. Brussels: CENELEC, 2006.

[32] CENELEC. *EN 50470-3:2006 Electricity metering equipment (a.c.) – Part 3: Particular requirements – Static meters for active energy (class indexes A, B and C)*. Brussels: CENELEC, 2006.

[33] OIML. *OIML R 46-1:2012 Electricity meters – Part 1: Metrological and technical requirements*. Paris: International Organization of Legal Metrology, 2012.

[34] OIML. *OIML R 46-2:2012 Electricity meters – Part 2: Metrological controls and performance tests*. Paris: International Organization of Legal Metrology, 2012.

[35] IEC. *IEC 62057-1:2023 Electrical energy meters – Test equipment, techniques and procedures – Part 1: Stationary meter test units (MTUs)*. Geneva: International Electrotechnical Commission, 2023.

[36] ACER. *Report on Distribution and Transmission Tariff Methodologies in Europe*. Ljubljana: Agency for the Cooperation of Energy Regulators, May 2021. Available from: https://acer.europa.eu

[37] CENELEC. *EN IEC 62056-6-1:2021 Electricity metering data exchange – The DLMS/COSEM suite – Part 6-1: Object Identification System (OBIS)*. Brussels: European Committee for Electrotechnical Standardization, 2021.

[38] LIMA, D. A., PADILHA-FELTRIN, A. a CONTRERAS, J. An overview on network cost allocation methods. *Electric Power Systems Research*. 2009, roč. 79, č. 5, s. 750–758. DOI 10.1016/j.epsr.2008.10.005.

[39] LI, N., HAKVOORT, R. A. a LUKSZO, Z. Cost allocation in integrated community energy systems – A review. *Renewable and Sustainable Energy Reviews*. 2021, vol. 144, no. 111001. DOI 10.1016/j.rser.2021.111001.

[40] LUMMI, K., MUTANEN, A. a JÄRVENTAUSTA, P. Calculation methodology to determine electricity distribution tariffs using an approach based on cost causation. *Energies*. 2024, vol. 17, no. 13. DOI 10.3390/en17133348.

[41] CENELEC. *EN 50160:2022 Voltage characteristics of electricity supplied by public distribution networks*. Brussels: European Committee for Electrotechnical Standardization, 2022.

[42] EUROPEAN PARLIAMENT and COUNCIL. *Directive (EU) 2019/944 of the European Parliament and of the Council of 5 June 2019 on common rules for the internal market for electricity and amending Directive 2012/27/EU*. *Official Journal of the European Union*. 14. June 2019, L 158, pg. 125–199.

[43] SINGH, N., MOHAPATRA, A. a SINGH, S. N. Loss allocation methods in distribution networks: Present status and challenges. *Electric Power Systems Research*. 2024, vol. 236, no. 110966. DOI 10.1016/j.epsr.2024.110966.

[44] EUROPEAN COMMISSION. *Commission Regulation (EU) 2017/2195 of 23 November 2017 establishing a guideline on electricity balancing*. *Official Journal of the European Union*. 28. November 2017, L 312, pg. 6–52.

[45] MWAMPASHI, M. M., NIKITOPOULOS, C. S. and RAI, A. From 30- to 5-minute settlement rule in the NEM: An early evaluation. *Energy Policy*. 2024, vol. 194, 114305. Available from: https://doi.org/10.1016/j.enpol.2024.114305

[46] MOHAMED, S. K., HASSAN, M. H. and DOMÍNGUEZ-GARCÍA, J. L. Optimal Power Flow Incorporating Renewable Energy Sources and FACTS Devices: A Chaos Game Optimization Approach. *IEEE Access*. 2024, vol. 12, pp. 23338–23362. DOI 10.1109/ACCESS.2024.3363237.

[47] RAEBER, M., HEINZELMANN, A. and OLIAPURAM, J. Analysis of a three-phase AC chopper with high power factor for the use in "PV-to-Heat" applications. In: *IECON 2019 – 45th Annual Conference of the IEEE Industrial Electronics Society*. IEEE, 2019, pp. 2319–2323. DOI 10.1109/IECON.2019.8926733.

[48] ČEPS, a.s. *Transmission System Code – Part II: Ancillary Services (AS). Rules for the Operation of the Transmission System*. Revision January 2025. Prague: ČEPS, 2025 (in Czech).

[49] TUTTELBERG, K. and KILTER, J. Real-time estimation of transmission losses from PMU measurements. In: *2015 IEEE Eindhoven PowerTech*. IEEE, 2015, pp. 1–5. DOI 10.1109/PTC.2015.7232313.

[50] KOTSONIAS, M., ASPROU, M., HADJIDEMETRIOU, L. and KYRIAKIDES, E. State Estimation for Distribution Grids With a Single-Point Grounded Neutral Conductor. *IEEE Transactions on Instrumentation and Measurement*. 2020, vol. 69, no. 10, pp. 8167–8177. DOI 10.1109/TIM.2020.2994011.

[51] EUROPEAN COMMISSION. *Commission Regulation (EU) 2016/631 of 14 April 2016 establishing a network code on requirements for grid connection of generators*. *Official Journal of the European Union*. 27 April 2016, L 112, pp. 1–68.

[52] *Distribution System Operation Rules – Grid Code (PPDS)*. Prague: ERÚ, 2020. (in Czech).

[53] PERETTO, L., WILLEMS, J. and EMANUEL, A. The effect of the integration interval on the measurement accuracy of rms values and powers in systems with nonsinusoidal waveforms. In: *Proceedings of the Seventh International Workshop on Power Definitions and Measurements under NonSinusoidal Conditions*. University of Cagliari, 2006, pp. 103–109.

[54] IEC. *IEC 62428:2007 Signal processing – Vocabulary*. Geneva: International Electrotechnical Commission, 2007.

[55] LANGELLA, R. and TESTA, A. A New Algorithm for Energy Measurement at Positive Sequence of Fundamental Power Frequency, Under Unbalanced Non-Sinusoidal Conditions. In: *2007 IEEE Lausanne Power Tech*. Lausanne: IEEE, 2007, pp. 1558–1563. DOI 10.1109/PCT.2007.4538547.

[56] CZARNECKI, L. S. Comments on active power flow and energy accounts in electrical systems with nonsinusoidal waveforms and asymmetry. *IEEE Transactions on Power Delivery*. 1996, vol. 11, no. 3, pp. 1244–1250. DOI 10.1109/61.517478.

[57] D-A-CH-CZ. *Technische Regeln für die Beurteilung von Netzrückwirkungen. Teil A: Grundlagen*. 2021 [online]. Available from: https://www.vde.com/resource/blob/2243774/835c8e1f4c150c0aeaeae21642fbf0f2/teil-a--technische-regeln-fuer-die-beurteilung-von-netzrueckwirkungen-data.pdf

[58] MEYER, J., MÖLLER, F., PERERA, S. and ELPHICK, S. General Definition of Unbalanced Power to Calculate and Assess Unbalance of Customer Installations. In: *2019 Electric Power Quality and Supply Reliability Conference (PQ) & 2019 Symposium on Electrical Engineering and Mechatronics (SEEM)*. Kärdla, Estonia: IEEE, 2019, pp. 1–6. DOI 10.1109/PQ.2019.8818268.

[59] DRECHSLER, R. *Measurement, Evaluation, and Quality of Electric Energy Consumption in Thyristor Equipment Operation*. Prague: SNTL – Technical Literature Publishing / ALFA, 1982. (in Czech).

[60] REPAK, M., OTCENASOVA, A., REGULA, M., BOLI, A. and BELANY, P. Design of power quality analyzer. In: *ELEKTRO 2018*. IEEE, May 2018, pp. 1–6. DOI 10.1109/ELEKTRO.2018.8398305.

[61] TEXAS INSTRUMENTS. *Power quality analyzer design resources*. [online]. Accessed 18 April 2025. Available from: https://www.ti.com/solution/power-quality-analyzer
[62] TEXAS INSTRUMENTS. *Electricity meter design resources*. [online]. Accessed 18 April 2025. Available from: https://www.ti.com/solution/electricity-meter?variantid=24375
[63] NXP. *AN13259 Low-Power Real-Time Algorithm for Metering Applications*. Rev. 0. June 2021.
[64] TESTA, A., GALLO, D. and LANGELLA, R. On the processing of harmonics and interharmonics: using Hanning window in standard framework. *IEEE Transactions on Power Delivery*. 2004, vol. 19, no. 1, pp. 28–34. DOI 10.1109/TPWRD.2003.820437.
[65] ANALOG DEVICES. *ADE 7758: Poly Phase Multifunction Energy Metering IC with Per Phase Information*. Data Sheet. Rev. E.
[66] BLAABJERG, F., TEODORESCU, R., LISERRE, M. and TIMBUS, A. V. Overview of control and grid synchronization for distributed power generation systems. *IEEE Transactions on Industrial Electronics*. 2006, vol. 53, no. 5, pp. 1398–1409. DOI 10.1109/TIE.2006.881997.
[67] SEVILMIŞ, F. and KARACA, H. Performance enhancement of DSOGI-PLL with a simple approach in grid-connected applications. *Energy Reports*. 2022, vol. 8, pp. 9–18.
[68] BLAABJERG, F., ed. *Control of Power Electronic Converters and Systems: Volume 1*. 1st ed. San Diego, CA: Academic Press, 2018. ISBN 978-0-12-805245-7.
[69] FEOLA, L., LANGELLA, R. and TESTA, A. On the effects of unbalances, harmonics and interharmonics on PLL systems. *IEEE Transactions on Instrumentation and Measurement*. 2013, vol. 62, no. 9, pp. 2399–2409. DOI 10.1109/TIM.2013.2270925.
[70] CARBONE, R., LANGELLA, R. and TESTA, A. Grid-Connected Photovoltaic Plants: Energy Account Problems. In: *102° Convegno Nazionale AEIT*. Catania, Italy, September 2009.
[71] CATALIOTTI, V., COSENTINO, A., LIPARI, A. and NUCCIO, S. Metrological Characterization and Operating Principle Identification of Static Meters for Reactive Energy: An Experimental Approach Under Nonsinusoidal Test Conditions. *IEEE Transactions on Instrumentation and Measurement*. 2009, vol. 58, no. 5, pp. 1427–1435. DOI 10.1109/TIM.2008.2009134.
[72] EMANUEL, E. *Power Definitions and the Physical Mechanism of Power Flow*. 2010. DOI 10.1002/9780470667149.
[73] CZARNECKI, L. S. Do Energy Oscillations Degrade Energy Transfer in Electrical Systems? *IEEE Transactions on Industry Applications*. 2021, vol. 57, no. 2, pp. 1314–1324. DOI 10.1109/TIA.2021.3051314.
[74] AKAGI, H., WATANABE, E. H. and AREDES, M. *Instantaneous Power Theory and Applications to Power Conditioning*. Hoboken, NJ: Wiley–IEEE Press, 2007.
[75] FRONIUS. *Fronius OhmPilot: Operating manual*.
[76] EGD. *Electricity Sharing* [online]. [Accessed 22 July 2025]. Available from: https://www.egd.cz/sdileni-elektriny (in Czech).
[77] BRUGEL. Décision relative aux modifications tarifaires au cours de la période 2022–2024 et portant principalement sur les tarifs de distribution applicables pour le partage d'énergie. *BRUGEL-DECISION-20220823-205*. Brussels, 23 August 2022 [online]. Available from: www.brugel.brussels
[78] FRANK BOLD SOCIETY. *Legal Framework for Community Energy in the European Union: Seven Recommendations for the Czech Republic*. Brno: Frank Bold, 2023 [online]. Available from: https://frankbold.org/sites/default/files/publikace/pravni_uprava_komunitni_energetiky_v_eu._sedm_doporuceni_pro_cr.pdf [Accessed 22 July 2025]. (in Czech).

[79] YU, Y., ZHAO, W., CHEN, L., WANG, Q. and HUANG, S. Power measurement accuracy analysis in the presence of interharmonics. *Measurement*. 2020, vol. 154, 107484. DOI 10.1016/j.measurement.2020.107484.

[80] DRÁPELA, J., HAVRÁNEK, Z. and JURKA, T. Immunity Issues Related to Revenue Meters. In: *IEEE PES General Meeting*. Denver, USA: IEEE, 2015 [presentation]. Available from: https://www.ieee-pes.org/presentations/gm2015/PESGM2015P-000911.pdf

[81] NOVOTNÝ, J., DRÁPELA, J. and TOPOLÁNEK, D. Frequency response of revenue meters in measured active energy. In: *2016 17th International Conference on Harmonics and Quality of Power (ICHQP)*. IEEE, 2016, pp. 524–529. DOI 10.1109/ICHQP.2016.7783309.

AUTHOR'S PUBLICATIONS

[A1] KLUSÁČEK, J., VRÁNA, M. a DRÁPELA, J. Demand Responsive Power Flow Controller Providing Resistive Load Perspective Regulation in Cooperation with Small Generation Units. In: *Proceedings of the 2020 21st International Scientific Conference on Electric Power Engineering (EPE)*. New York: IEEE, 2020, s. 1–6. ISBN 978-1-7281-9479-0. NY,USA: IEEE, 2020. p. 1-6. ISBN: 978-1-7281-9479-0.

[A2] VOJTEK, M., DRÁPELA, J., MASTNÝ, P., MORÁVEK, J., VRÁNA, M. a KLUSÁCEK, J. Analysis and Verification of Operating Characteristics of Hybrid Inverter with External Power Meter. In: *Proceedings of the 2022 22nd International Scientific Conference on Electric Power Engineering (EPE)*. New York: IEEE, 2022, s. 89–93. ISBN 978-1-6654-1057-1.

[A3] VRÁNA, M., KLUSÁCEK, J., DVORÁCEK, J., MORÁVEK, J., DRÁPELA, J. a MASTNÝ, P. Impact of three-phase inverter-based generating units with asymmetrical power redistribution on the low-voltage network operation. In: *27th International Conference on Electricity Distribution (CIRED 2023)*. Rome: IET, 2023, s. 3909–3913. ISBN 978-1-83953-855-1. ISSN 2732-4494.

[A4] KLUSÁCEK, J., VRÁNA, M., DRÁPELA, J., MORÁVEK, J. a MASTNÝ, P. Advanced Design of Heat Accumulation Responsive Demand Control for Energy Management of Prosumers. In: *The 26th International Conference and Exhibition on Electricity Distribution (CIRED 2021)*. IET, 2021, s. 986–990. ISBN 978-1-83953-591-8. ISSN 2732-4494.

[A5] KLUSÁCEK, J., DRÁPELA, J. a LANGELLA, R. Control Strategies for Energy Diverters based on Revenue Meters' Metrics. In: *Proceedings of the 2023 23rd International Scientific Conference on Electric Power Engineering (EPE)*. New York: IEEE, 2023, s. 211–216. ISBN 979-8-3503-3593-4.

[A6] KLUSÁČEK, J. et al. Feed-in Energy Controllers for Prosumer Installations: Development of Commercial Devices with Power-Quality Considerations. *Conference ČK CIRED*. Tábor, 2022, s. 31 (in Czech).

[A7] KLUSÁCEK, J., DRÁPELA, J. Voltage Control in Medium Voltage Grids Employing Distributed Power Sources. In: *Proceedings II of the 27th Conference STUDENT EEICT 2021*. Brno: Brno University of Technology, Faculty of Electrical Engineering and Communication, 2021, s. 224–228. ISBN 978-80-214-5943-4.

[A8] DVORÁCEK, J., KLUSÁCEK, J., DRÁPELA, J. a TOPOLÁNEK, D. Dispatch Reactive Power Sharing Concept for Power Generating Plants in Medium Voltage Distribution Systems. In: *Proceedings of the 2022 22nd International Scientific Conference on Electric Power Engineering (EPE)*. New York: IEEE, 2022, s. 125–130. ISBN 978-1-6654-1057-1.

[A9] KLUSACEK, J., DRAPELA, J. a LANGELLA, R. Power Symmetrical Components as Grid Usage Indicator for Unbalanced Prosumers. In: *2022 20th International Conference on Harmonics & Quality of Power (ICHQP)*. Naples: IEEE, 2022, s. 1–6. DOI 10.1109/ICHQP53011.2022.9808706.

[A10] KLUSACEK, J., DRAPELA, J., LANGELLA, R. a MEYER, J. Revenue Metrics Ability to Correctly Register Bidirectional Active Energy Flows in Active Distribution Networks. In: *2023 IEEE 13th International Workshop on Applied Measurements for Power Systems (AMPS)*. Bern: IEEE, 2023, s. 1–6. DOI 10.1109/AMPS59207.2023.10297185.

[A11] KLUSÁCEK, J., LANGELLA, R., MEYER, J. a DRÁPELA, J. Performance of Smart Revenue Meters Under Bidirectional Active Energy Flows in Energy Communities. *IEEE Transactions on Instrumentation and Measurement*. 2024, roč. 73, č. 1, s. 1–12. ISSN 1557-9662.

[A12] KLUSÁCEK, J., DRÁPELA, J. a LANGELLA, R. Revenue Metering of Unbalanced Prosumers in Energy Communities. *IEEE Open Access Journal of Power and Energy*. 2023, roč. 10, č. 1, s. 426–437. ISSN 2687-7910.

LIST OF ABBREVIATIONS

∑1ph	Algebraic active power
3ph	Vectorial active power
A/D	Analog-to-Digital Converter
AC	Alternating Current
AK	Allocation Key
AUX	Auxiliary load
CAPEX	Capital Expenditures
CHP	Combined Heat and Power
CON	Consumer
COSEM	Companion Specification for Energy Metering
DC	Direct Current
DER	Distributed Energy Resources
DLMS	Device Language Message Specification
DQ	DQ-domain algorithm
DSP	Digital Signal Processor
DS	Distribution System
DSO	Distribution System Operator
DTS	Distribution Transformer Substation
EEPROM	Electrically Erasable Programmable Read-Only Memory
EMC	Electromagnetic Compatibility
EMS	Energy Management System
FEED	Feeder (main supply line in a distribution system)
FILT	Filtering algorithm
FPGA	Field Programmable Gate Array
FT	Fourier Transform algorithm
HV	High Voltage
I/O	Input/Output
LED	Light-Emitting Diode
LP	Load Profile
LV	Low Voltage
MAN	Signal-manipulation algorithm
MCU	Microcontroller Unit
MID	Measuring Instruments Directive
MV	Medium Voltage
OBIS	Object Identification System
OPEX	Operational Expenditures
P+	Positive-sequence active power controller
P∑	Vectorial active power controller
P2P	Peer-to-Peer
PCC	Point of Common Coupling
PO	Pulse Output
PLL	Phase-Locked Loop
PMU	Phasor Measurement Unit
PoC	Point of Connection
PoM	Point of Measurement
Pph	Algebraic active power controller
PRO	Prosumer (general form)
PV	Photovoltaic
PWR	Pulse-Width Regulation
RAM	Random Access Memory
RES	Renewable Energy Sources
RM	Revenue Meter
RMS	Root Mean Square
SD	Secure Digital (memory card)
STD	Standard algorithm
SYM	Positive sequence active power
THD	Total Harmonic Distortion
VC	Virtual Conditioner

BIBLIOGRAPHY

Jan Klusáček was born in Nové Město na Moravě, Czech Republic, on October 4, 1995. He received the B.Sc. and M.Sc. degrees in electrical engineering from the Brno University of Technology (BUT), Faculty of Electrical Engineering and Communication (FEEC), Brno, Czech Republic, in 2018 and 2020, respectively. His bachelor's thesis focused on the control of drives using inverters with active front-ends, and his master's thesis concerned the design of controllers for energy flows in prosumer installations and their impact on voltage quality in distribution networks.

Since 2020, he has been pursuing the Ph.D. degree at the BUT, focusing on the impacts of energy sector decentralization, particularly the influence of active customers not only on voltage quality but also on deviations and accuracy of electrical energy and power measurements, both at the level of individual devices and with in the broader measurement framework, including definitions of measured components. His research interests further include requirements on measuring instruments, power theories, control algorithms for active power flow management, EMC aspects of commercial power hardware and mitigation techniques, as well as related standards and legislation. He has actively participated in several national research projects funded by TAČR, GAČR, and the Czech Ministry of Industry and Trade, as well as in contract-based research. Through these projects, he has gained expertise in topics such as allocation of voltage disturbance contributions from consumers, control and design of converters for railway traction power supply systems and their contribution to voltage distortion, reactive power control of converters with active front-ends for voltage support in distribution/transmission grids, and laboratory testing of commercial photovoltaic inverters.

Ing. Klusáček has actively participated in national and international conferences focused on the development and operation of distribution and transmission systems (including conferences and working group meetings organized by the Czech National Committee of CIRED, the international CIRED conferences, EPE conference), power quality (ICHQP), electrical measurements (AMPS workshop), as well as student conferences (e.g. EEICT). He has authored 14 papers in international conference proceedings and 2 journal papers in IEEE journals (TIM, OAJPE), sharing the results of his work with both professional and academic communities. He is a student Member of IEEE and a member of CIGRE. In addition to his research activities, he has supervised two successfully defended bachelor's theses and two master's theses, and has taught laboratory and numerical classes in the courses of Electricity Consumption and Use, Power Quality, and Electrical Power Distribution at BUT.